Analysis of Power Converter's Control Techniques in Grid-Tie and AC Micro/Smart Grid

Abdulgafor Mohammed Alfares
Marquette University

ANALYSIS OF POWER CONVERTER'S CONTROL TECHNIQUES IN GRID –TIE
AND AC MICRO/SMART GRID

by

Abdulgafor Mohammed Alfares , B.S.

A Thesis Submitted to the Faculty of the Graduate School,
Marquette University,
in Partial Fulfillment of the Requirements for
the Degree of Master of Science

Milwaukee, Wisconsin

May 2014

ABSTRACT
ANALYSIS OF POWER CONVERTES' CONTROL TECHNIQUES
IN GRID-TIE AND AC MICRO/SMART GRID

Abdulgafor Alfares , B.S.

Marquette University, 2014

Power converters have an outstanding potential in micro and smart grid applications that require flexible and fast power control as well as rigid voltage regulation at the point of common coupling. Power converters are required to properly operate under several modes of operation such as grid-tie and micro-grid modes of operations. In addition, the control system should be designed to enable proper load sharing between several units.

Several control techniques have been proposed in the literature to address most of the control requirements of the power converters under different operating modes mentioned above. However, references found in the literatures are usually centered on the analysis of the system under only one mode of operation and using a single control strategy. Comprehensive study that combines an in depth analysis of the power converters control under several modes are very scarce in the literature.

In this thesis, a detailed survey and analysis of power converter control techniques in Grid-Tie and AC Micro/Smart Grid applications are introduced. This analysis is based on detailed nonlinear time domain simulations as well as average and small signal models for system stability assessment and performance evaluation.

ACKNOWLEDGMENTS

Abdulgafor Alfares , B.S.

TABLE OF CONTENTS

CHAPTER 3: GRID FILTER DESIGN

CHAPTER 4: MICROGRID SYSTEM IN STAND-ALONE APPLICATION

CHAPTER 5: MICROGRID SYSTEM IN STAND-ALONE WITH SHARING SOURCE

LIST OF TABLES

LIST OF FIGURES

CHAPTER 1: INTRODUCTION

1.0   INTRODUCTION

The goal of renewable energy is to provide energy that originates from natural resources such as sunlight, wind, rain, and other sources. Since the use of green energy enhances the environment and reduces global energy consumption, the attention of research in this field has been focused on methods of developing green energy resources. As a result of using natural resources, the need for microgrid energy systems will be increasing. Moreover, such a system will require small energy storages, small and large loads, and microgenerators, leading to the introduction of a unique category of distributed generation systems known as microgrid.

1.1   MICROGRID AND SMART GRID SYSTEMS:

- **Microgrid:**

A microgrid is defined as a small scale standard power grid, shaped by a distributed generation, electric energy sources, and loads which are electrically connected and controlled in the ability to operate with a grid-connected mode or as an islanded system mode, as shown in Fig 1.1a and Fig 1.1b [3]. The microgrid can be feeding the grid, supporting the grid or can run in a stand-alone mode . The high power quality in the microgrid is very important and desirable to obtain from these new resources of energy. To achieve the efficient and safe operation of these systems, the concept of Droop

Control Method (DCM) is used to control the microgrid. This theory is discussed in

Chapter 5.
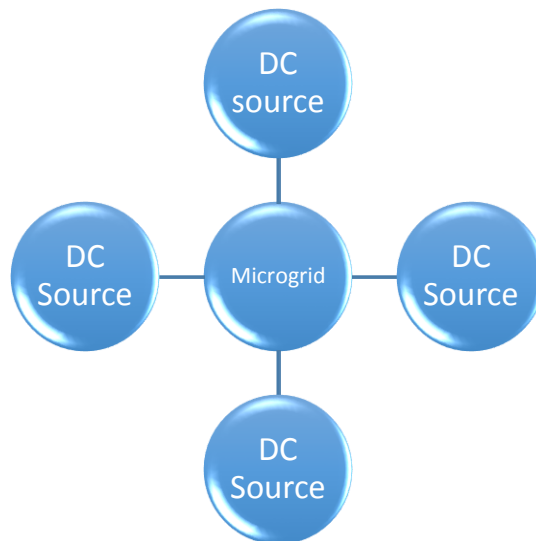
Fig. 1.1a Simple configuration of microgrid.
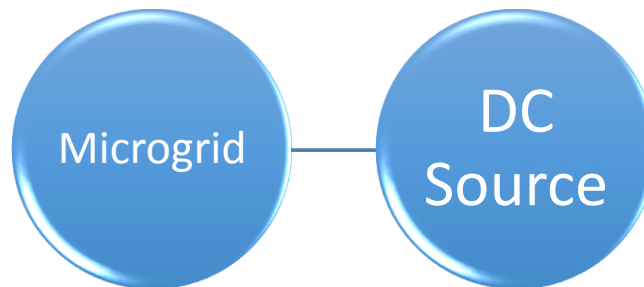
Fig. 1.1b: Simple configuration of microgrid.

- **Smart Grid :**

    The old traditional structure of an electric power system contains thousands of

miles of transmission lines, substations, and large transformers. Furthermore, the cost of

the old system is very high because of factors including insulation and maintenance.

Smart grid construction does not need thousands of miles of transmission lines and

substations. This new system is small, and it includes a smart grid technique that controls

the renewable energy resources. Smart grid represents distributed power since it has

many supplies and many loads and different types of controls at various location [1].

A simple smart grid could consist of any two or more power sources such as an

AC power source and a DC power source where all the power sources must be converted

to an AC power source. A typical smart grid system is shown in Fig 1.2.
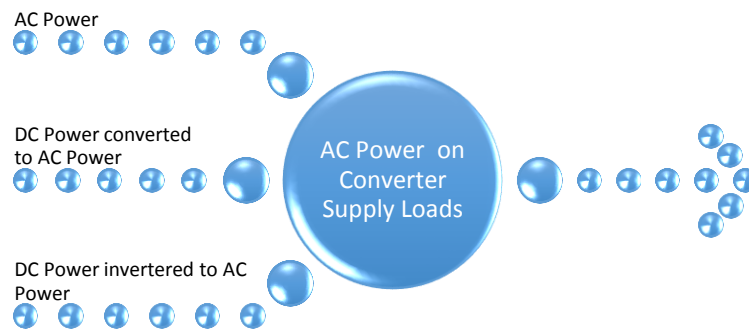
Fig. 1.2: Simple smart grid structure.

The renewable energy resources are assumed to be the source of the DC power in

this thesis; however, this DC power source is assumed to be constant. The power grid is a

network of short transmission and distribution systems for distributing the electric power

from the suppliers to the customers. In addition, a smart grid uses several methods of

energy generation and distribution [1]. The future concept for the modern city of electric

power system structure is represented in Fig 1.3 [10].
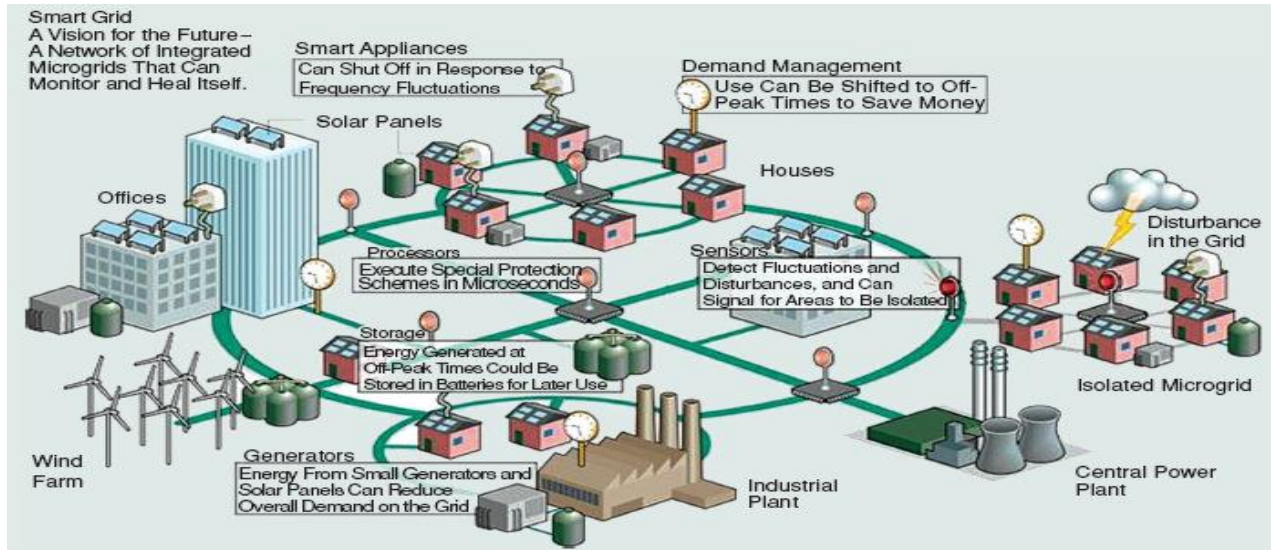
Fig. 1.3: Smart grid and microgrid source [10].

- **The Difference Between Smart Grid and Microgrid:**

The difference between a smart grid and a microgrid is the scale of standard power. Smart grids are considered at the utility and national grid level, which include the large transmission and distribution lines, while smart microgrids are considered at a smaller scale which includes small energy storages, small loads, and microgenerators. As a result of this, microgrids have shorter commissioning time. A microgrid could be independent with one power source with only one utility or more as seen in Fig 1a.1 and Fig 1b.1. However, the microgrid is still part of the smart grid, and if the smart grid is developed the microgrid will have better power quality [7].

- **Achievement of Smart Grid and Microgrid:**

The modern electric system has renewable energy storage and eliminates the need for long-distance transmission lines, since the new concept is to generate a small amount of power in several distributed power stations, rather than a huge amount of power in one power station.

Smart grids rely on using modern technology to convert the different energy and power supply systems into a reliable, stable, and smart network that uses the environmental resources with secure ways of controls. Research in smart grids focuses on addressing the following issues:

- Efficiency of the system, including power quality and system reliability

- Size of energy storage systems

- Distribution of the renewable energy resource generation

- Control methods of the microgrid systems, including power management.

The concept of smart grids is based on using modern technology to transfer the energy from generator to the customers. This approach will allow home electric utilization because it is affordable and low-cost. In addition, the approach will allow customers to have access to basic control for the smart grid to measure the quality of power and the system overall [2]. This area of research plays a main role in societal economics; therefore, many investigations have been centered on developing renewable alternatives for fossil fuels and nuclear energy.

1.2 THE IMPORTANCE OF RENEWABLE ENERGY RESOURCES:

In order to organize the need for renewable energy resources, let us discuss the disadvantages of the current energy resources as follows:

- **Nuclear Power Plant :**

It is well known that nuclear power is one of the most efficient sources of energy, and it is guaranteed to provide the utilities' power requirements. However, the

catastrophic consequences in the case of catastrophic accidents of nuclear power plants discourage their expansion.

- **Fossil Fuel:**

Natural gas and oil are provided by certain countries to the world at a very high price and are the main cause of pollution in the environment. Global warming is a great example of the results of using fossil fuel as a source of energy. The time needed to develop different energy sources is shown below.

Energy Production	Time
Solar/Heat/Electricity	Direct Use
Wind Energy	Hours/Days
Hydro-electro Power	Weeks
Biomass	Month/Years
Oil	Many Years

Table 1.1: Time required for production of different types of energy [1].

Close observation of Table 1.1 shows the historical use of energy. Our early energy was wood, then coal replaced it, and after a while oil has dominated until today. However, with the new Industrial Revolution and the colossal pollution of oil, this type of fuel is going to be replaced. From Tables 1.2 and 1.3, the carbon footprint of fossil fuels is the highest; this is one of the reasons of the pollution's effects on the earth and global warming, while renewable energy sources are the "friendliest" to our environment and to our earth. A great example of renewable energy—especially in Texas, some regions in the south of the USA, and Middle Eastern countries—is Solar Photovoltaic because these areas are sunny and hot. Also, the wind power system is useful in very windy areas such as Chicago, which is in the Midwest of the USA.

Fuel Type	CO2 Footprint (Ib)
Wood	3.306
Coal-Fired Plant	2.117
Gas-Fired Plant	1.915
Oil-Fired Plant	1.314
Combined-Cycle Gas	0.992

Table 1.2: Carbon footprint of various fossil fuels for production of 1kWh of electric energy [1].

Fuel Type	CO2 Footprint(Ib)
Hydroelectric	0.008
Wind	0.03306
PV	0.2204

Table 1.3: Carbon footprint of renewable source for production of 1kWh of electric energy [1].

After the disadvantages of current energy resources were introduced, the need to search for alternative energy resources has become essential. A great example of this substitute energy resource is renewable energy, represented as follows:

- **Fuel Cells:**

A fuel cell is a device that converts fuel from chemical energy to electricity by using a chemical reaction with oxygen or another oxidizing agent. Fuel cells can produce electricity frequently as long as these inputs are provided. The basic concept of fuel cells' function is that two chemical reactions happen at the interfaces of the three diverse segments. The net outcome of the two reactions is that fuel is consumed, carbon dioxide or water is generated, and an electric power is generated. This could be used to power electrical devices or other loads [5].

- **Solar and Photovoltaic:**

Solar and Photovoltaic (PV) energies are current significant renewable energy sources. The sun is the first source of energy that provides electromagnetic waves and light. Sunlight produces about 1 kilowatt (kW) per square meter at sea level and 0.8 sunlight about 800 W/meter square. It is prudent for hot weather countries to invest in this huge energy from the sun and use it for renewable energy purposes. Fig1.4 is an example of Solar Thermal Generation [10].

Sun

Solar energy

Focused solar collector dishes

Stream turbine (superheated stream to 600C

Generator

Grid

End consumer
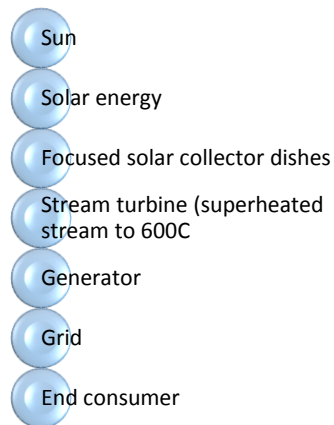
Fig. 1.4: Solar system.

The structure above is a simple and basic development for a solar system. The solar system needs solar collector dishes to collect all the solar energy and convert it to electrical energy. In some cases, there is a need use energy storage since the solar energy does not last too long and does not have a good efficiency yet. Research in this area focuses on trying to increase the efficiency of this type of energy.

- **Wind Power Development:**

The Wind Turbine System (WTS) is made of two parts, electrical and mechanical. The electrical parts contain power electronics and grid supply, while the mechanical parts contain the rotor and gearbox. This is illustrated in Fig. 1.5 [4].

| Rotor (Power conversion and power control | Gearbox (Power transmission) | Generator (Power conversion) | Power electronics (power conversion and power control) | Supply grid (power transmission) |
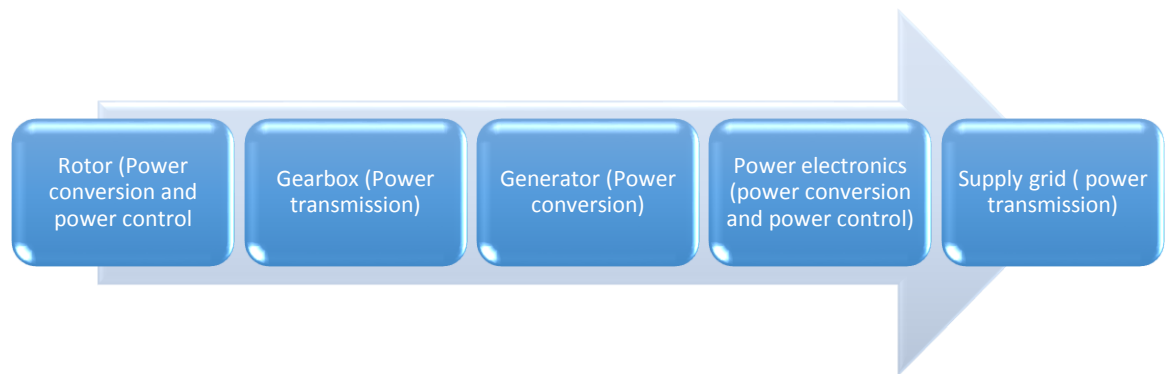
Fig. 1 .5: Basic power conversion wind turbine system [4].

From the previous discussion, research and development efforts focus on the best way to put these green energies to use. One of the most complex issues of using renewable energy is to find how to properly control these energy sources.

A smart grid is a complex system to build, containing many symbiotic technologies and alternative approaches. Therefore, it is imperative to understand the control system in order to guarantee both quality of supply and the power management supervising load sharing. Also, a basic issue on small grids is the control of the number of microgrid resources. The scope of this thesis is centered on the approaches to regulate microgrid assuming the power source at the DC side of the power converter is supplied by well-controlled and regulated energy sources, so the DC voltage can be represented by a constant voltage. This is typically the case for many renewable energy sources such as PV systems and fuel cells.

1.3   THE SCOPE OF THIS THESIS:

A survey regarding smart grid, microgrid structures, and the control of power converters is given in this thesis. A detailed investigation of the key operating modes and control configurations for systems belonging to smart grids and microgrids at the Distributed Generator (DG) will be provided. In addition to the first chapter, the content of this thesis is as follows:

The main control structures used for grid power converter are introduced in Chapter 2. The control is divided into three types:

1. Voltage Oriented Control (VOC).

2.   Direct Power Control (DPC).

3. Virtual Direct Torque Control (VDTC).

Also, details of the VOC are introduced and compared to the DPC and VDTC.

The power converter of VOC is investigated in Chapter 3 by using a detailed time domain simulation and the state space technique to model the control system.

The microgrid system in a stand-alone mode is studied in Chapter 4 by using detailed time domain simulation in an open loop mode, and closed loop using an outer voltage control loop and an inner current control loop.

In Chapter 5, the model utilized in Chapter 3 is further simplified, and a control system has been designed for proper load sharing between several operating units.

Future Work, Summary, and Conclusion are presented in Chapter 6.

CHAPTER 2: CONTROL TECHNIQUES OF MICROGRID POWER CONVERTER

2.0   INTRODUCTION:

Control technology of the microgrid has been developed widely during the last decade. This development has indebted its growth to the advancements in control methods. Before describing in detail the microgrid structure, let us discuss a high-level overview of control techniques for the smart grid. Due to the fact that the smart grid model contains AC and DC power sources, it is necessary to understand the basic idea of power flow. The control of the renewable energy DC source is out of the scope of this thesis; and the input to the power converter is assumed to be a regulated DC source. Thus, the general model of smart grids could be simplified by two AC voltage sources of the same frequency connected through a pure inductor with an impedance "X" as shown in Fig. 2.1.
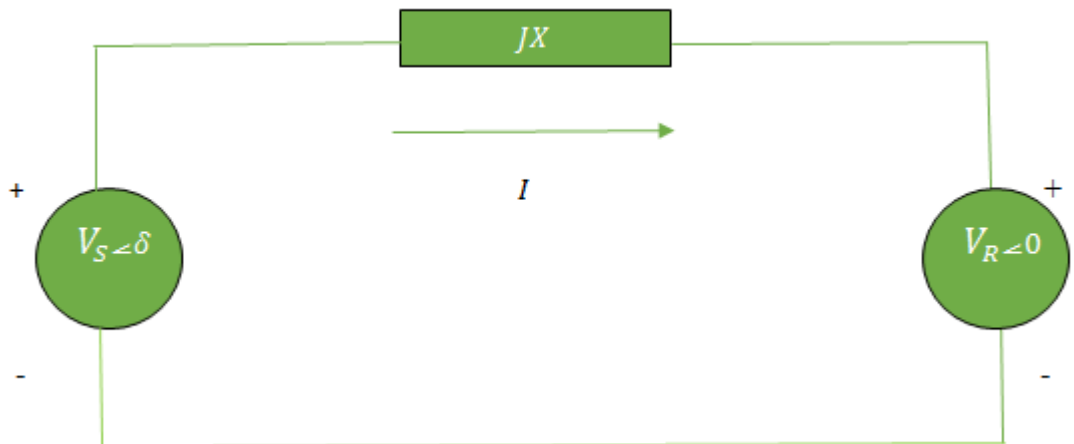
Fig. 2.1: Power transfer between tow AC systems.

The voltage V_R is assumed to be the converter voltage with a zero phase angle and

V_s is assumed to be the source voltage with δ phase angle. In the circuit of Fig. 2.1,

$$\bar{I} = \frac{\bar{V}_S - \bar{V}_R}{JX} \qquad (2.1)$$

At the receiving end, the complex power can be written as

$$S_R = P_R + JQ_R = V_R I^* \quad (2.2)$$

By using the complex conjugate from (2.1) into (2.2)

$$P_R + JQ_R = V_R \left(\frac{V_S \angle (-\delta) - V_R}{-JX} \right) = \frac{V_S V_R \, Sin\delta}{X} + J \left(\frac{V_S V_R \, Cos\delta - V_R^2}{X} \right) \qquad (2.3)$$

Where $\frac{V_S V_R \, Sin\delta}{X}$ is the active power, while $J \left(\frac{V_S V_R \, Cos\delta - V_R^2}{X} \right)$ is the reactive power [6].

From the basic scheme in Fig. 2.1, a smart grid can be controlled by either VOC, VDTC,

or DPC with different modes of the controller, as will be discussed later.

2.1   MODES OF CONTROLLER IN SMART GRIDS:

When the converter operates as a current source, the controller does not regulate

the voltage at the Point of Common Coupling (PCC). On the other hand, when the

converter is in a stand-alone mode or a grid support mode, it means the voltage and

frequency at PCC are regulated by the power converter. As a result, the operation of the

AC source in a smart grid or a microgrid will determine the type of control as either grid-

feeding, grid-support, or stand-alone [3].

A. Grid-Feeding Power Converters:

Grid-feeding power converters are used to provide active power (P) and reactive

power (Q) to the grid by using a current-controlled voltage source converter, which

emulates a current source in parallel with and high impedance connected to the grid as shown in Fig. 2.2.
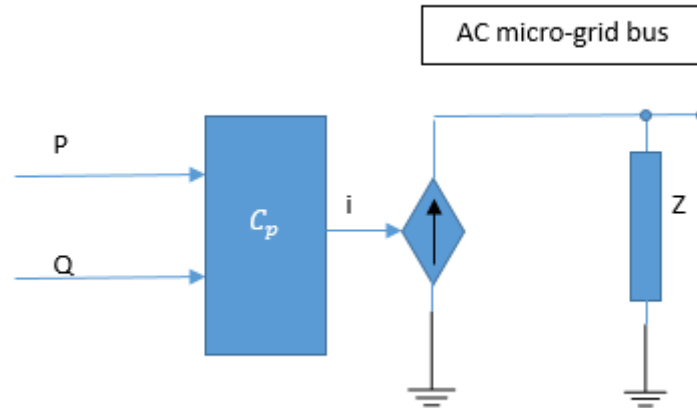
Fig. 2.2: Simplified parallel grid-feeding [3].

B. Grid-Supporting Power Converters:

Grid-supporting converters can be characterized by an ideal AC-voltage source in series with a link impedance, or as an ideal AC current source in parallel to shunt impedance with a link impedance, as shown in Fig. 2.3(a) and 2.3(b). Output voltage and output frequency are regulated by these converters [3].
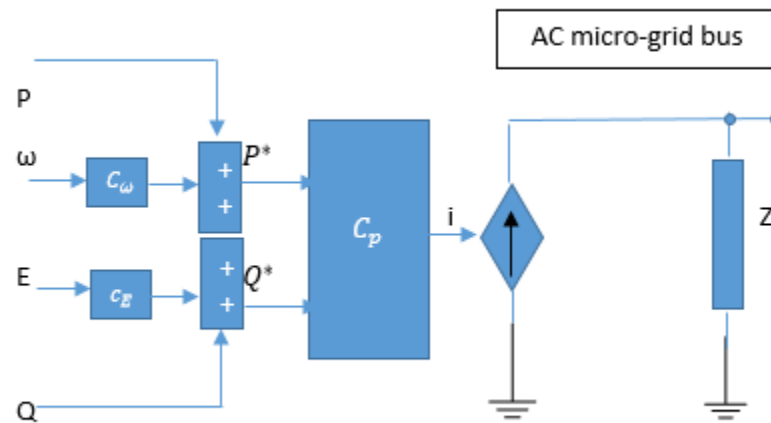
Fig. 2.3a: Simplified current source based grid supporting [3].
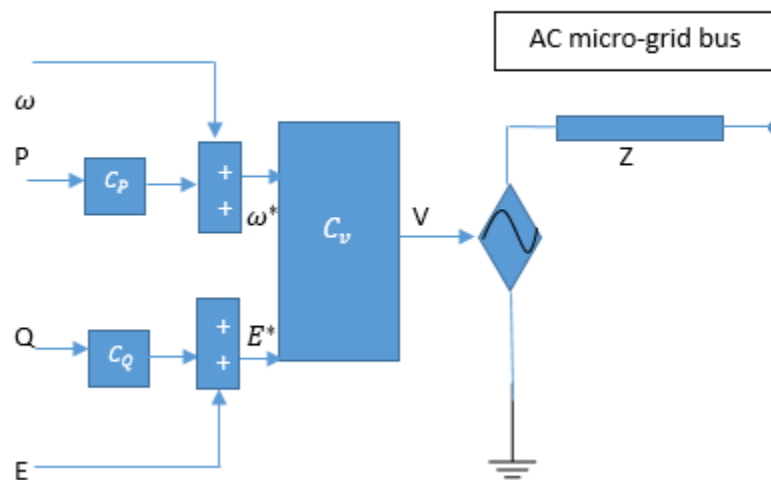
Fig. 2.3b: Simplified voltage source based grid supporting [3].

C. Stand-Alone Mode:

A microgrid in stand-alone mode is similar to supporting the grid, but without

using an AC source or infinite AC bus, as shown in Fig. 1.3. The basic concept is output

voltage, frequency, and load sharing regulated by the converters. Consequently, the

Distributed Generation (DG) is able to give better power quality to the loads.

The control of the grid converter is characterized by three levels:

1. Outer voltage control loop and inner current control loop which are typically applied in a stand-alone microgrid.

2. Outer active and reactive power control loops with an inner current control loop, such as VOC in grid feeding.

3. Only active and reactive power control loop, such as DPC and VDTC in grid feeding.

In view of high-performance control, VOC, DPC, or more lately VDTC, are used.

Using these methods, both a smart grid and microgrid could be controlled even in various

applications in power electronic systems. VOC, DPC, and VDTC are control strategies

that allow active power and reactive power to be decoupled and controlled independently.

VOC and DPC have better quality of control, while VDTC has a faster response [9]. A

comparative study of VOC, DPC, and VDTC follows.

2.2   VIRTUAL DIRECT TORQUE CONTROL (VDTC):

The concept of Direct Torque and Flux Control (DTFC) originated from drives

and machines [22]. In the past, Direct Torque Control (DTC) was established in 1971 by

Japanese and German researchers for high power drives purposes [9]. After this concept

was developed in drives and proved to be effective, it was extended to a microgrid for

control purposes by using the idea of VDTC. VDTC is a technique that uses the concept

of Space Vector (SV) to control active power and reactive power of the AC power

source. This includes calculating the active and reactive power based on the measured

voltages and currents of the converter. Active power is calculated from voltages and currents originated from the converter and is then compared with their reference values. If either the estimated reactive or active power deviates from the reference more than the allowed tolerance, the transistors of the power converter are turned off and on in such a way that the reactive and active errors will return to their tolerant bands as quickly as possible. Thus DTC is a form of the hysteresis control, as shown in Fig. 2.4.
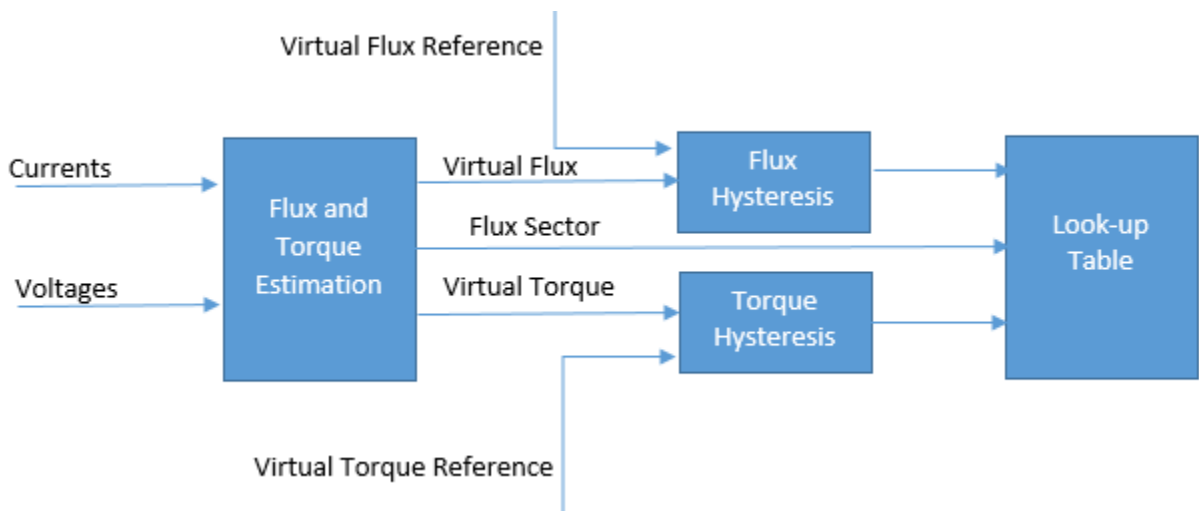
Fig. 2.4: Simplified block diagram of Virtual Direct Torque Control.

Finally, the look-up table gives the transistor signal control Sa, Sb, and Sc, and the switching table determines the switching state. The model in Fig. 2.5 is based on a MATLAB's Demo, modified to control active and reactive power in a smart grid system instead of torque and flux in an electrical machine. The voltages and currents are simply measured from both power sources, while the measured feedbacks for active and reactive power are calculated as follows [23]:

1. $P = v_a\, i_a\ +\ v_b\, i_b\ +\ v_c\, i_c$ \qquad\qquad (2.1)

2. $Q = \frac{1}{\sqrt{3}} [v_{ab} \; i_c + \; v_{bc} \; i_a + \; v_{ca} \; i_b]$ (2.2)

Where v_a , v_b and v_c are the phase voltages of phases *A, B* and *C* respectively, and

i_a , i_b and i_c are the phases currents of phases *A, B* and *C* respectively.
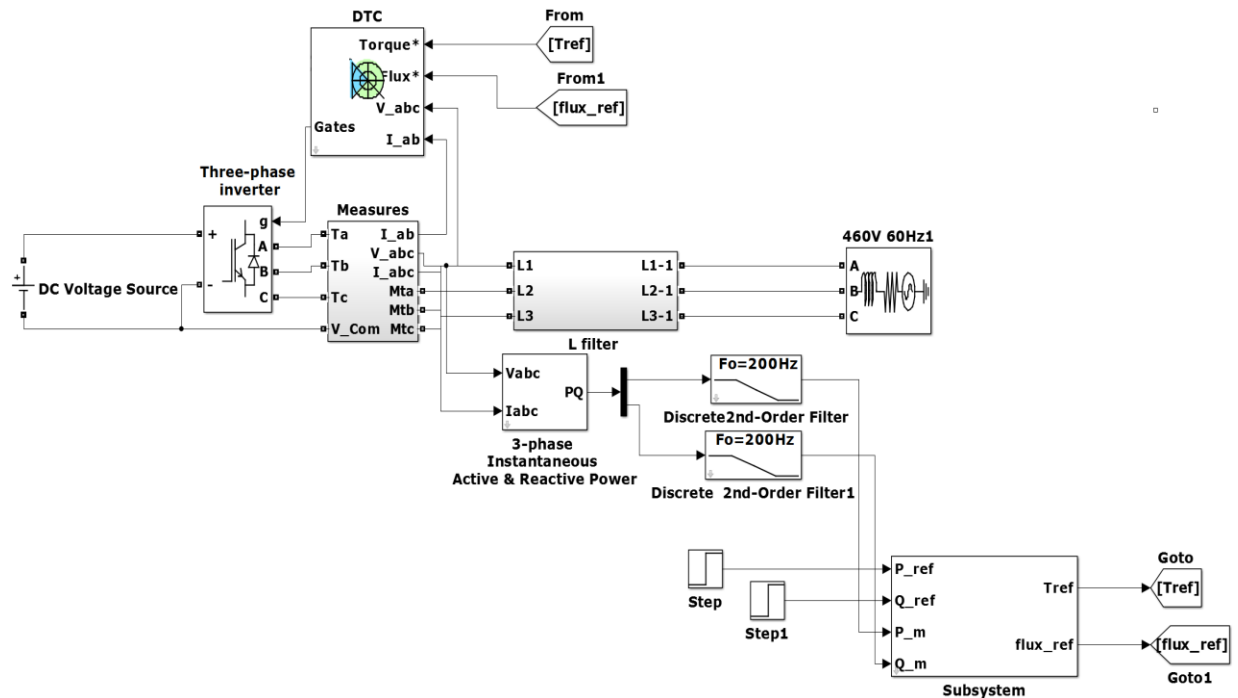
Fig. 2.5: Basic Virtual Direct Torque Control scheme for smart grid (VDTC).

VDTC control techniques of this system are based on three levels: 1) calculating the active and reactive power, 2) hysteresis control, and 3) a look-up table for generating the proper switching vector, as seen in Fig. 2.6.

- **Virtual Torque and Flux Calculation:**

Virtual Torque and flux are calculated from measured voltages and currents by using (2.3) and (2.5). Virtual torque and flux represent active power (P) and reactive power (Q), as shown in equations (2.3) and (2.5) respectively.

$P = Torque_{virtual} * \omega_{base}$ (2.3)

$\emptyset = \int (V - IR) \, dt$ (2.4)

When $R \approx 0$

$$\emptyset = \int V \, dt \qquad\qquad (2.5)$$

The reactive power can be estimated from equation (2.2) and equation (2.5).

- **Hysteresis Control:**

    The basic implementation of hysteresis control is based on deriving the switching signals depending on the comparison of the signal error with a fixed tolerance band. This control relies on the comparison of the actual phase variable with the tolerance band around the reference variable associated with that phase. Hence, hysteresis control is treating signals as vectors to have them in a specific domain. Therefore, a relay is needed to conduct this type of control as shown in Fig. 2.6. With all of these conditions, the hysteresis control will drive the signal into a fast path in a short amount of time.
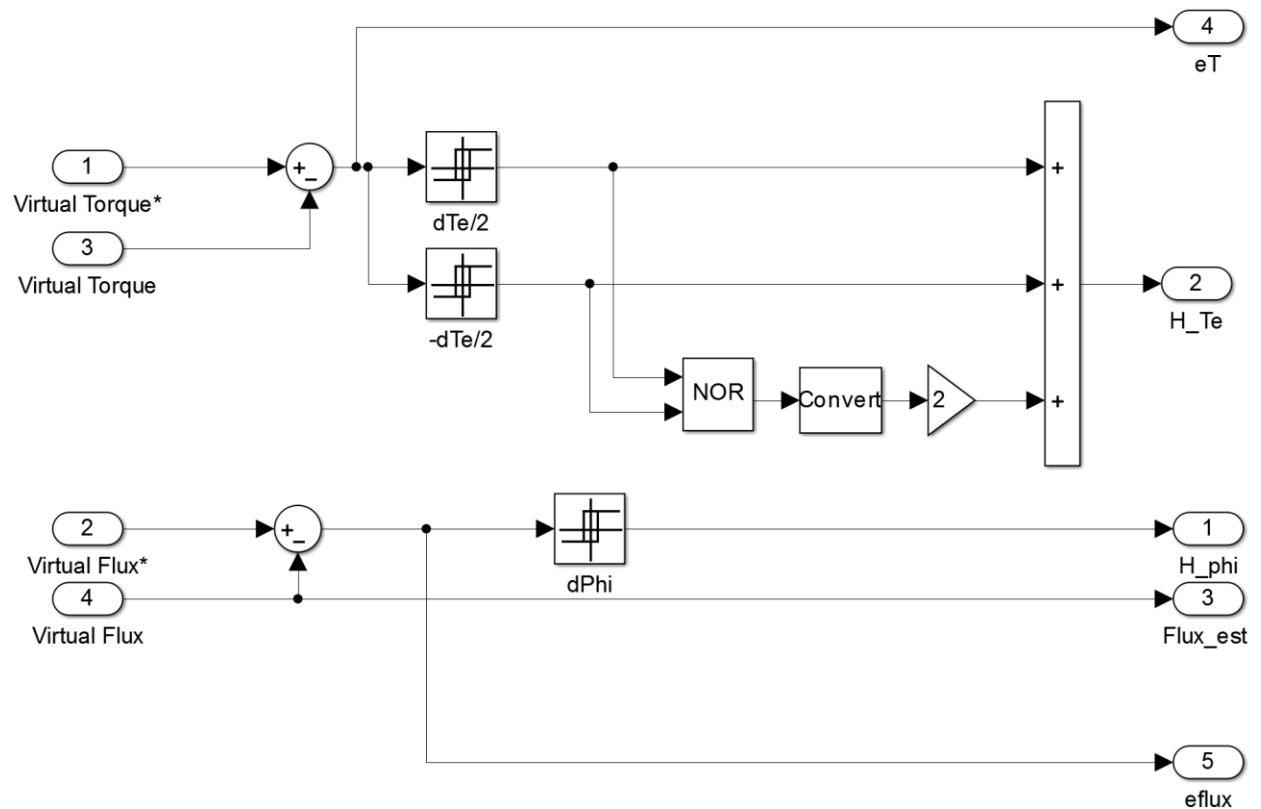
Fig. 2.6: Virtual Torque and flux hysteresis control.

- **Look-Up Table and Control:**

The main sectors for the inverter are shown in Fig. 2.7.
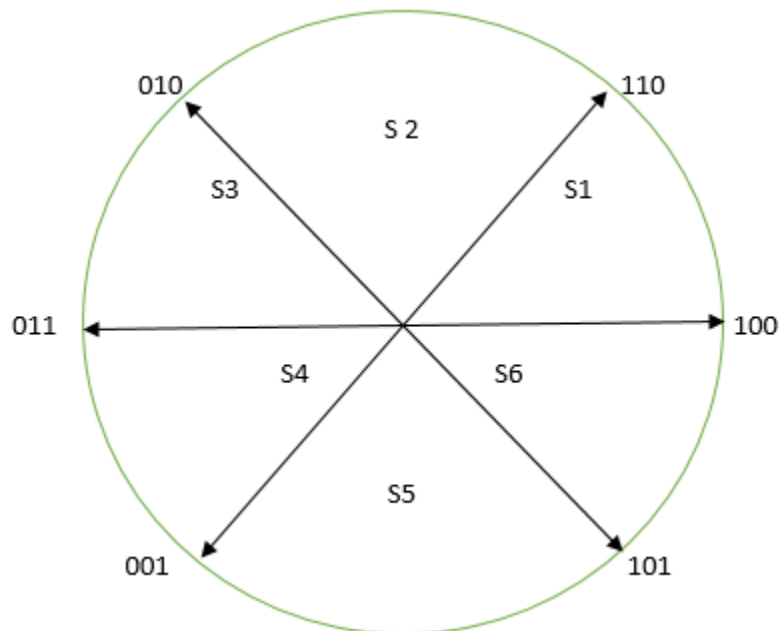
Fig. 2.7: Principle of Space Vector modulation.

Sectors	Start	End
S1	(1 0 0)	(1 1 0)
S2	(1 1 0)	(0 1 0)
S3	(0 1 0)	(0 1 1)
S4	(0 1 1)	(0 0 1)
S5	(0 0 1)	(1 0 1)
S6	(1 0 1)	(1 0 0)

Table 2.1: Sectors locations.

A VDTC scheme is shown in Fig. 2.6; the torque is compared in a three-level hysteresis control defining the error torque as *dTe/2* in modulus and sign. The flux is defining the error flux as *dPhi*. With this information, a voltage selector determines the

converter voltage required to increase or decrease the variables' active and reactive

power according to the demands. The switching states and look-up table are summarized

in Table 2.2. The used switching states are sector-dependent and are applied according to

the error states *dTe/2* and *dPhi* given by the flux and torque comparators.

State	Sa	Sb	Sc	Switching Vector
0	OFF	OFF	OFF	0 0 0
1	ON	OFF	OFF	1 0 0
2	ON	ON	OFF	1 1 0
3	OFF	ON	OFF	0 1 0
4	OFF	ON	ON	0 1 1
5	OFF	OFF	ON	0 0 1
6	ON	OFF	ON	1 0 1
7	ON	ON	ON	1 1 1

	flex logic dPhi = -1			flex logic dPhi = 1		
sector	dTe/2 =-1	dTe/2=0	dTe/2=1	dTe/2 =-1	dTe/2=0	dTe/2=1
S1	5	0	3	6	7	2
S2	6	7	4	1	0	3
S3	1	0	5	2	7	4
S4	2	7	6	3	0	5
S5	3	0	1	4	7	6
S6	4	7	2	5	0	1

Table 2.2: States switching and look-up table.

2.2.1 SUMMARY OF VDTC:

The VDTC was developed as an analogy to the well-known Direct Torque

Control used for drive. In VDTC, internal current loops and a PWM modulator block are

not used. Instead, the converter switching states are appropriately selected by a switching

table based on instantaneous errors between the commanded and estimated values of active and reactive power. The idea is to model the grid as a virtual electrical machine and estimate the virtual equivalent air-gap flux for control purposes. The estimation obtained while integrating the measured grid voltage can be used for synchronization purposes and for estimating the power injected into the grid for controlling a smart grid or microgrids.

2.3   VOLTAGE ORIENTED CONTROL:

The control of VOC in the modes supporting and feeding the grid is dependent on instantaneous apparent power. From the relation $S = Re\ \{V\ I^*\}$ for rms-value single phase and for three-phase system will be proportional to, $Re\ \{v^s\ (i^s)^*\} = Re\ \{v^{dq}\ (i^{dq})^*\}$ (2.4)

The power formula is independent of the coordinate system. Also, the time argument *(t)* is deleted from the SV definition for simplification.

$$v^s\ (i^s)^* = \left(\frac{2}{3}\ K\right)^2 \left(v_{a+}v_b\ e^{j\left(\frac{2\pi}{3}\right)} + v_c\ e^{j\left(\frac{4\pi}{3}\right)}\right)\left(i_a\ +\ i_b\ e^{j\left(\frac{2\pi}{3}\right)} + i_c\ e^{j\left(\frac{4\pi}{3}\right)}\right)^*$$

$$= \left(\frac{2}{3}\ K\right)^2 \left(v_a i_a\ +\ v_b i_b\ +\ v_c i_c\ + j\frac{1}{\sqrt{3}}\ (v_a(i_c\ -\ i_b)+\ v_b(i_a\ -\ i_c)+\ v_c(i_b\ -\right.$$

$$\left. i_a)\right)\ (2.5)$$

Then, the real part represents the active power

$$P = \left(\frac{2}{3}K\right)^2 Re\ \{v^s\ (i^s)^*\} =\ Re\ \{v^{dq}\ (i^{dq})^*\} =\ \left(\frac{2}{3}\ K\right)^2\ (v_a i_a\ +\ v_b i_b\ +\ v_c i_c)$$

(2.6)

Also, with an imaginary part represents the reactive power

$$Q = \left(\frac{2}{3}K\right)^2 Im\{v^s\ (i^s)^*\} = Im\{v^{dq}\ (i^{dq})^*\}$$

$$= \left(\frac{2}{3}K\right)^2 \left(j\frac{1}{\sqrt{3}}\ (v_a(i_c - i_b) +\ v_b(i_a - i_c) + v_c(i_b - i_a))\right)$$

(2.7)

Where K is a scaling constant and the transformation from $ABC\text{-}to\text{-}\alpha\beta$ is dependent on the scaling constant K. Refer to APPENDIX A for details [8].

The main control of the power converter can be carried out of a stationary $\alpha\beta$ frame, natural frame abc, or the dq synchronous frame, as shown in Fig. 2.8.
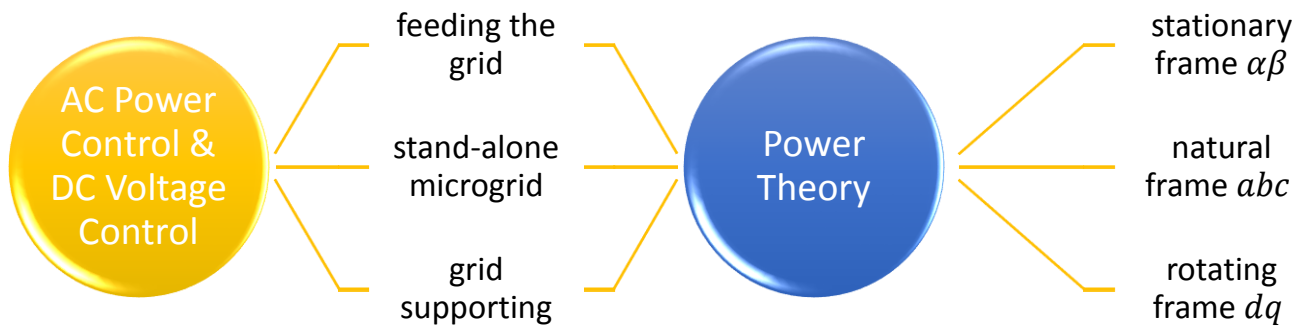
Fig. 2.8: Basic scheme of VOC.

Generally, VOC is based on the use of dq reference frame rotating at ω speed, and the circulation angle is chosen such that the d axis is aligned on the grid voltage vector, as shown in Fig. 2.9 [4].
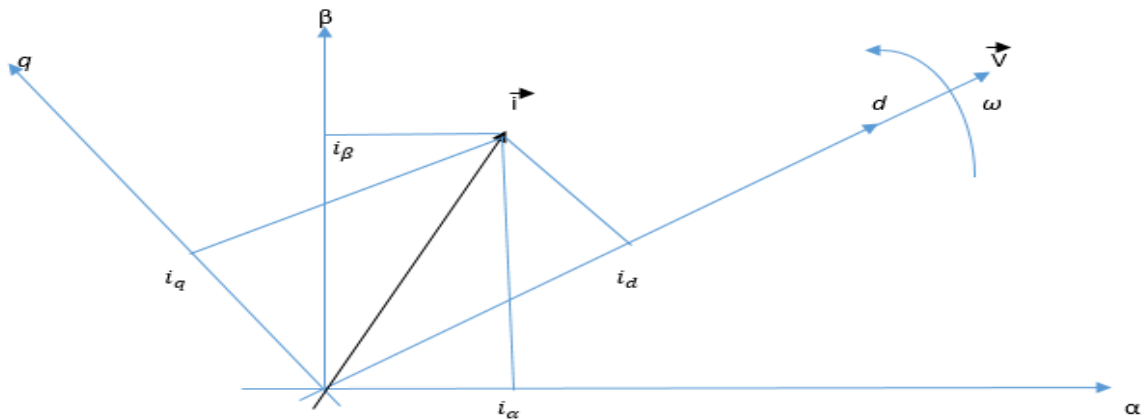
Fig. 2.9: Stationary $\alpha\beta$ frame and rotating dq frame (4).

The easiest direct implementation of VOC is achieved by using a current regulator implemented in a synchronous dq frame, as shown in Fig. 2.10. This is in addition to the outer active and reactive power loop. The active and reactive power are calculated in terms of the $d\text{-}q$ currents and voltages components in a synchronous frame of reference, as shown in the following equations and matrices:

$$S = VI^* \tag{2.8}$$

$$\lfloor P + JQ \rfloor = (V_d + J\,V_q)(I_d - J\,I_q) \tag{2.9}$$

$$= V_d I_d - J\,V_d\,I_q + JV_q I_d + V_q\,I_q$$

$$\lfloor P + JQ \rfloor = (V_d I_d + V_d\,I_q) + J(-V_d I_q + V_q\,I_d) \tag{2.10}$$

$$\begin{pmatrix} P \\ Q \end{pmatrix} = \begin{pmatrix} V_d & V_q \\ V_q & -V_d \end{pmatrix}\begin{pmatrix} I_d \\ I_q \end{pmatrix} \tag{2.11}$$

Now, find the inverse of the active and reactive matrix to get

$$\begin{pmatrix} P \\ Q \end{pmatrix} = \begin{pmatrix} V_d & V_q \\ V_q & -V_d \end{pmatrix}^{-1}\begin{pmatrix} I_d \\ I_q \end{pmatrix} \tag{2.12}$$

$$\begin{pmatrix} i_d \\ i_q \end{pmatrix} = \frac{1}{V_d{}^2 + V_d{}^2} \begin{pmatrix} V_d & -V_q \\ V_q & V_d \end{pmatrix} \begin{pmatrix} P \\ Q \end{pmatrix} \qquad (2.13)$$

The reference current i_d controls the active power and the DC voltage, while the reference i_q controls the reactive power and utility power angle [4].
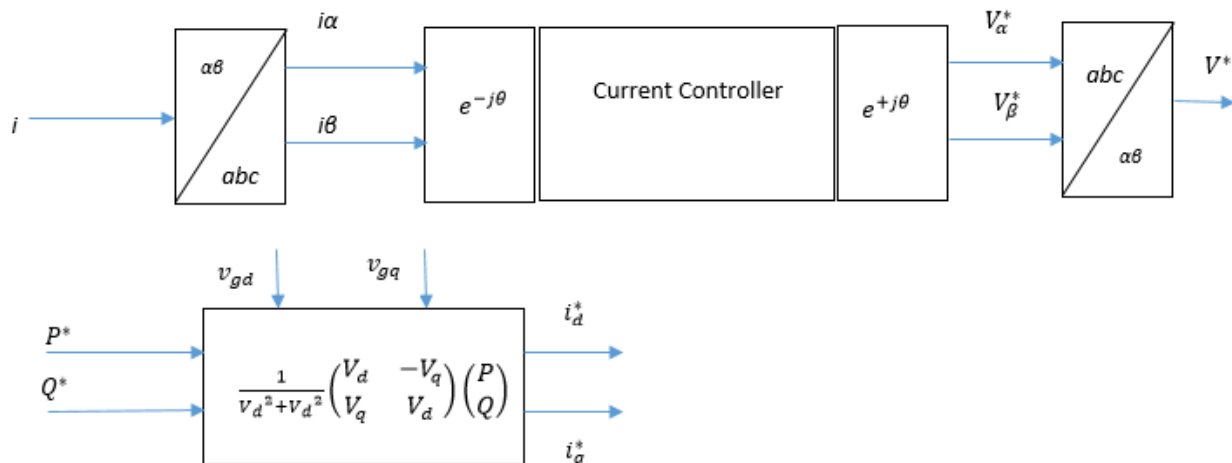
Fig. 2.10: PQ-loop and inner current loop [4].

The VOC is based on transforming the voltage and current from the ABC frame of reference to the DQ frame of reference. The angle and the frequency of the input line voltage are needed for this transformation. The Phase Locked Loop PLL plays a critical role of estimating the angle and the frequency of this transformation. Its aim is to provide the voltage angle θ of the three-phase system. This angle is then used for all of the dq transformed in the model. The three-phase line voltages and currents are measured and transferred to a synchronous frame of reference. The control of VOC consists of two loops, as shown in Fig. 2.11:

1. Outer active and reactive power control loops.

2. Inner current control loop.

The control strategy for the voltage and current is shown in Fig. 2.10. The observation is that v_d and v_q are used to feed forward the d-axis and the q-axis to provide good disturbance rejection. The inner control loops of the d-axis and the q-axis are the current control loops. The active and reactive power are calculated by using the measured voltage and current at PCC. The main function of the outer control loops is to regulate active and reactive power fed to the grid. The output of the power control loop is the common reference current for the inner current control loops [4].
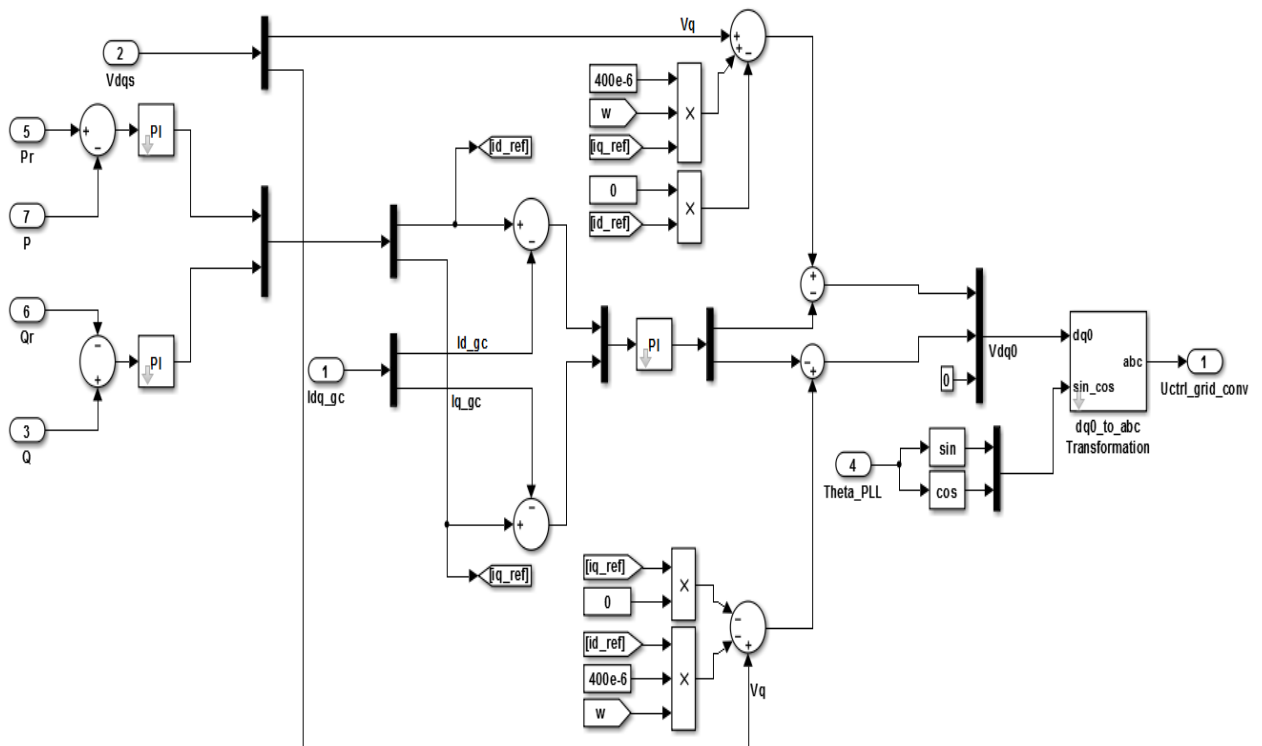
Fig. 2.11: PQ closed loop voltage-oriented control based on synchronous dq frame.

2.3.1 SUMMARY OF VOC:

The idea of VOC is based on instantaneous power theory for decoupling active and reactive power. This strategy guarantees fast transient response and high static

performance via an internal current control loop. Consequently, the performance depends upon the current control loop. The VOC's implementation is based on a *dq* frame of reference.

2.4   DIRECT POWER CONTROL (DPC):

DPC is a special case of VOC. They both have similar implementation and structures, such as the PWM modulator block and Proportional Integrator (PI) controller. Moreover, DPC is based on the instantaneous power theory for decoupling active and reactive power, and the PLL's output angle is used for *dq* transformation. However, the main difference between them is that in DPC there are no i_{dq} current loops, as shown in Fig 2.12. Hence, the control in *dq* transformation can be done by using only one loop, which is designed to regulate active and reactive power. The feed forward v_{dqs} is designed to regulate the voltage at the PCC.
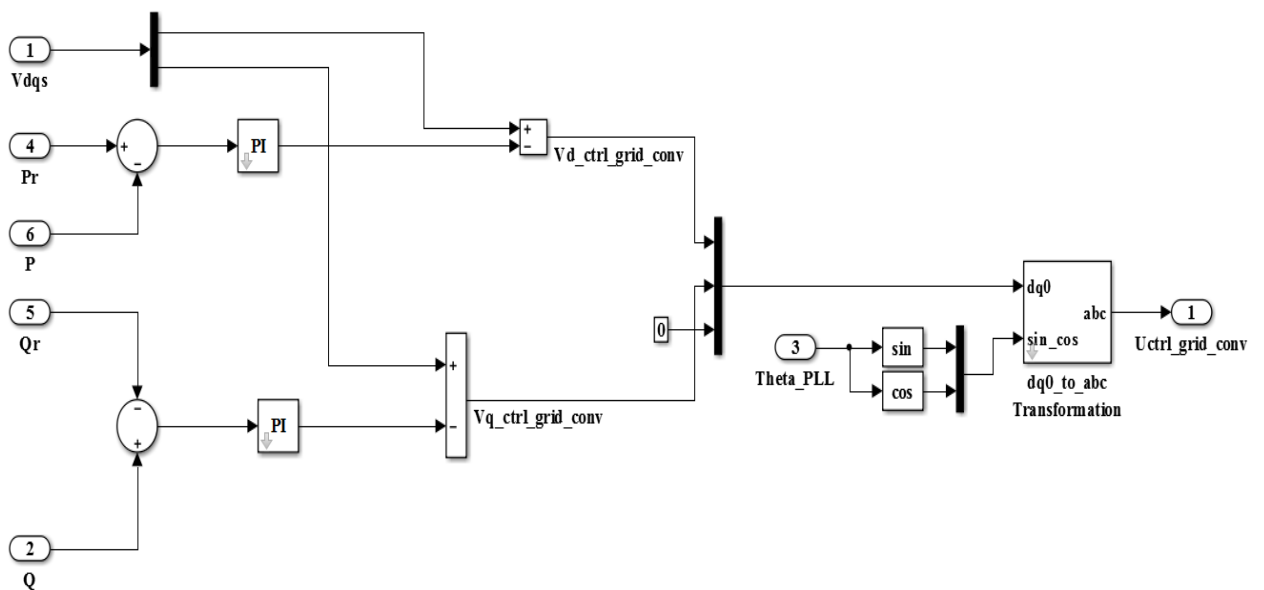
Fig 2.12: Scheme of DPC.

In Fig. 2.12, P is the measured active power and Pr is the reference active power, while Q is the measured reactive power and Qr is the reference reactive power.

The DPC will be discussed in section 2.5.

2.5   COMPARISON BETWEEN VDTC, VOC, AND DPC:

The disadvantages of the VDTC technique are as follows [8]:

a. The fast change of estimated values requires high sampling frequency.

b. Since the switching frequency is not constant, high inductance value is needed.

c. It is hard to design an input filter due to non-constant values of the switching frequency.

d. The line currents have higher Total Harmonic Distortion (THD), as shown in Fig. 2.14a.

e. Switching frequency harms the power quality. From Fig. 2.13,

$$I_L = \frac{V_{CONV}}{J\omega L} = \frac{V_{CONV}}{J\,2\,\pi\,f_{sw}L} \qquad (2.14)$$

It is preferable to obtain high f_{sw}; however, f_{sw} may cause losses in power devices. It is well known that any device losses are switching losses and conduction losses.
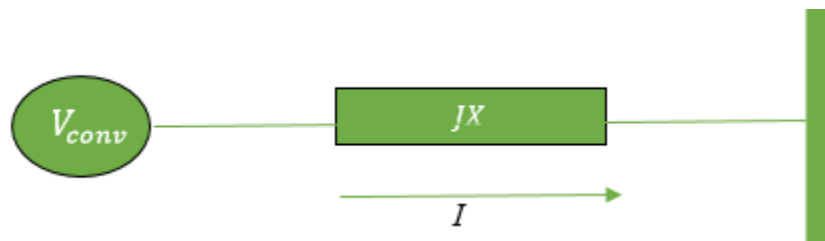
Fig. 2.13: Smart grid simple configuration.

One the other hand, the following are characteristics of the VOC [8]:

      a. Lower sampling frequency.

      b. The line currents have lower THD, as seen in Fig. 2.14b.

      c. It is observed that VOC has a better dynamic to decoupled active and reactive power control.

      d. High dynamic and static performance through an internal current control loop.

      e. It is observed that the DTC has high switching ripples, with a THD of 10.46% as compared to a THD of 7.71% in the case of the VOC. See Fig. 2.15.

The parameters of the simulations are shown in table 2.3:

Parameters	VDTC	VOC	DPC
Sampling Time	Ts=10 μ sec	Ts=100 μ sec	Ts=100 μ sec
Three-Phase Voltages	Vll=480 V	Vll=480 V	Vll=480 V
Frequency	F =60 Hz;	F =60 Hz;	F =60 Hz;
Voltage Direct Current	$Vdc=Vll*\sqrt{2}$ = (V)	$Vdc=Vll*\sqrt{2}$ = (V)	$Vdc=Vll*\sqrt{2}$ = (V)
AC Current	I =300 (A)	I =300 (A)	I =300 (A)
Power	P =Vll*I = (W)	P =Vll*I = (W)	P=Vll*I = (W)
Inductance	L=400 μ H	L=400 μ H	L=400 μ H
Switching Frequency	fs = 4 k Hz	fs = 4 k Hz	fs = 4 k Hz

Table 2.3: Simulations parameters.
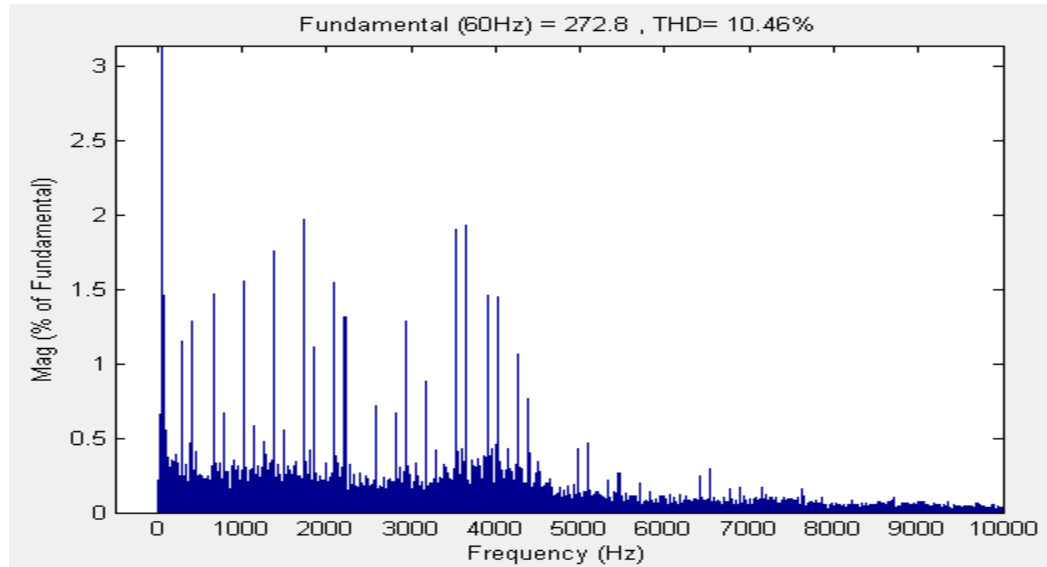
Fig. 2.14a: Fast Fourier Transform (FTT) for currents in: a) VDTC
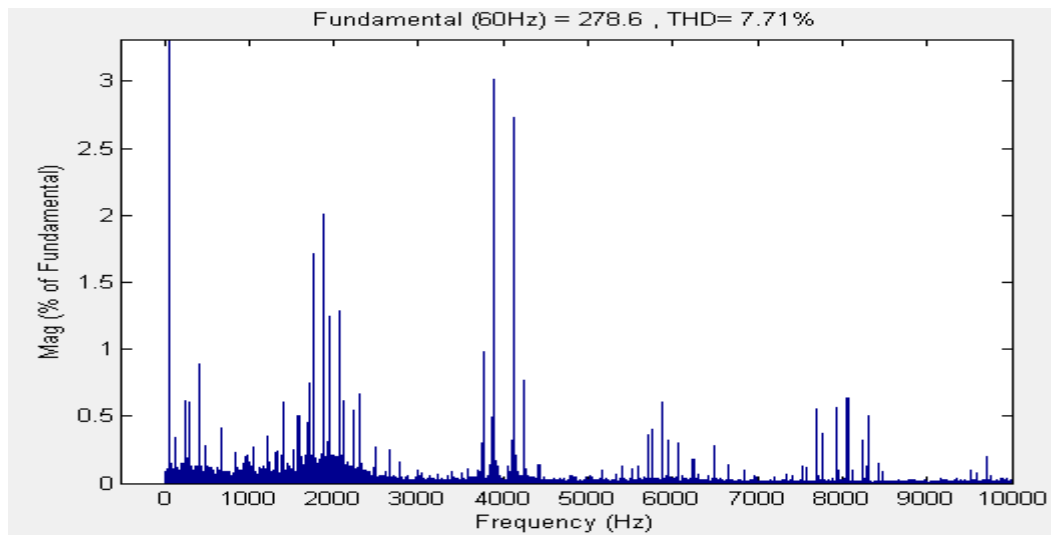
Fig. 2.14b: Fast Fourier Transform (FTT) for currents in: b) VOC.
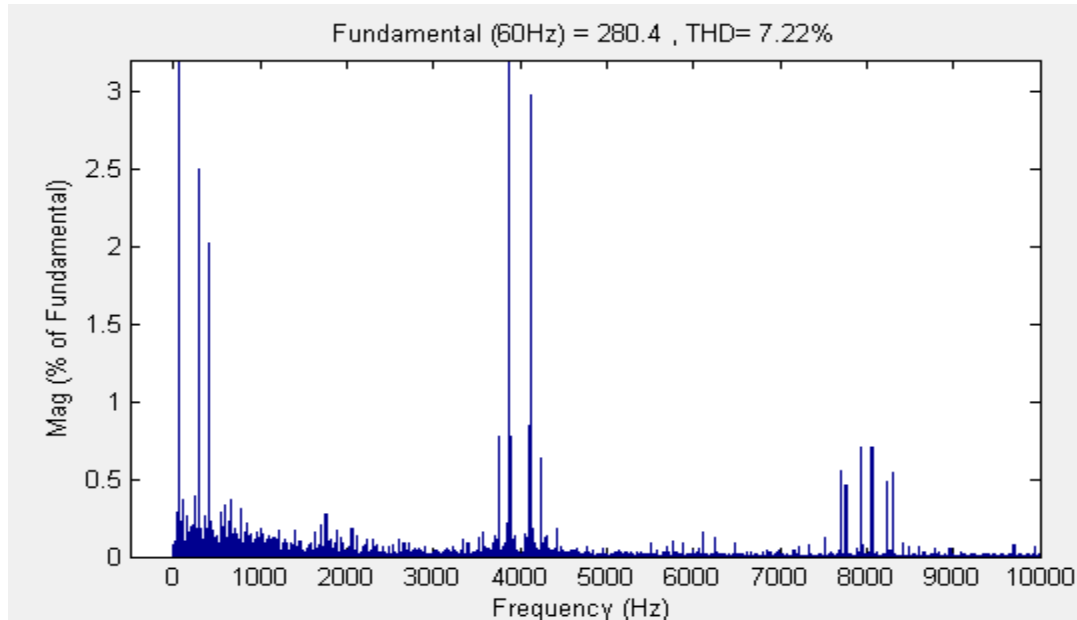
Fig. 2.14c: Fast Fourier Transform (FTT) for currents in c) DPC.

The advantage of VDTC [8]:

    a. It has faster response since the internal current control loop and PWM modulator block do not exist.

    b. The switching state and the switching table determine the commanded and estimated values of active and reactive power based on the instantaneous errors.

    c. PI controllers and coordinate transformation are not required.

    d. Easy calculation for active and reactive power.

The disadvantage of VOC [8]:

    a. The decoupling between active and reactive components with coordinate
transformation is required.

    b. Complex and intensive algorithm.

- **DPC vs. VOC:**

    VOC and DPC are both based on the transformation between a natural frame *abc*

and synchronous reference frame *dq.* This strategy promises fast transient response with

high dynamic performance. Even though this performance depends on the quality of the

inner current control loop, DPC can provide faster transient response without inner

current loop as shown in Fig. 2.15 and Fig. 2.16. The observation is that the response is

faster without an inner current loop. In addition, VOC and DPC provide some advantages

compared to VDTC. First, low sampling frequency for better performance; and second,

fixed switching frequency leads to easier design of input filter. On the other hand, both

VOC and DPC share the same previously mentioned disadvantage about VOC.
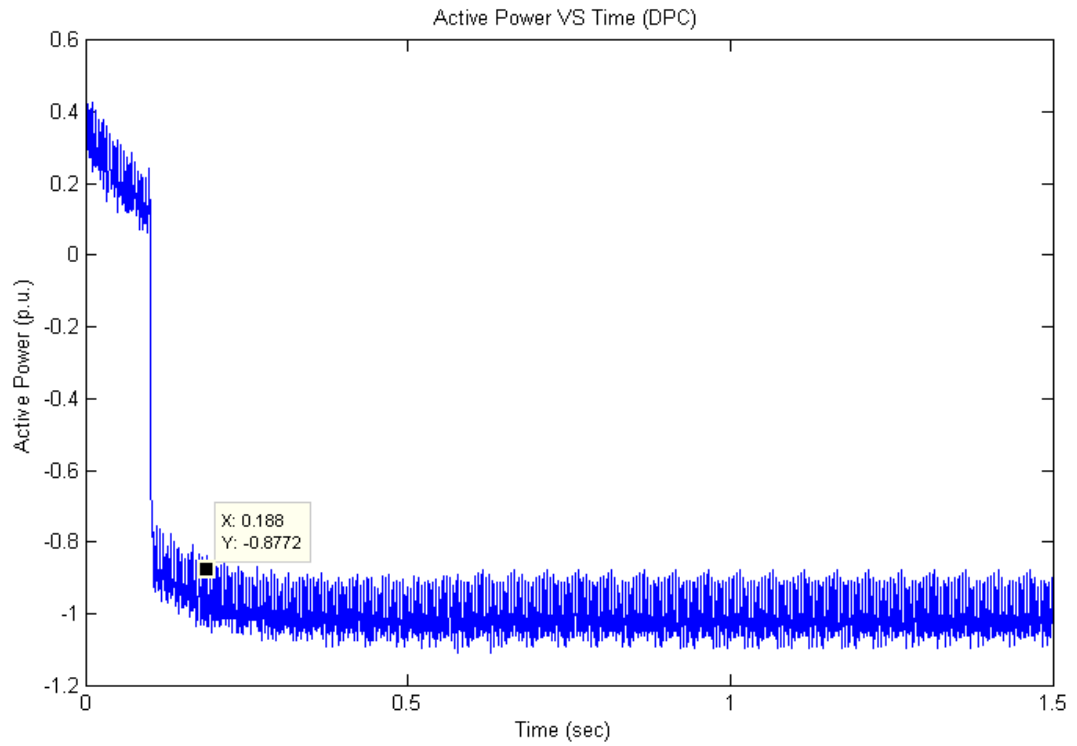
a)
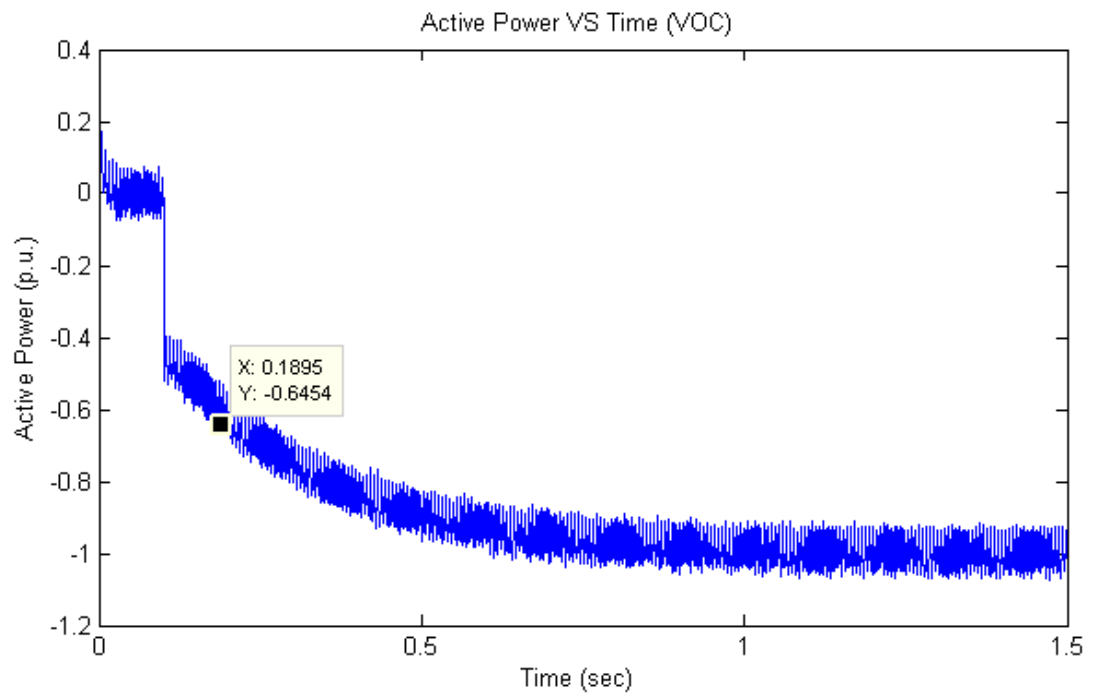
b)

Fig. 2.15 Active power for a) DPC and b) VOC.
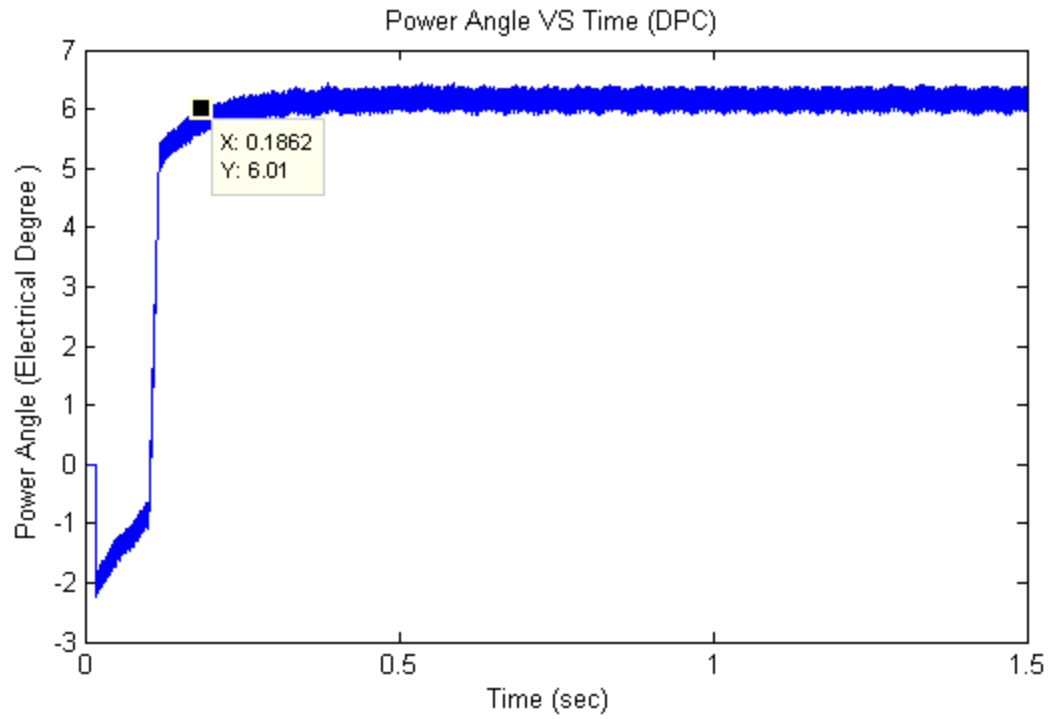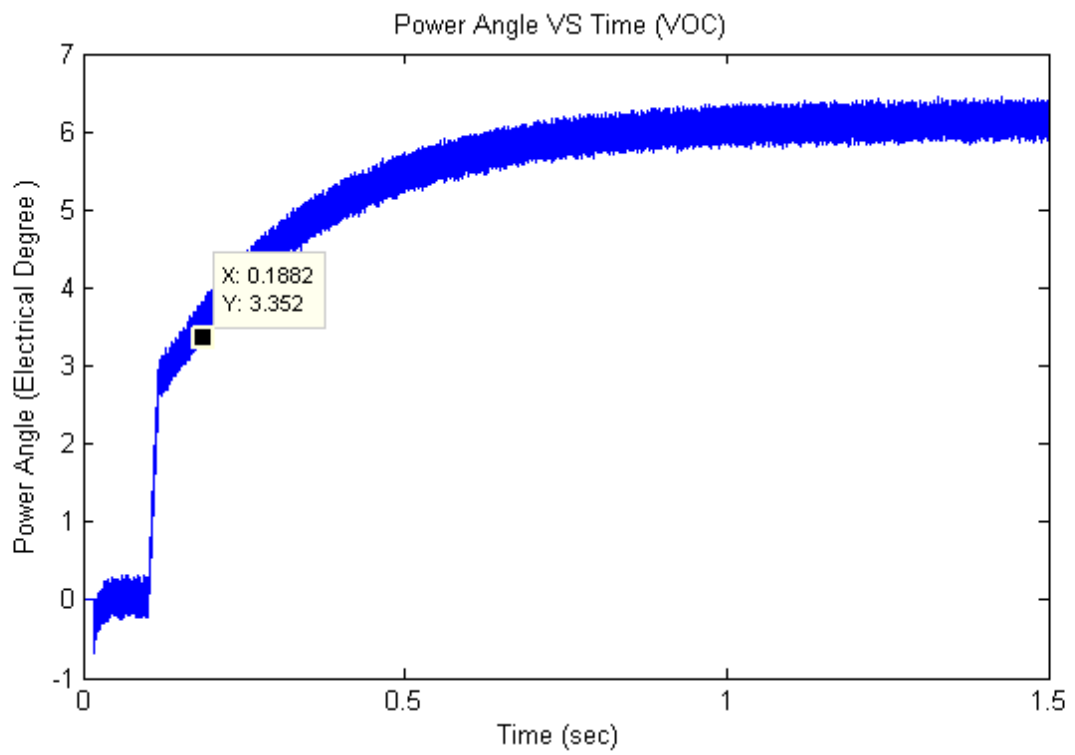
Fig. 2.16: Power angle: a) DPC and b) VOC.

2.6 SUMMARY OF THE COMPARISON BETWEEN VDTC, VOC AND DPC:

TECHNIQUE	ADVANTAGES	DISADVANTAGES
VDTC	• No PWM block required • No inner current loop • No coordinate transformation • Decent dynamics • Simple algorithm • Decoupled active and reactive power control	• High inductance and sample frequency needed • Power and voltage estimation should be avoided at the moment of switching • Variable switching frequency
VOC	• Fixed switching frequency. leads easier design input filter • Advanced PWM strategies can be used • Better quality and performance • Control of power factor angle • Low THD line currents distortion	• Coordinating transformation and decoupling between active and reactive components is required • Complex algorithm
DPC	• Simple and noise-resistant power estimation • Low THD of line currents with distortion • No current regulation loop • Good dynamics	• Coordinating transformation and decoupling between active and reactive components is required • Lower power quality than VOC

Table 2.4: Comparison summary of VTPC, VOC, and DPC [8].

After the main control structures for a grid power converter are investigated, the VOC appears to have the best power quality among other techniques, as shown in Figs. 2.17, 2.18, and 2.19 Therefore, the remainder of this thesis will investigate the VOC in more detail with various applications.
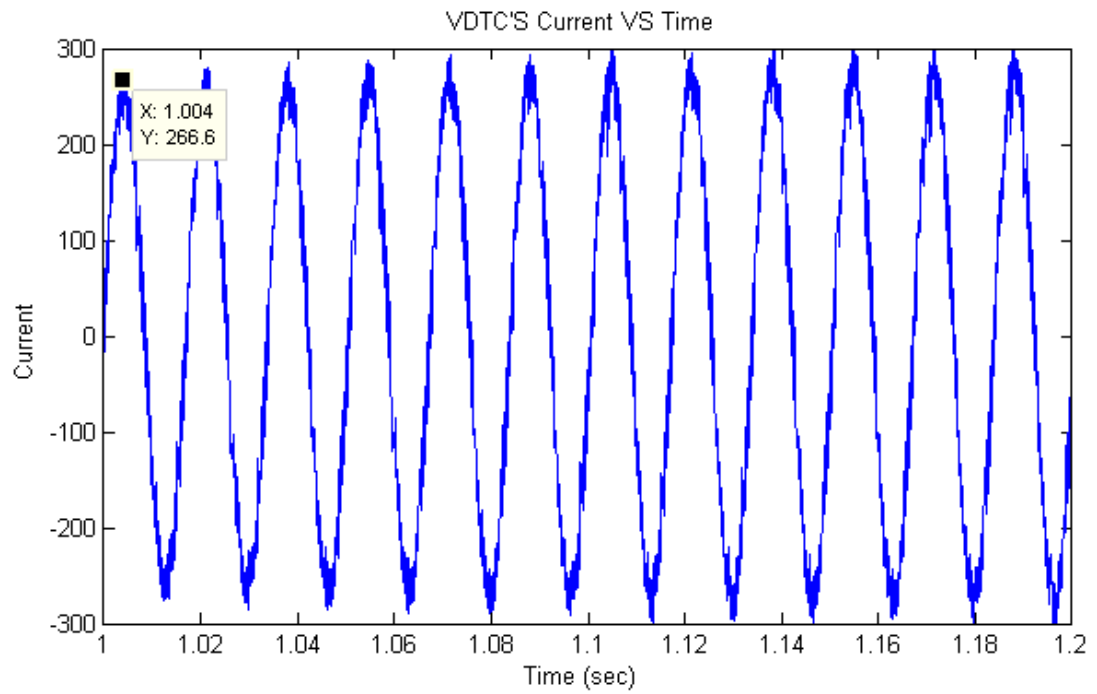
a)
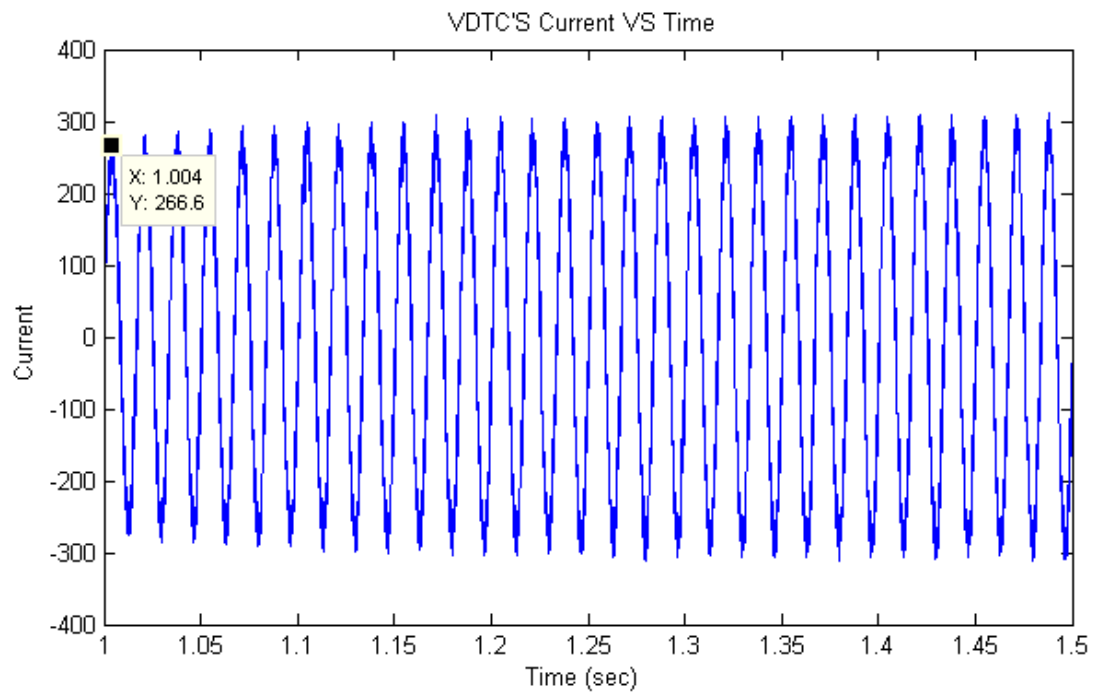
b)

Fig. 2.17: VDTC's Current vs. Time: a) from 1s to 1.5s and b) 1s to 1.2s.
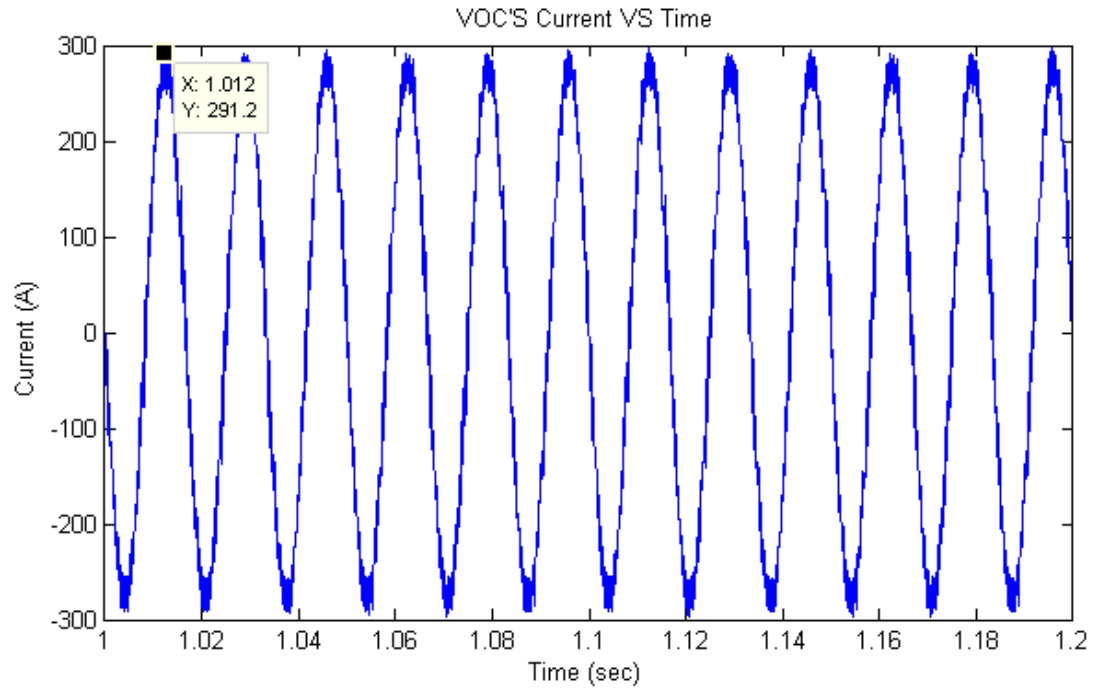
a)
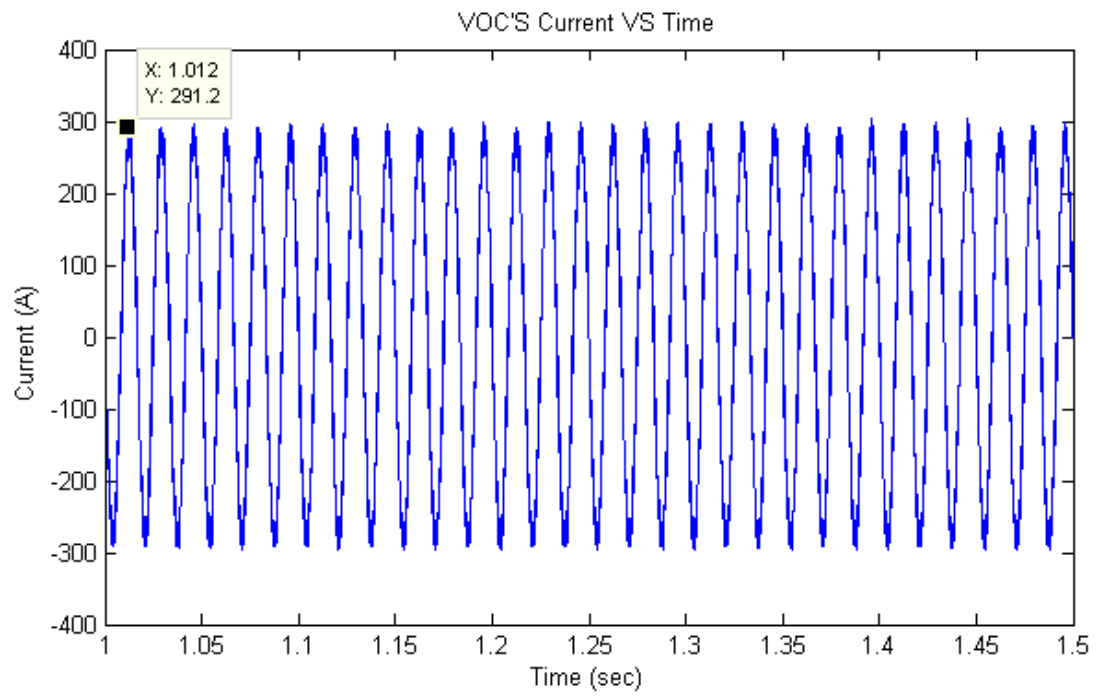
b)

Fig. 2.18: VOC's Current vs. Time: a) from 1s to 1.2s and b) 1s to 1.5s.
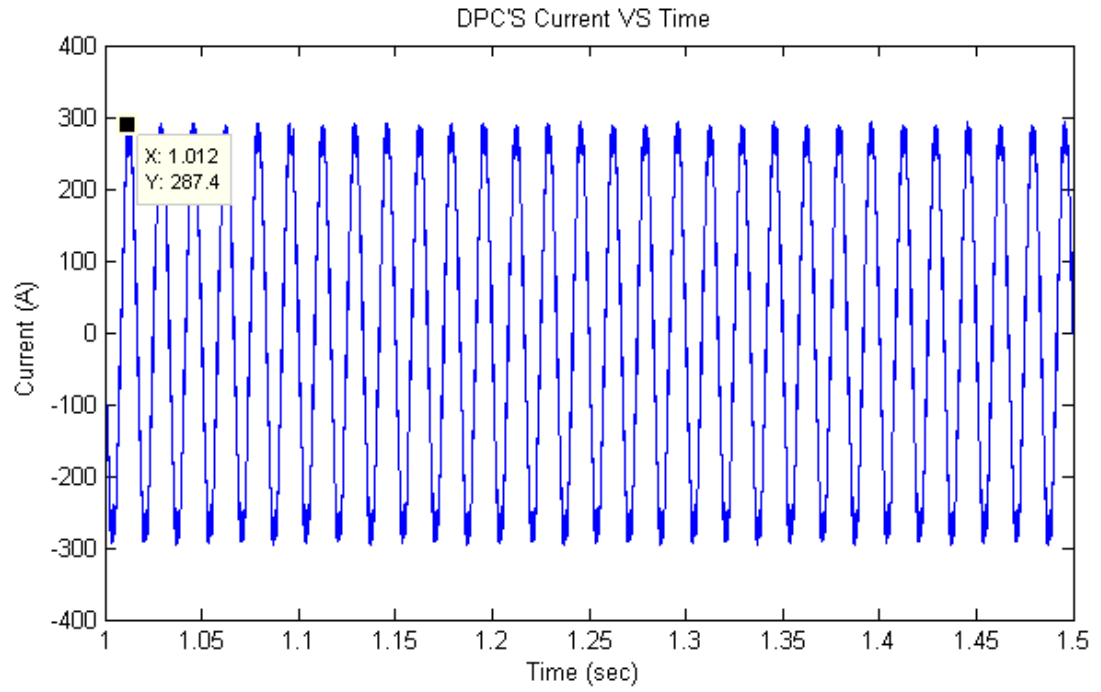
a)
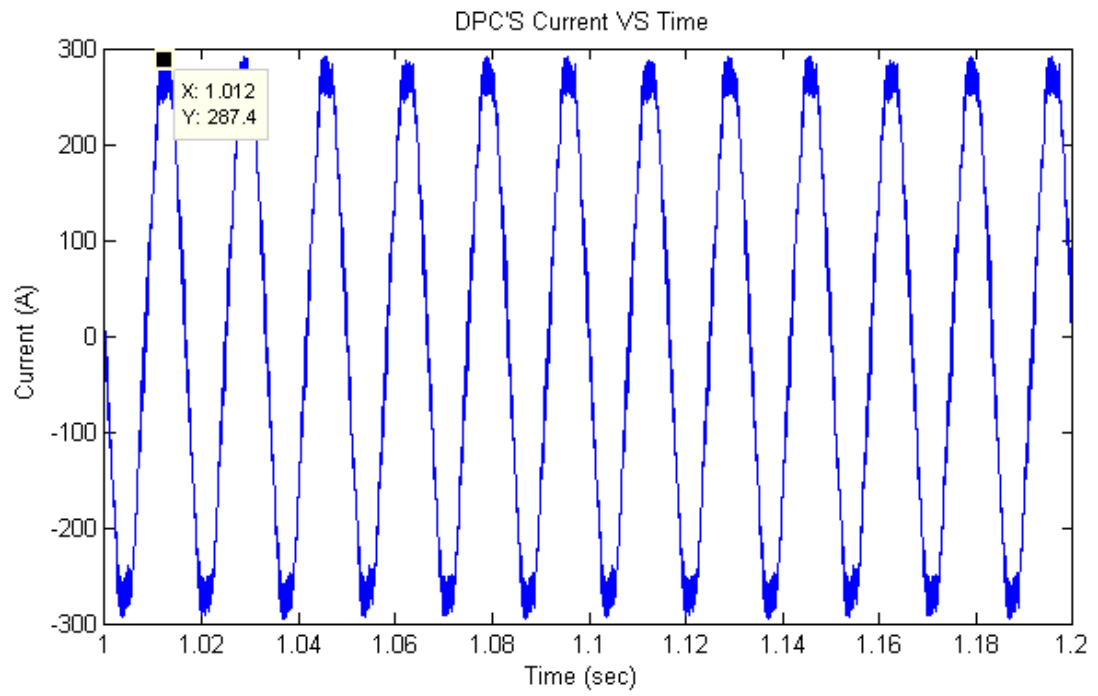
b)

Fig. 2.19: DPC's Currents vs. Time: a) from 1s to 1.5s and b) 1s to 1.2.

CHAPTER 3: GRID FILTER DESIGN

3.0   INTRODUCTION:

The need for a higher order filter that can be used to connect the grid converter to the utility will be discussed in this chapter. The design of the filter, the problems related to the variation of grid parameters, and the stability problems will also be investigated in this chapter. It is desirable to have the switching frequency as low as possible to limit switching losses. However, a large inductor will be required to reduce harmonics in the line currents [4]. The purpose of the AC chocks is to smooth the line current and act as energy storage elements.

A major disadvantage of using an LCL-filter is that it may result in resonance under certain operating conditions. Resonance occurs when a system is able to store and easily transfer energy between two or more different storage modes. Usually there are some losses from cycle to cycle due to the resistance of the inductors and capacitors. When the resistance is small, the resonant frequency is approximately equal to the natural frequency of the system, which is a frequency of unforced oscillations. Some systems have multiple, distinct, resonant frequencies [4].

Another important topic discussed in this chapter is the description of the power angle. The power angle is a well-known variable in classic power system analysis. The analysis in this chapter demonstrates how the power angle is indirectly controlled by the power converter.

3.1   TYPES OF FILTERS:

There are two types of filters typically used: L-filter and LCL-filter. The L-filter is a first-order filter that can be used by installing an inductor in each phase between the converter and the PCC. It is required to operate the converter with a high switching frequency to achieve sufficient attenuation of the harmonics if an L-filter is only used. An LCL-filter is obtained by connecting the capacitor in wye or delta on the line side of the L-filter. An additional inductor is connected on the line side of the capacitor. In order to tune the resonance frequency of the filter, the inductors on the lines of the capacitors are used. Reactive power is produced because capacitors are used in an LCL-filter [14]. The LCL filter provides a better attenuation of the switching ripple compared to an L-filter, as it is a third-order filter [15]. The LCL-filter increases the average efficiency of the converter mainly due to the reduced harmonic distortion. Furthermore, the THD decreases by using LCL-filters [17]. Consequently, this renders the LCL-filter the most appropriate selection in many applications.

3.2 DESIGN CONSIDERATIONS FOR AN LCL-FILTER:

The main factor in choosing LCL-filter parameters is related to power due to the displacement between the voltage and current caused by the reactive elements installed in the filter. Also, one must consider the equivalent impedance at the fundamental frequency since it is strictly dependent on the location of the voltage and current sensors, assuming that the voltage and current are in phase.

The LCL-filter design can be organized in three steps [12]:

1. Ripple analysis and converter-side inductor choice.

2. Harmonic attenuation of an LCL-filter and choice of the resonance frequency.

3. LCL-filters optimization and choice of grid-side inductor, capacitor, and damping method and value.

The LCL-filter is the point of connection between the converter and the grid. A lumped model parameter of the LCL-filter consists of resistor R_{cov} and inductor L_{cov} representing the equivalent circuit of the converter side inductor. On the other side is the resistor R_{grid} and inductor L_{grid} representing the equivalent circuit of the grid side inductor. Also, a capacitor C in series with damping resistor R_c is used, as shown in Fig. 3.1.
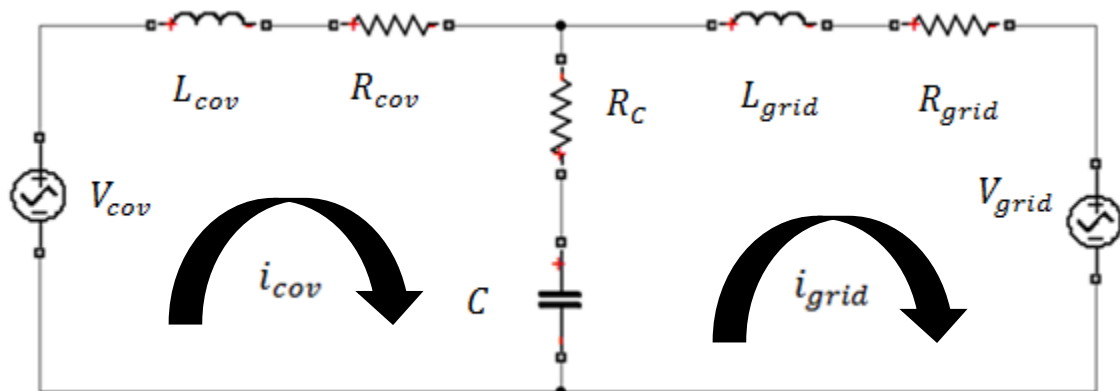
Fig. 3.1: LCL-filter.

In summary, the reasons for using the LCL-filter are [12], [13], and [14]:

a. Separating the energy between the converter and the grid.

b. To filter out current harmonics resulting from switching action of the power converter.

c. The LCL-filter has a relatively high attenuation, therefore, the converter switching frequency can be reduced, which improves the system efficiency.

The state space model of the LCL-filter in an *abc* stationary reference frame is shown below. Refer to APPENDIX B for derivation details.

$$\frac{d}{dt}\begin{bmatrix} i_{cova} \\ i_{covb} \\ i_{covc} \\ i_{grida} \\ i_{gridb} \\ i_{gridc} \\ v_{ca} \\ v_{cb} \\ v_{cc} \end{bmatrix} = \begin{bmatrix} \frac{-R_{cov}-R_c}{L_{cov}} & 0 & 0 & \frac{R_c}{L_{cov}} & 0 & 0 & \frac{-1}{L_{cov}} & 0 & 0 \\ 0 & \frac{-R_{cov}-R_c}{L_{cov}} & 0 & 0 & \frac{R_c}{L_{cov}} & 0 & 0 & \frac{-1}{L_{cov}} & 0 \\ 0 & 0 & \frac{-R_{cov}-R_c}{L_{cov}} & 0 & 0 & \frac{R_c}{L_{cov}} & 0 & 0 & \frac{-1}{L_{cov}} \\ \frac{R_c}{L_{grid}} & 0 & 0 & \frac{-R_c-R_{grid}}{L_{grid}} & 0 & 0 & \frac{1}{L_{grid}} & 0 & 0 \\ 0 & \frac{R_c}{L_{grid}} & 0 & 0 & \frac{-R_c-R_{grid}}{L_{grid}} & 0 & 0 & \frac{1}{L_{grid}} & 0 \\ 0 & 0 & \frac{R_c}{L_{grid}} & 0 & 0 & \frac{-R_c-R_{grid}}{L_{grid}} & 0 & 0 & \frac{1}{L_{grid}} \\ \frac{1}{C} & 0 & 0 & \frac{-1}{C} & 0 & 0 & 0 & 0 & 0 \\ 0 & \frac{1}{C} & 0 & 0 & \frac{-1}{C} & 0 & 0 & 0 & 0 \\ 0 & 0 & \frac{1}{C} & 0 & 0 & \frac{-1}{C} & 0 & 0 & 0 \end{bmatrix}$$

$$\begin{bmatrix} i_{cova} \\ i_{covb} \\ i_{covc} \\ i_{grida} \\ i_{gridb} \\ i_{gridc} \\ v_{ca} \\ v_{cb} \\ v_{cc} \end{bmatrix} + \begin{bmatrix} \frac{1}{L_{cov}} & 0 & 0 & 0 & 0 & 0 & 0 & 0 & 0 \\ 0 & \frac{1}{L_{cov}} & 0 & 0 & 0 & 0 & 0 & 0 & 0 \\ 0 & 0 & \frac{1}{L_{cov}} & 0 & 0 & 0 & 0 & 0 & 0 \\ 0 & 0 & 0 & \frac{-1}{L_{grid}} & 0 & 0 & 0 & 0 & 0 \\ 0 & 0 & 0 & 0 & \frac{-1}{L_{grid}} & 0 & 0 & 0 & 0 \\ 0 & 0 & 0 & 0 & 0 & \frac{-1}{L_{grid}} & 0 & 0 & 0 \\ 0 & 0 & 0 & 0 & 0 & 0 & 0 & 0 & 0 \\ 0 & 0 & 0 & 0 & 0 & 0 & 0 & 0 & 0 \\ 0 & 0 & 0 & 0 & 0 & 0 & 0 & 0 & 0 \end{bmatrix} \begin{bmatrix} v_{cova} \\ v_{covb} \\ v_{covc} \\ v_{gridb} \\ v_{gridc} \\ v_{grida} \\ 0 \\ 0 \\ 0 \end{bmatrix} \qquad (3.1)$$

V_{cov} is the converter output voltage.

V_{grid} is the grid output voltage.

i_{cov} is the converter current.

i_{grid} is the grid current.

v_c is the capacitor voltage.

Where V_{cov} and V_{grid} are the inputs of the three-phase system for phase a, phase

b, and phase c respectively, while i_{cov}, i_{grid} and v_c are the three states of the three-

phase system for phase a, phase b, and phase c respectively, as shown in Fig. 3.1.

Then, the following transfer function can be written as follows:

$$H(s) = \frac{I(s)_{cov}}{v(s)_{cov}} = \frac{L_{grid} \, C \, s^2 + R_C \, C \, s + 1}{L_{cov} \, L_{grid} \, s^3 + R_C \, C \, (L_{cov} \, L_{grid}) s^2 + (L_{cov} \, L_{grid}) s} \quad (3.2)$$

The following design elements play a critical role in LCL-filter performance [15].

The total inductance value has to be lower than 10% to limit the DC-link voltage. The

value of the capacitor is limited by decreasing the power factor at rated power (less than

5%) [13]. The resonance frequency has to be included in a range between 10 times the

line frequency and one-half of the switching frequency to prevent resonance problems in

the lower and higher parts of the harmonic spectrum. The passive resistor has to be

chosen as a compromise between the necessary damping and losses in the system. The

values used for filter parameters are shown in Table 3.1:

Parameters	Actual Values	p.u. Values
R_C	$100 \, m \, \Omega$	0.072
C	$100 \mu \, F$	0.02720j
L_{cov}	$100 \, \mu H$	0.027
L_{grid}	$300 \, \mu H$	0.081
R_{grid}	$0 \, \Omega$	0
R_{cov}	$0 \, \Omega$	0

Table 3.1: LCL-filter parameters.

Where: R_C is the damping series resistor.

C is the grid capacitor.

L_{cov} is the converter inductor.

L_{grid} is the grid inductor.

R_{grid} and R_{cov} are the resistors of the grid side and of the converter side respectively.

In order to obtain frequency response and the pole location of the LCL-filter, the bode diagram and pole map of the LCL-filter are shown in Fig. 3.2 and Fig. 3.3.
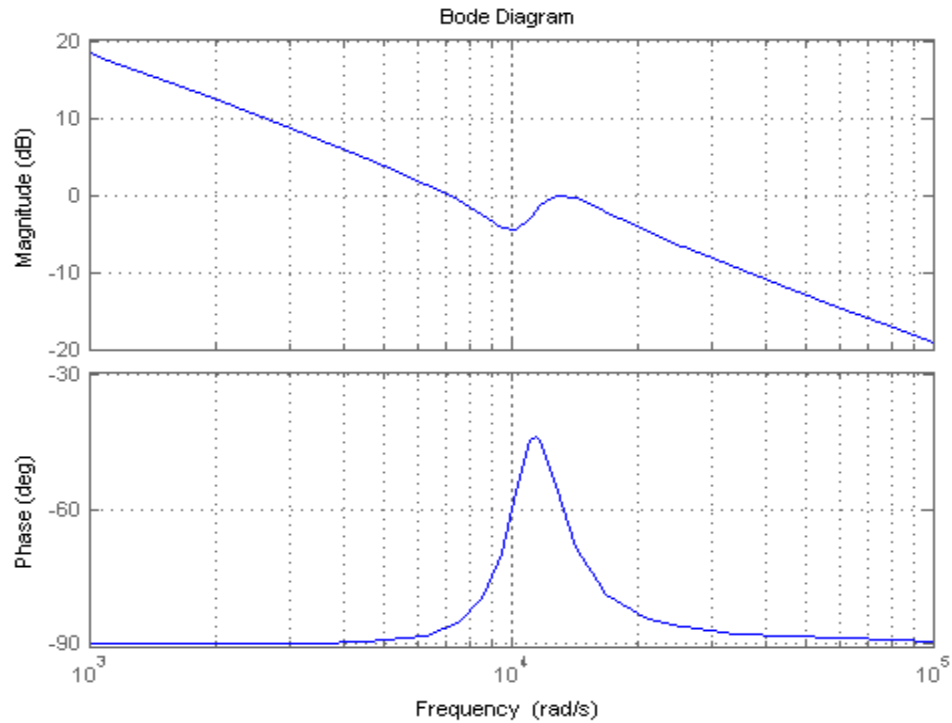
Fig. 3.2: Bode plot for LCL-filter with damping resistor.
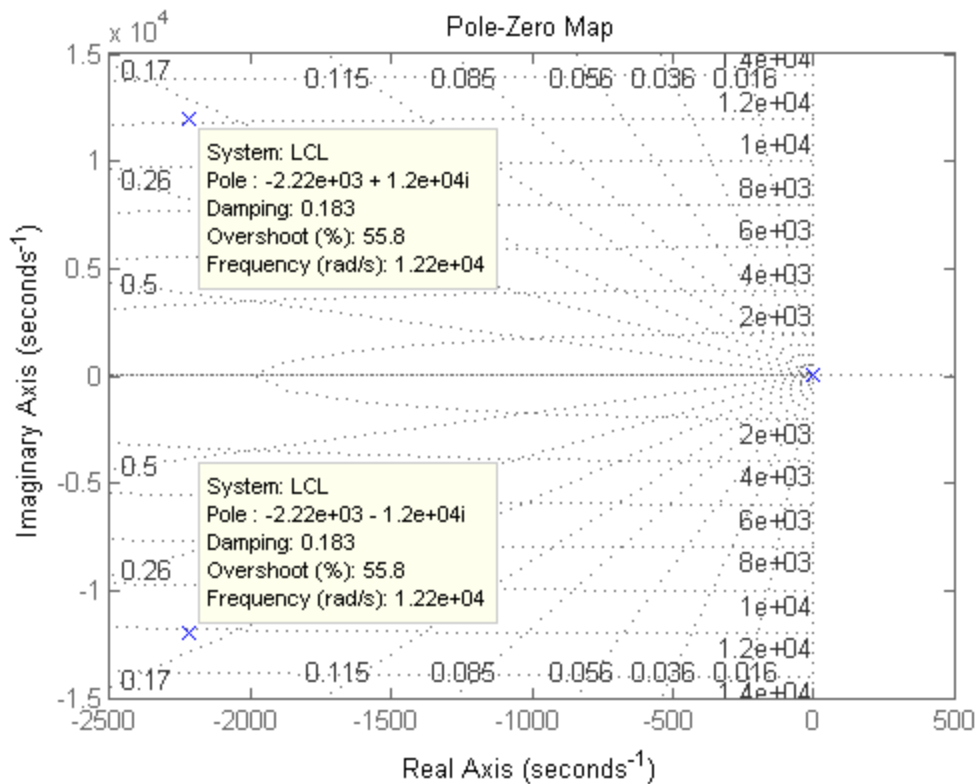
Fig. 3.3: Pole map for LCL-filter with damping resistor.

From Fig. 3.2, the LCL-filter has three poles. Now let us consider the damping resistor R_c is zero. The following transfer function can be written:

$$H(s) = \frac{I(s)_{cov}}{v(s)_{cov}} = \frac{L_{grid}\, C\, s^2 + 1}{L_{cov}\, L_{grid}\, s^3 + \left(L_{cov}\, L_{grid}\,\right)s} \quad (3.3)$$

In spite of the fact that the passive resistor (R_c) may result in an increase in system losses, it provides better damping for the system. When the passive resistance is zero, resonance may occur, as shown in Fig. 3.4. In addition, Fig 3.5 shows the Pole map for LCL-filter when $R_c = 0$. [27].
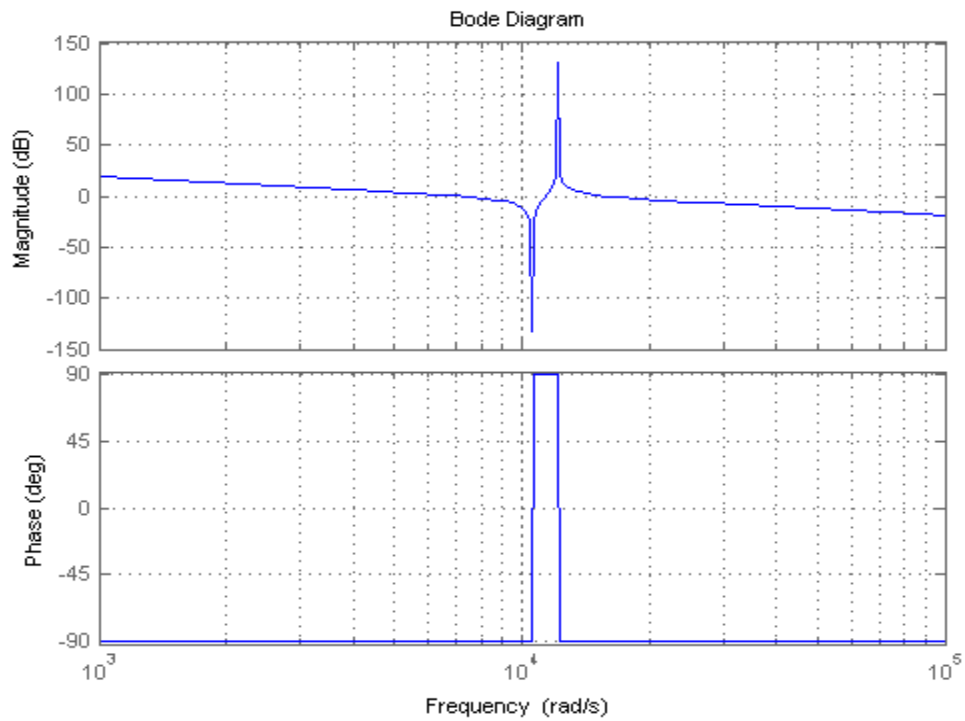
Fig. 3.4: Bode plot for LCL-filter when $R_c = 0$.
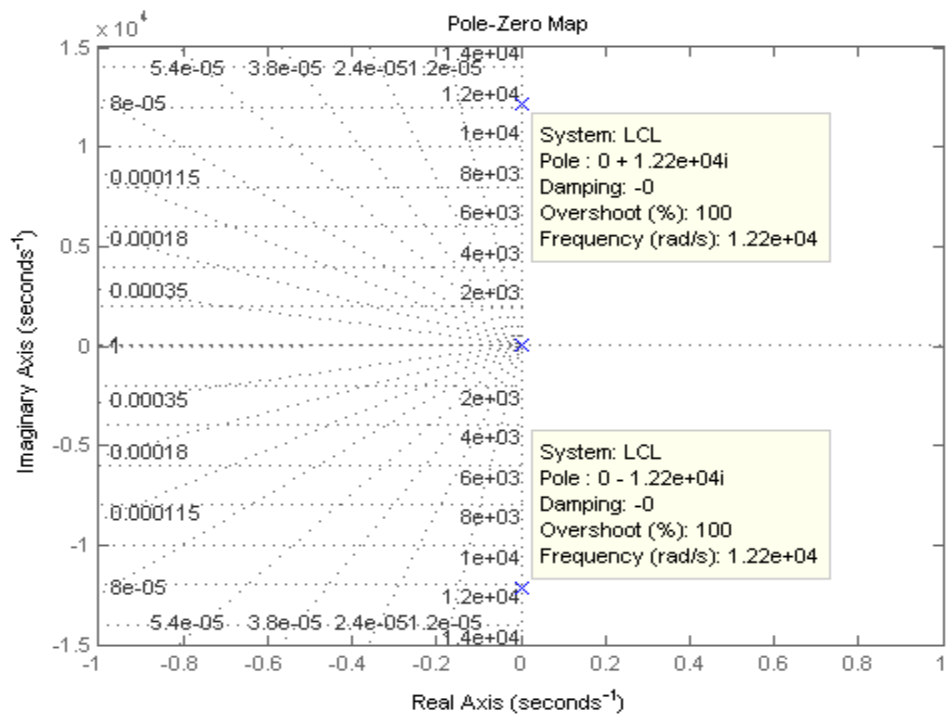
Fig. 3.5: Pole map for LCL-filter when $R_c = 0$.

3.3   POWER FLOW, AND POWER ANGLE ANALYSIS:

The primary advantage of a smart grid is the stability and quality of power delivered to the loads. Nowadays, modern DG systems provide higher controllability and operability to the grid [3]. Therefore, DG is a crucial issue for the development of modern control systems, but the majority of technical control matters are associated with voltage stability and power flow limitations. The case study discussed in this chapter consists of a power converter connected to the grid and three loads.
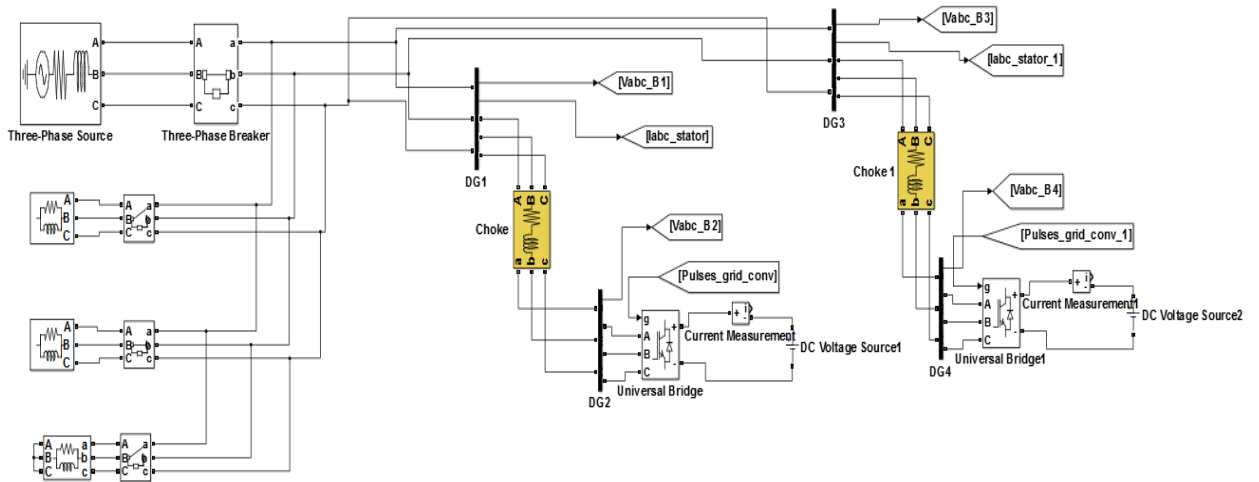
Fig. 3.6: A smart grid scheme with many sources and loads sharing.

Under steady state condition at a frequency *f*, the complex power *S*, the relative power *P* power angle expresses how effectively the real power *P* is transferred from one DG to the load.

Traditionally in power system applications, the power angle is used to analyze system performance. In this section, it will be shown that the power angle is indirectly affected when the reference power is changed. This is an attempt to link the standard

power system analysis and control of VOC power converters. To simplify this analysis,

an inductor-based filter is considered. The relation between the delivered power and the

power angle can be expressed as follows:

$$P_T = \frac{V_s V_R}{X} \sin \delta_{DGs} \qquad (3.4)$$

Where P_T is the power transferred to DG1 or DG3.

V_s is the grid voltage.

V_R is the converter output voltage.

δ is the power angle between $\overline{V_s}$ and $\overline{V_R}$.

Where the angle between DG1 and DG2 is $\delta_{1,2}$, and the angle between DG3 and DG4 is

$\delta_{3,4}$

To examine the stability of this system, three cases will be presented where the

reference powers are changed in every case, as follows:

First case: generate 0.5 p.u. reference power from DG1 and DG3. The simulation
results are shown in Fig. 3.8, Fig. 3.9, and Fig. 3.10.

Second case: generate 1 p.u. reference power from DG1 and generate 0.5 p.u.
reference power from DG3. The simulation results are shown in Fig. 3.11, Fig. 3.12, and
Fig. 3.13.

Third case: consume 1 p.u. reference power from DG1 and consume reference
power 0.5 p.u. from DG3. The simulation results are shown in Fig. 3.14, Fig. 3.15, and
Fig. 3.16.

All simulations and results of the system are based on parameters summarized in

Table 3.1.

Parameters	At First DG	At Third DG
Sampling Time	T_S=100 μ sec	T_S=100 μ sec
Three-Phase Voltages	V_{ll}=480 V	V_{ll}=480 V
Frequency	F =60 Hz;	F =60 Hz;
DC Voltage	$V_{dc} = V_{ll}\sqrt{2}$ = (V)	$V_{dc} = V_{ll}\sqrt{2}$ = (V)
AC Current	I =300 (A)	I =300 (A)
Power	$P = V_{ll}I$ = (W)	$P = V_{ll}I$ = (W)
Inductance	L=400 μ H	L=400 μ H

Table 3.2: Parameters of a smart grid in Fig. 3.3.

The results of the case study are shown in Table 3.3.

Case	DG	Power Reference (p.u.)	Active Power (p.u.)	Power Angle (E.dg.)	Reaching steady states (sec)	Current (A)	Figures
First	1	generate 0.5	-0.5	3.1	0.62	149.5	3.8a,3.9a,3.10a
	3	generate 0.5	-0.5	3.1	0.62	149.5	3.8b,3.9b,3.10b
Second	1	generate 1.0	-1	5.9	0.62	273	3.11a,3.12a,3.13a
	3	generate 0.5	-0.5	3.1	0.62	149.5	3.11b,3.12b,3.13b
Third	1	consume 1.0	1	-5.9	0.62	283	3.14a,3.15a,3.16a
	3	consume 0.5	0.5	-3.1	0.62	147	3.14b,3.15b,3.16b

Table 3.3: Simulations results for the case study.

The observation from Table 3.3 is that there is a relation between reference powers, active powers, power angles, and currents. From the first case, when the power reference generates 1 p.u. at DG1, the power angle $\delta_{1,2}$ responds to this change after the active power changed. Moreover, from the third case, when the power reference consumes 0.5 p.u. at DG3, the power angle $\delta_{3,4,}$ reacts to this change after the active

power changed; as is likewise in all other cases. It is important to note that all three cases reached the steady state within 0.62 sec.

The control of the DGs of the power system can be achieved by changing the values of the power references. This leads to a change in the performance of a smart grid as explained earlier in the case study. This is the new way of using the DGs to make the utilities have the basic control over their local grid. This relation in the smart grid is summarized in Fig. 3.7.
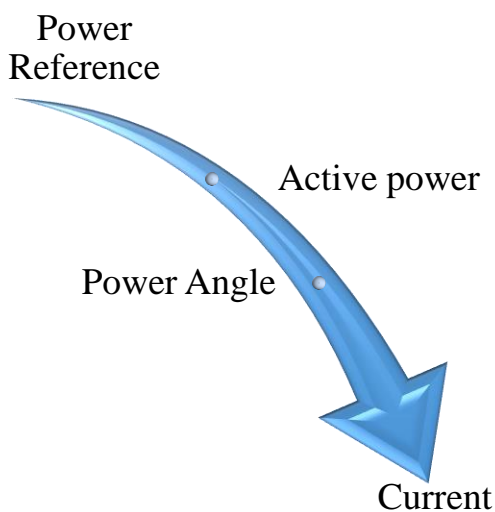
Fig. 3.7: Reference power relations.

The change in the power reference leads to a change in the delivered active power. Consequently, the power angle and the currents also changed.
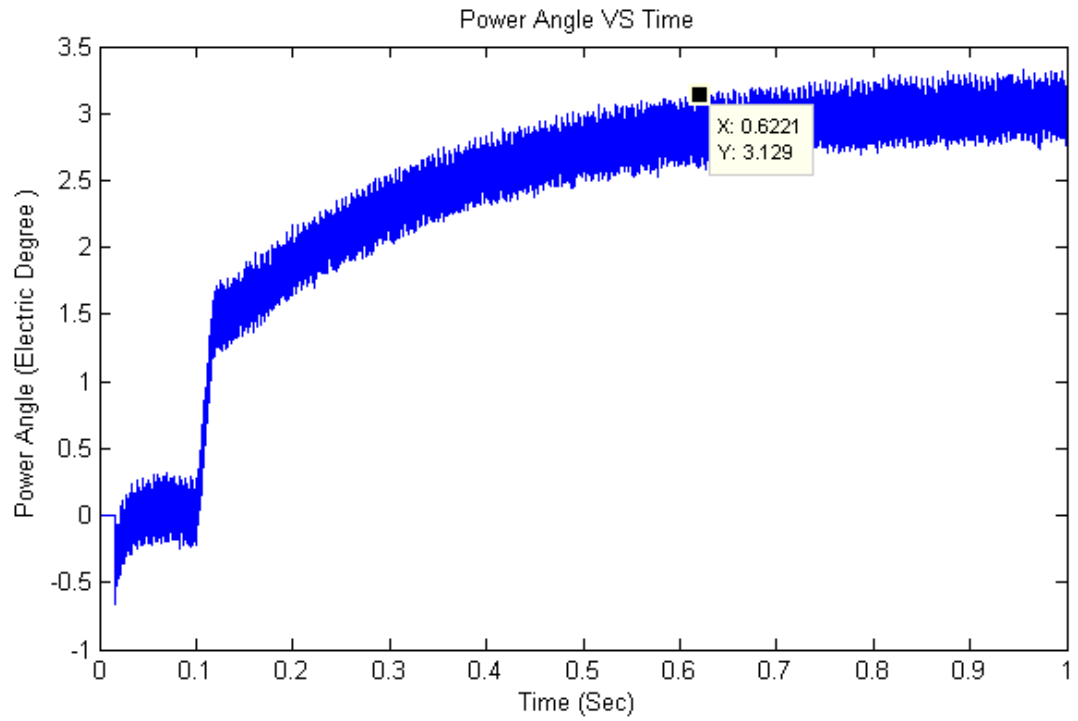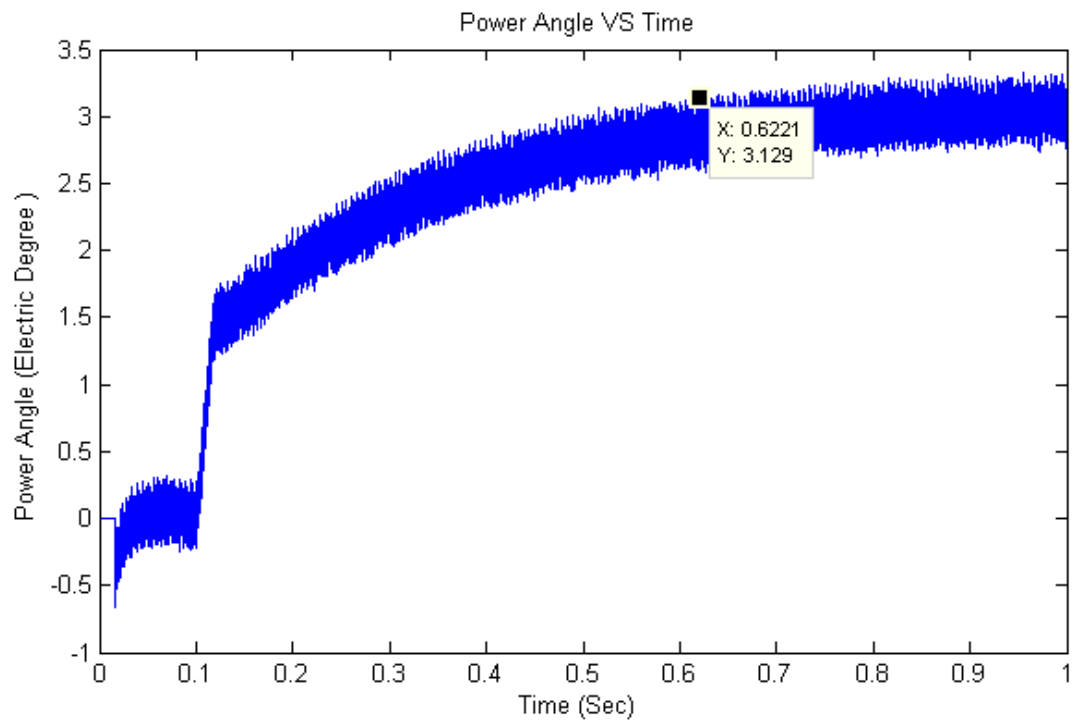
Fig. 3.8: Power Angle at a) DG1 and b) DG3.
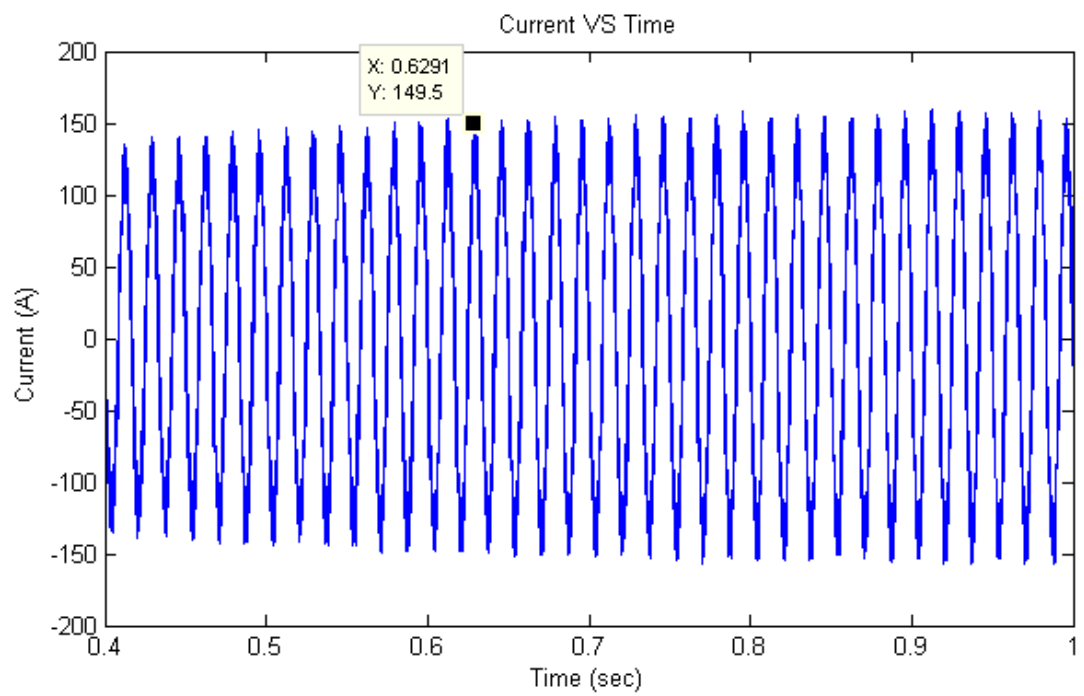
a)
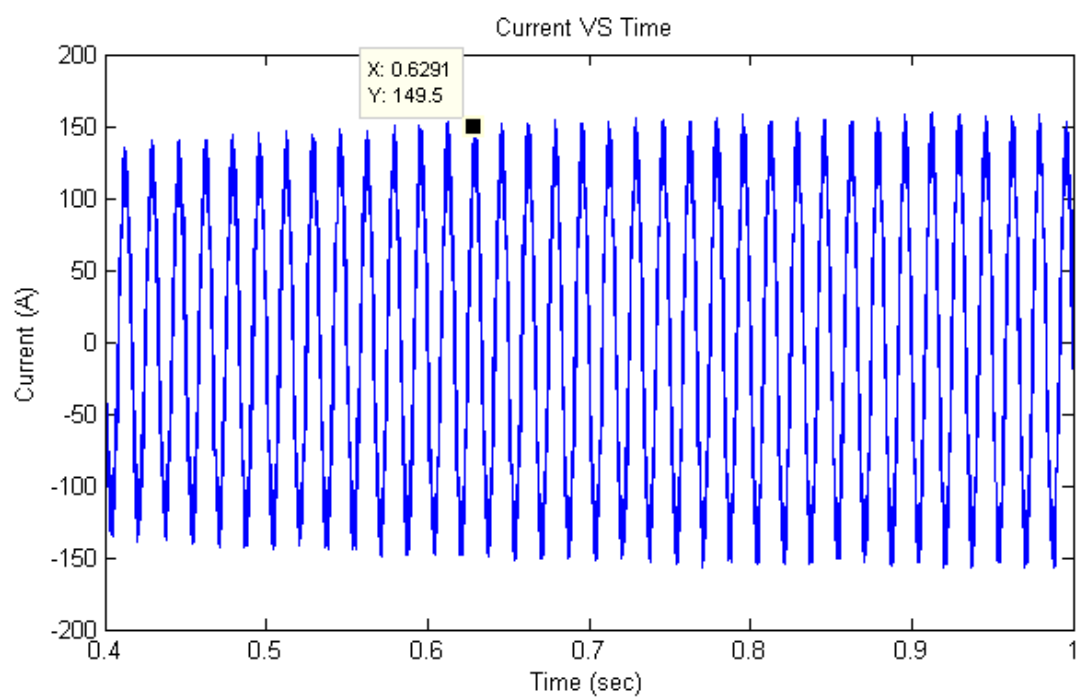
a)

Fig. 3.9: Currents at a) DG1 and b) DG3.
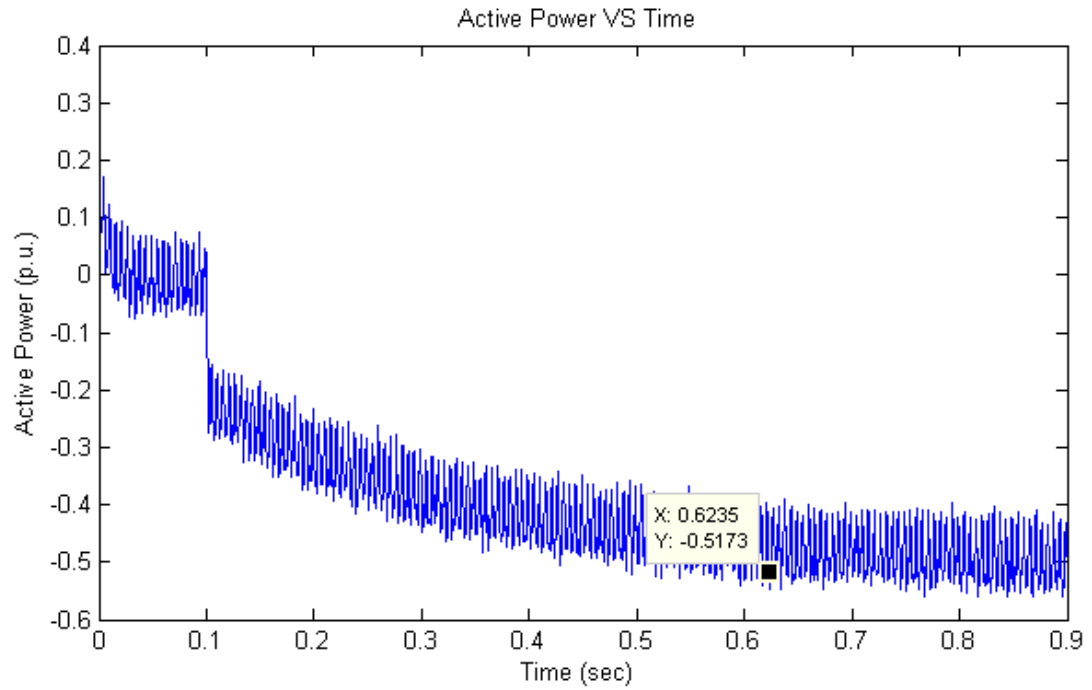
a)
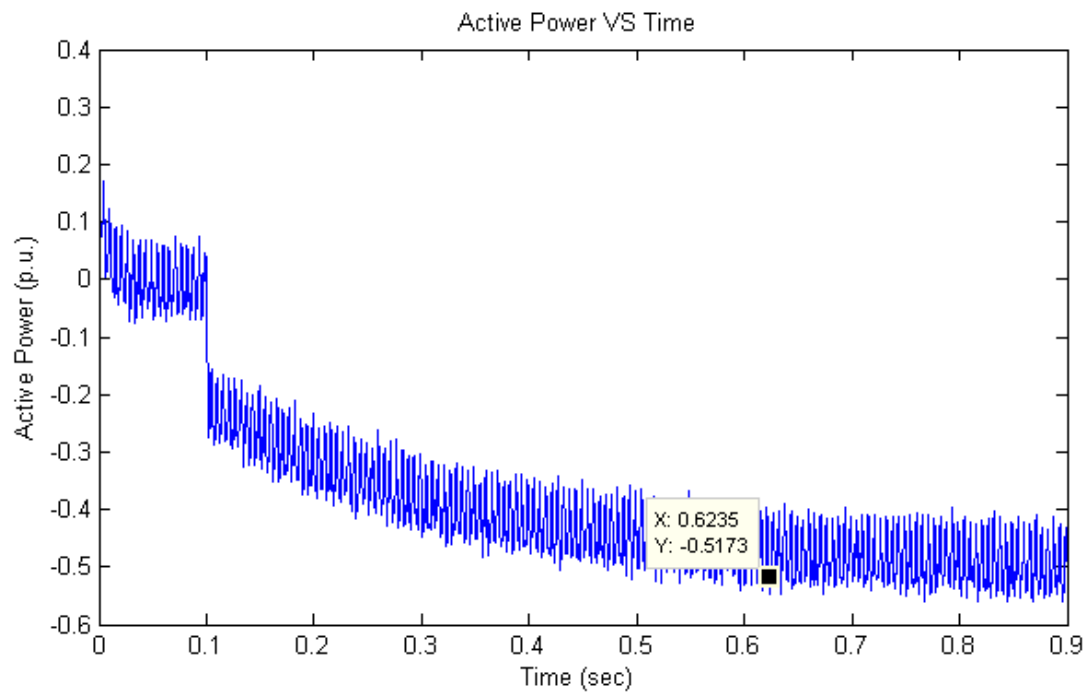
b)

Fig. 3.10: Active Power at a) DG1 and b) DG3.
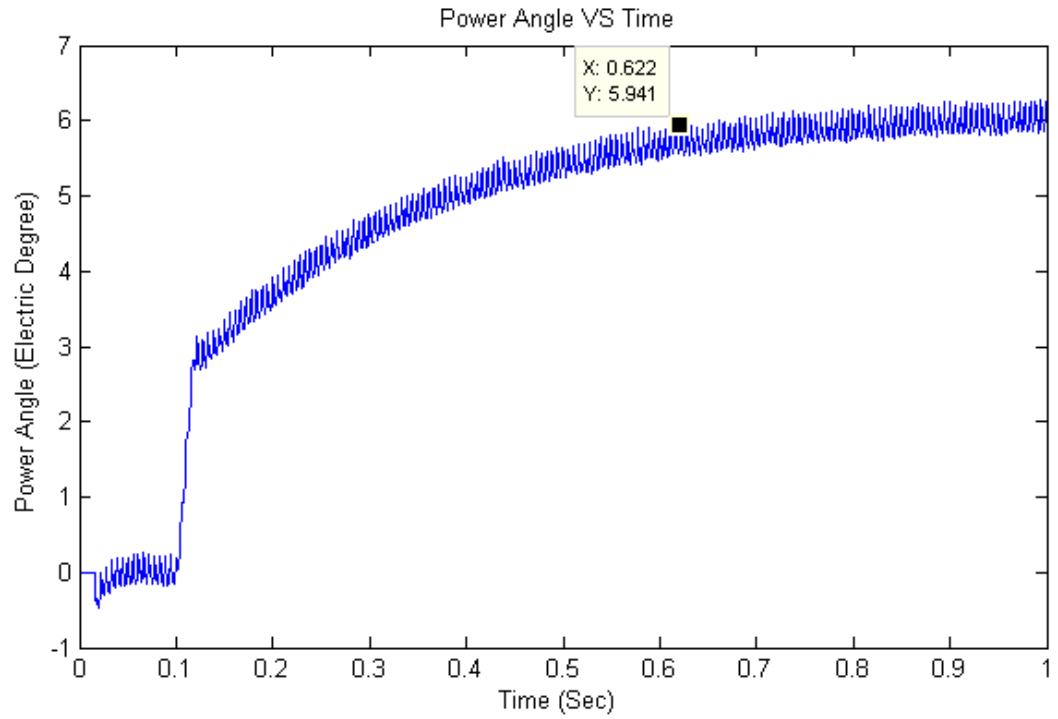
a)
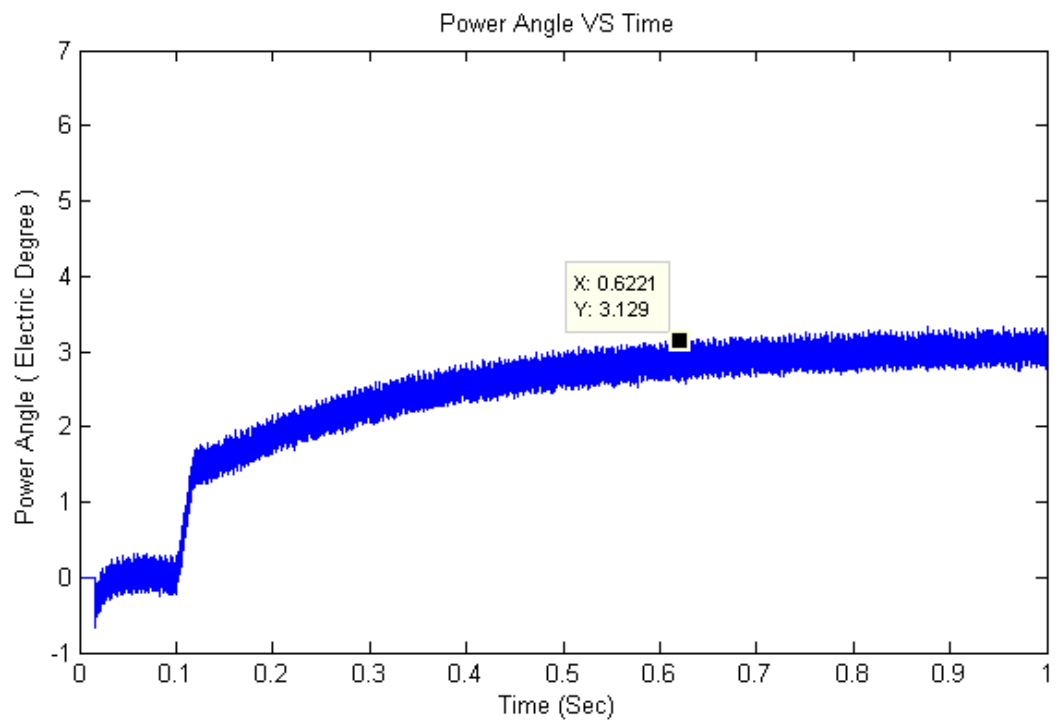
b)

Fig. 3.11: Power Angle at a) DG1 and b) DG3.
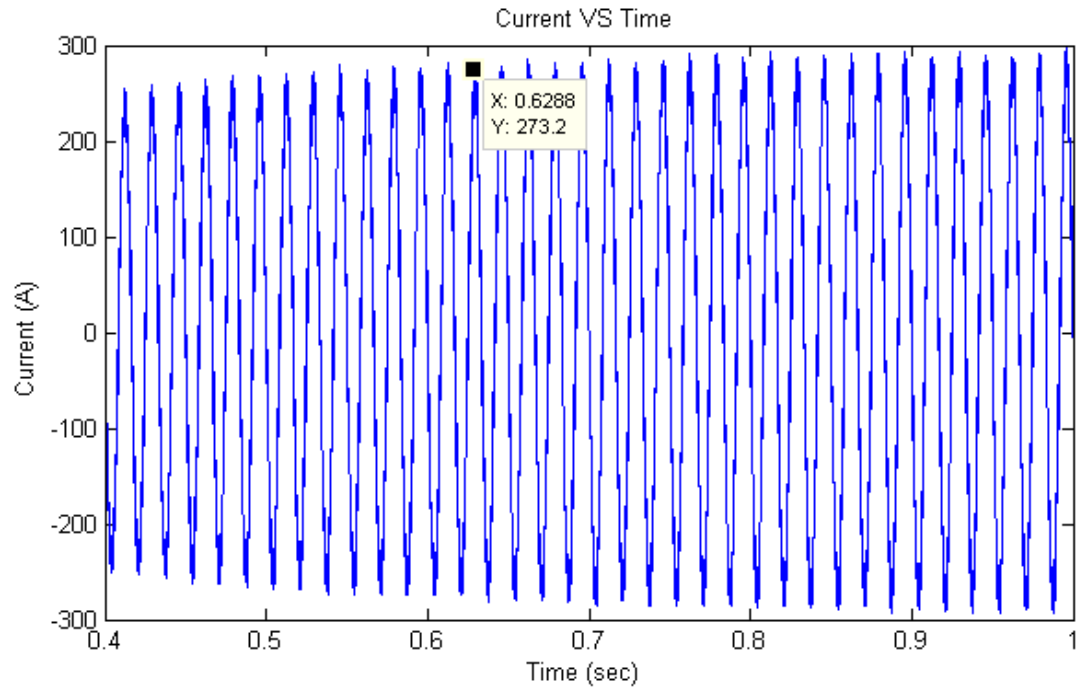
a)
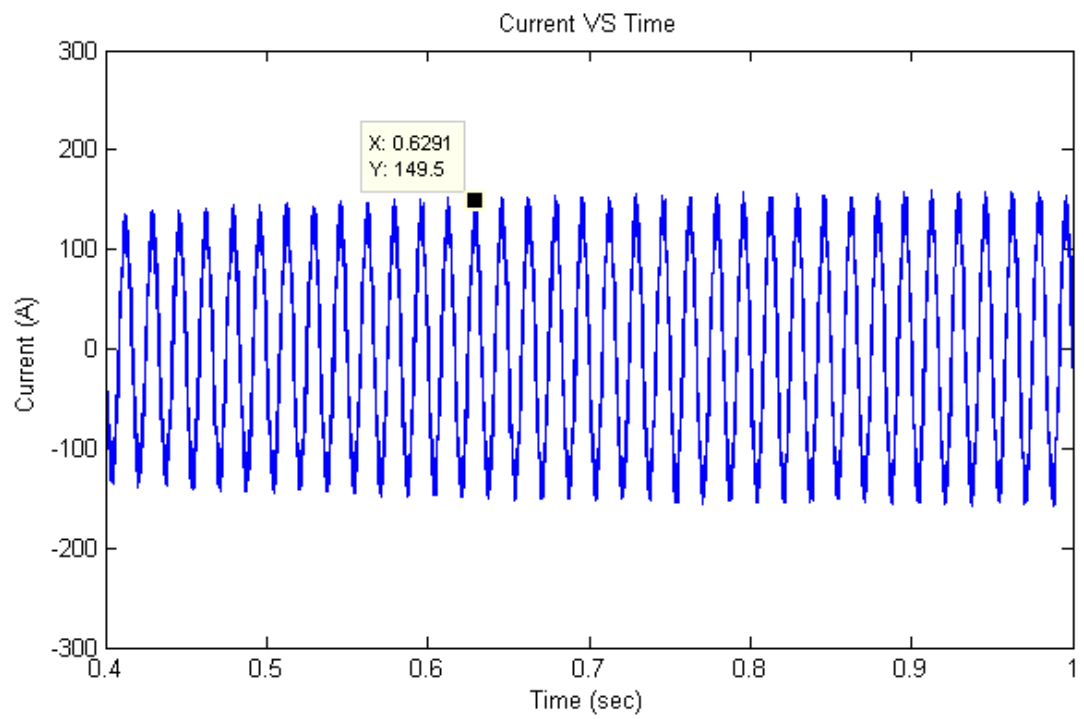
b)

Fig. 3.12: Currents at a) DG1 and b) DG3.
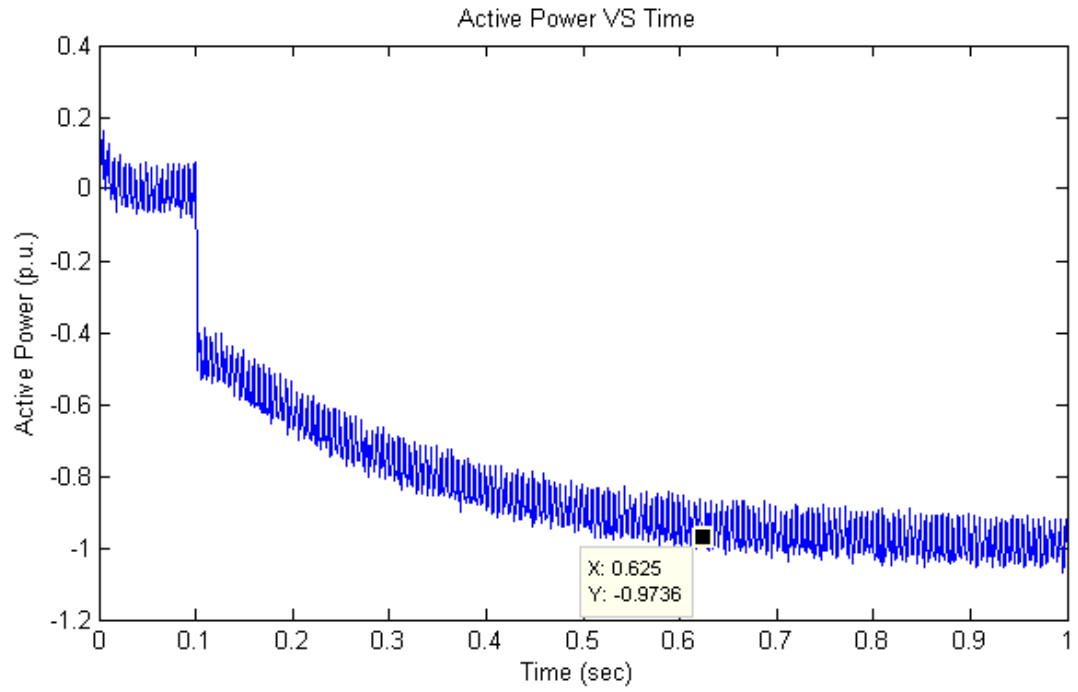
a)
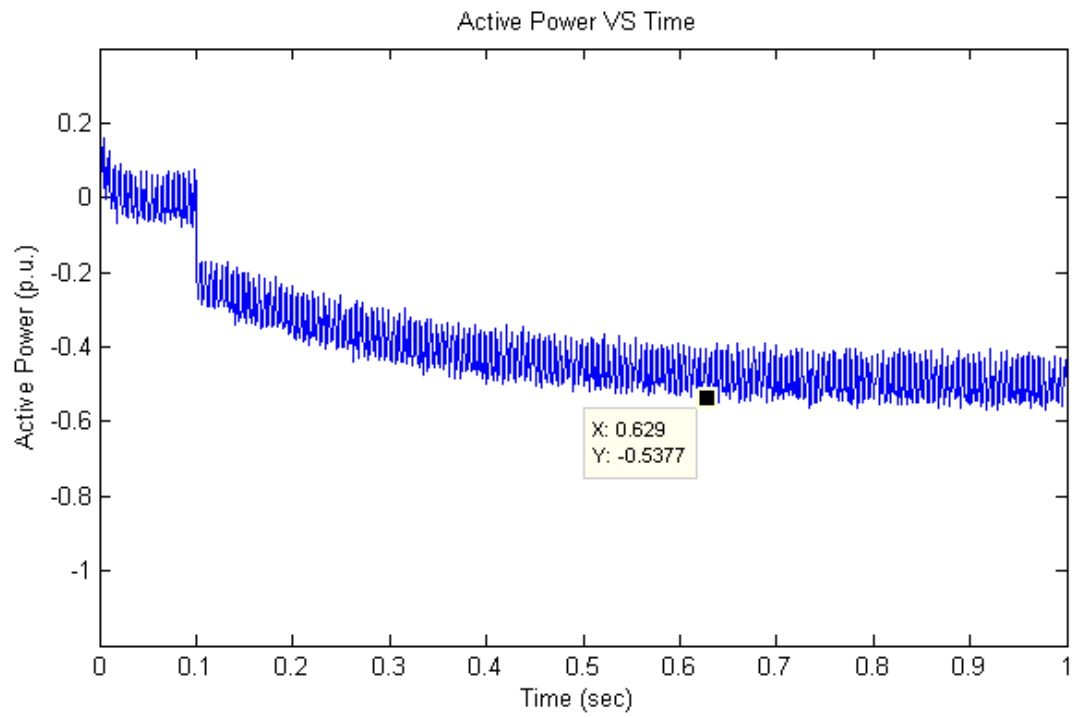
b)

Fig. 3.13: Active Power at a) at DG1 and b) DG3.
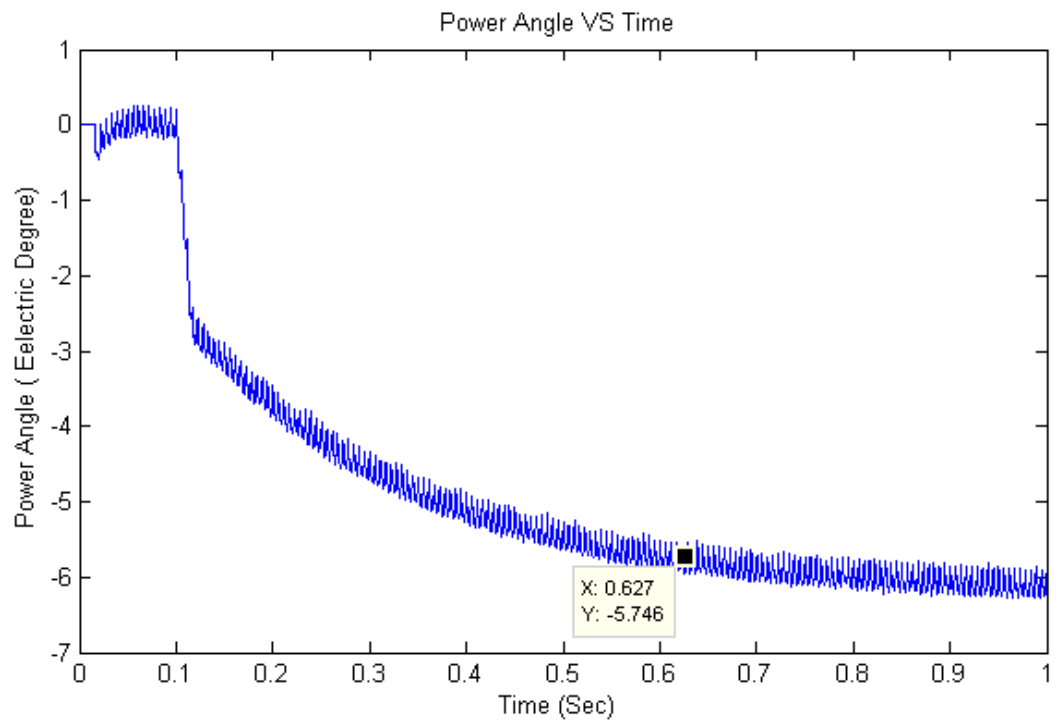
a)
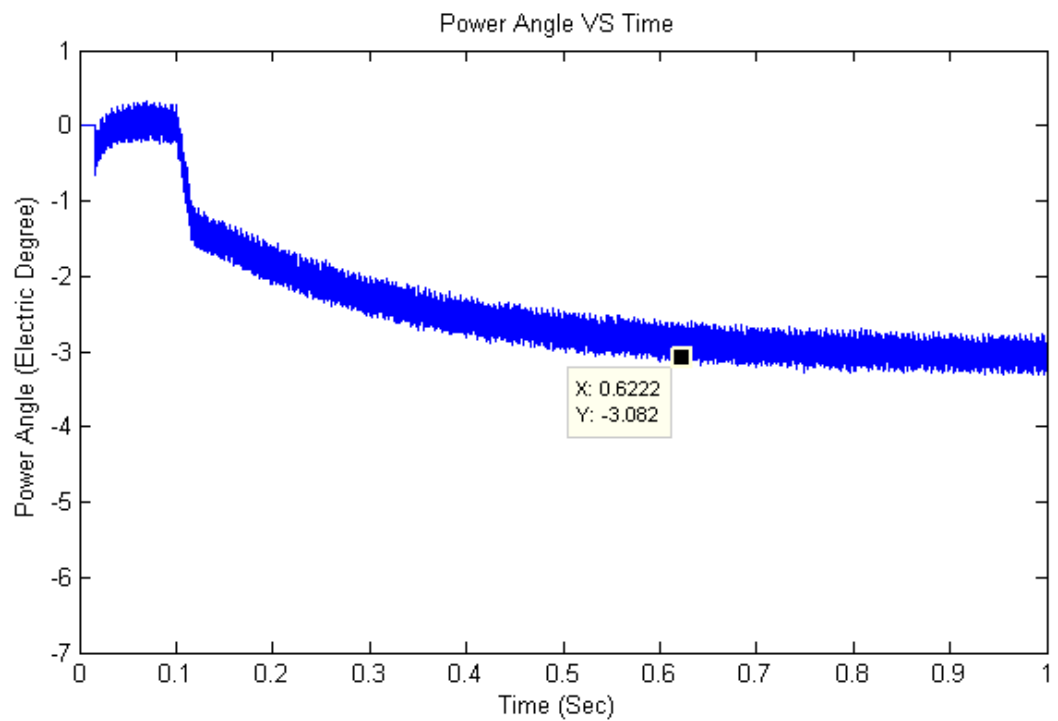
b)

Fig. 3.14: Power Angle at a) DG1 and b) DG3.
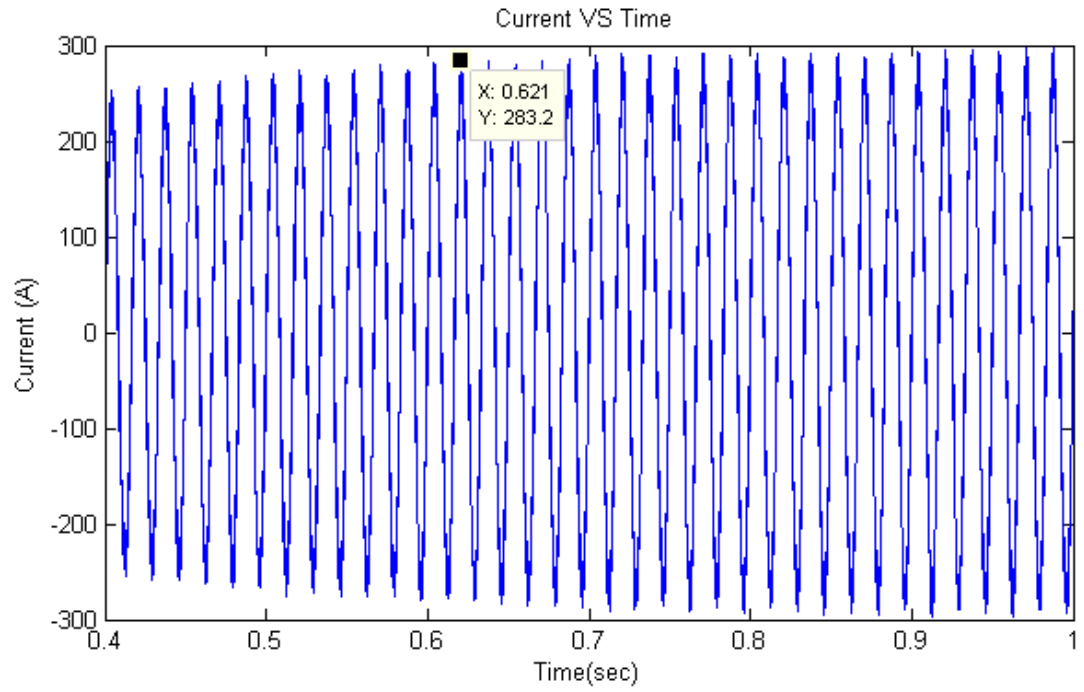
a)
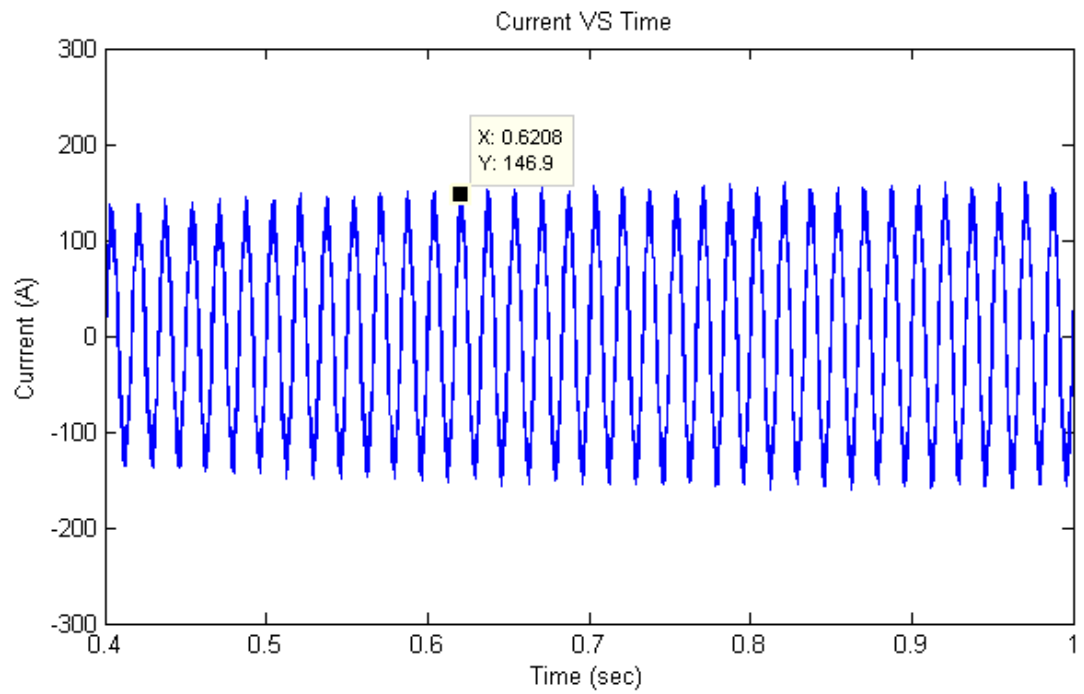
b)

Fig. 3.15: Current at a) DG1 and b) DG3.
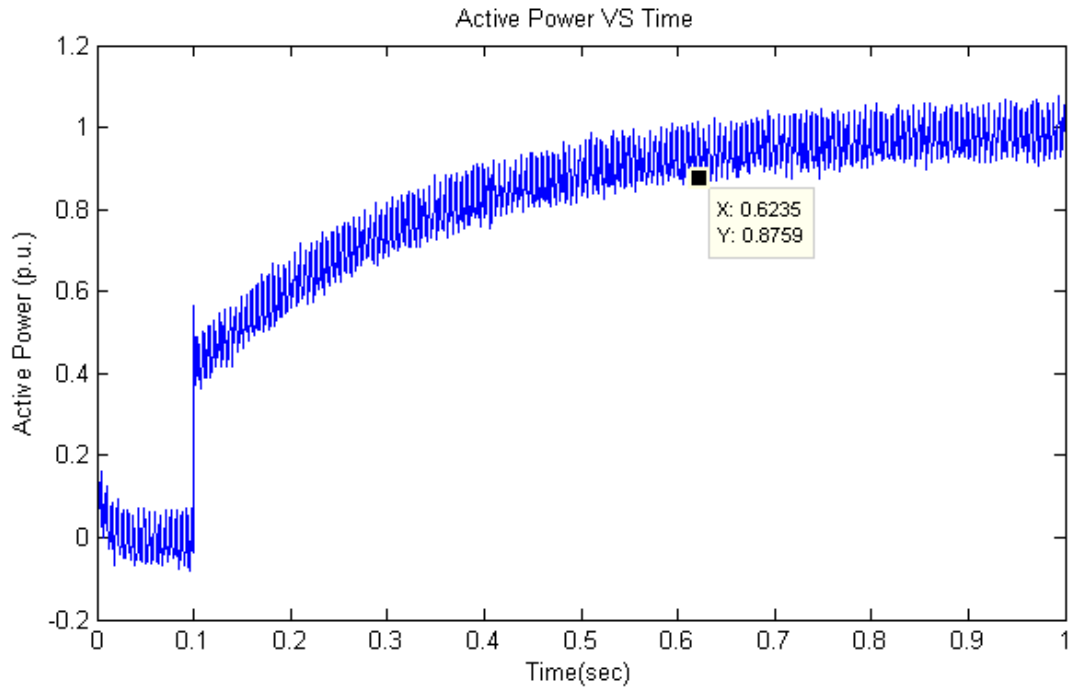
a)
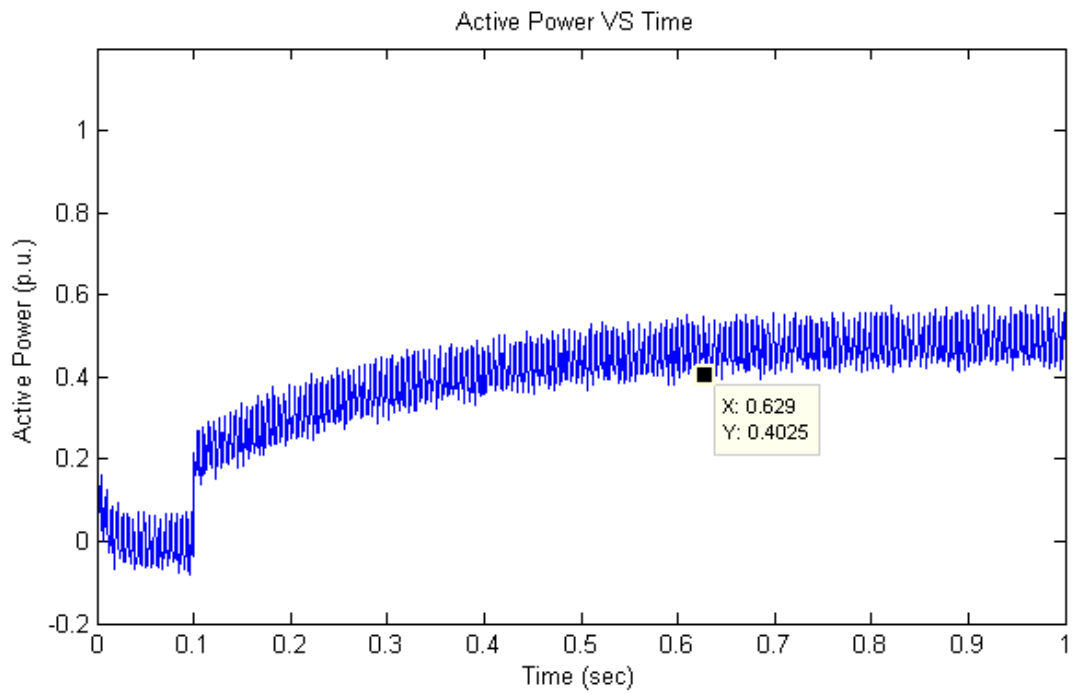
b)

Fig. 3.16: Active Power at a) DG1 and b) DG3.

3.4   SUMMARY OF CHAPTER 3:

The DC/AC power conversion represents a significant concern when operating an AC smart grid. The link between an AC grid and DC power source is important for power sharing between both sides since it helps solve major problems, such as voltage instability on the main grid. Also, the design of the filter, and the stability problems were investigated in this chapter.

The description of the power angles and how they are affected by loading in parallel operation systems were also investigated in this chapter.

CHAPTER 4: MICROGRID SYSTEM IN STAND-ALONE APPLICATION

4.0   INTRODUCTION:

Various microgrid configurations have been recently suggested. The majority of these configurations illustrate the technical complexity of controlling the operation of a microgrid. In a microgrid, many subsystems interact, such as power electronic converters, controllers, grid voltages, and many loads. In this chapter, a microgrid is studied in the case of operating in an isolated mode when supplied by a regulated DC power source [15], [16]. The concept of a microgrid is based on small photovoltaic sources or wind generator storages that are connected to the grid through an LCL-filter or chock. The overall system consists of the following elements: the DC power source, inverter, and loads. A power converter is integrated with a DC power source, DGs, loads, and an LCL output filter, as shown in Fig. 4.1.
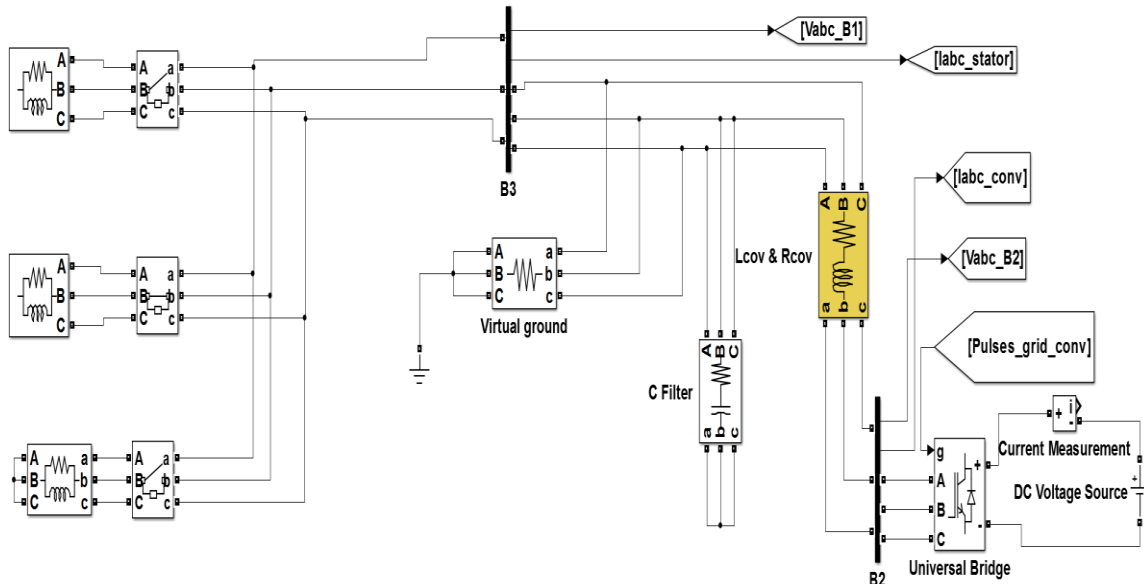
Fig. 4.1 Basic schematic diagram of a power microgrid in islanding mode.

In a microgrid, DG technologies depend on the type of resources (oil, gas, sun, wind, water, etc.) and also on the mode of operation (grid-feeding, grid-supporting, and islanding mode). Consequently, a microgrid involves several control structures to guarantee an acceptable system operation under generic operating conditions, such as different operating modes or grid-fault. These controllers are required to have better performance to ensure a fast time response under any operating conditions. In spite of the fact that the complexity of the closed loop control system is higher than the open loop control system, closed loop control yields better results.

4.1   THE STRUCTURE OF A MICROGRID IN STAND-ALONE MODE WITHOUT POWER SOURCE SHARING:

DC distribution was recommended as one of the best methods for electrical power delivery. This idea is motivated by the probability of efficient and small distributed

generation units [18], [19]. It has higher efficiency due to the absence of a reactive power component and the fact that the majority of the applications operate using DC voltage. [20], [21]

When the DC distribution systems are not connected to the main grid, it is called isolated, or forming a microgrid. The microgrid output power may vary from kWs to MWs. The fundamental reasons that cause this system to be isolated from the main grid are:

    a. Distance (high losses, poor quality of supply, far from grid).

    b. Size of load.

    c. Difficult terrain.

The analysis of DC microgrids is out of the scope of this thesis; however, it will be considered in future work as discussed in Chapter 6. In the next section, the AC microgrid is investigated.

4.1.2 FIRST CONTROL: REGULATE THE CURRENTS AND THE VOLTAGES:

The power converter at DG1 in the microgrid can be controlled either by using only a voltage control loop, as shown in Fig. 4.1, or by using an outer voltage control loop and an inner current control loop, as shown in Fig. 4.2. Furthermore, the first control can be achieved by using closed and open loops as follows:
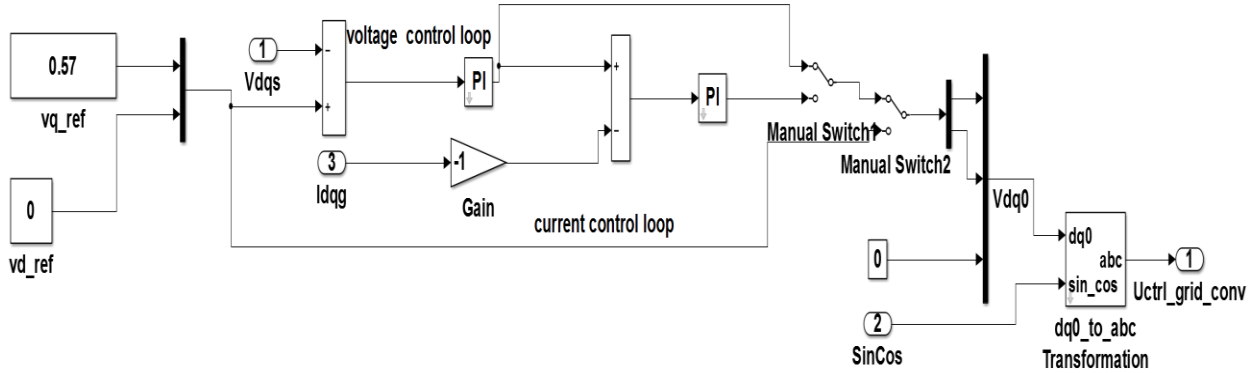
Fig. 4.2: VOC is used to regulate the microgrid.

The parameters for the case study system are shown in Table 4.1:

Parameters	Values
Sampling Time	Ts=100μ sec
Frequency	60 Hz
DC Power Source	720 V
Inductor (L)	400 μ H

Table 4.1: Fig. 4.2 Parameters and Values.

A. Closed Loop:

A type of control system that automatically changes the output based on the difference between the feedbacks values to the references values, as shown in Fig. 4.3. This control can be done by using one of the following techniques:
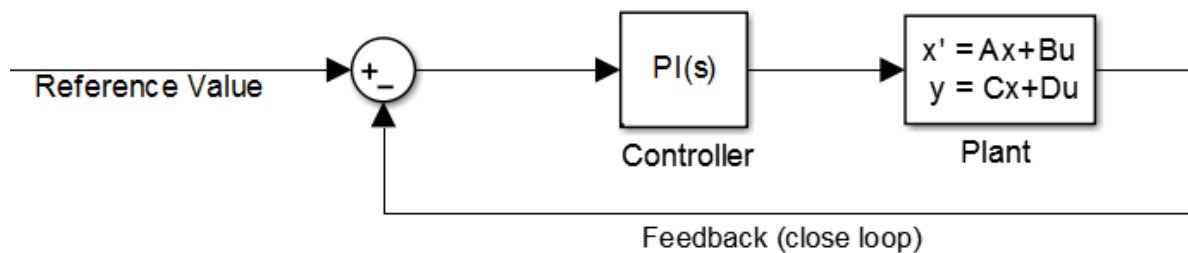
Fig. 4.3: Closed loop control.

1. Closed Loop Voltage Control:

The steady state and transient performance depend mainly on the closed loop voltage control, as shown in Fig. 4.3. The response of this closed control loop depends mainly on the Pl controller and the plant. At the steady state, the peak of the output current is 163.A and the peak of the output voltage is 376.3 V, with the percentage of total harmonic distortion around 3.61%, as shown in Fig. 4.4.

2. An Outer Voltage Control Loop and an Inner Current Control Loop:

The steady state and transient performance depend mainly on the outer voltage control loop, the inner current control loop, and the plant, as shown in Fig. 4.3. The response of this closed loop depends mainly on the Pl controller setting for the voltage control loop, the current control loop, and plant. The output of the first PI controller voltage presents a reference current signal that is forwarded to the current control loop. The voltage and current controller are both implemented by the second PI controller. When the current control was at the steady state, the peak of the output current was approximately 164.5.A and the peak of the output voltage is 376.3 V, with the percentage of total harmonic distortion around 2.91%, as shown in Fig. 4.5.
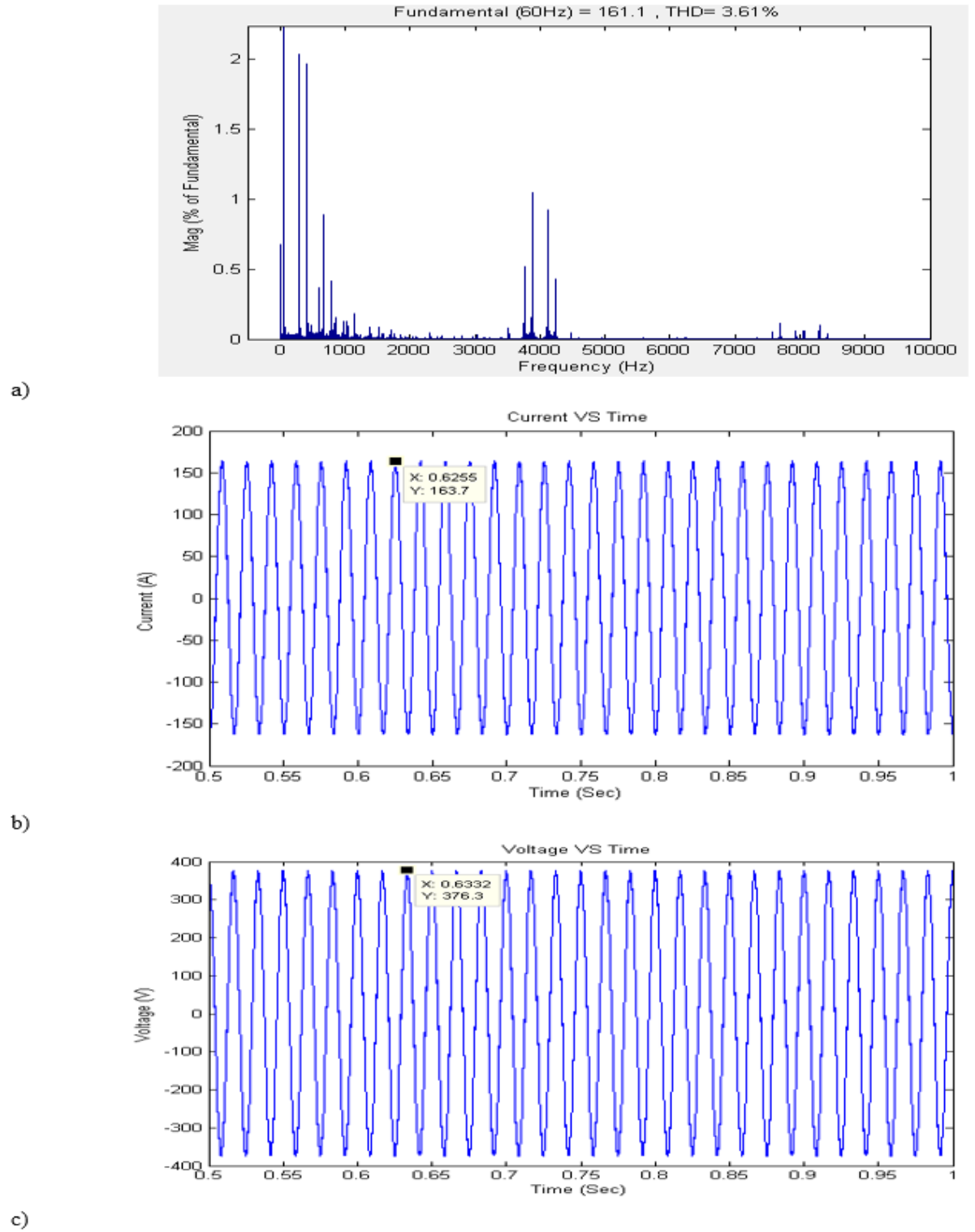
Fig. 4.4: Simulations results for closed loop voltage control: a) FFT for the current, b) current, and c) voltage.

a)

b)

c)
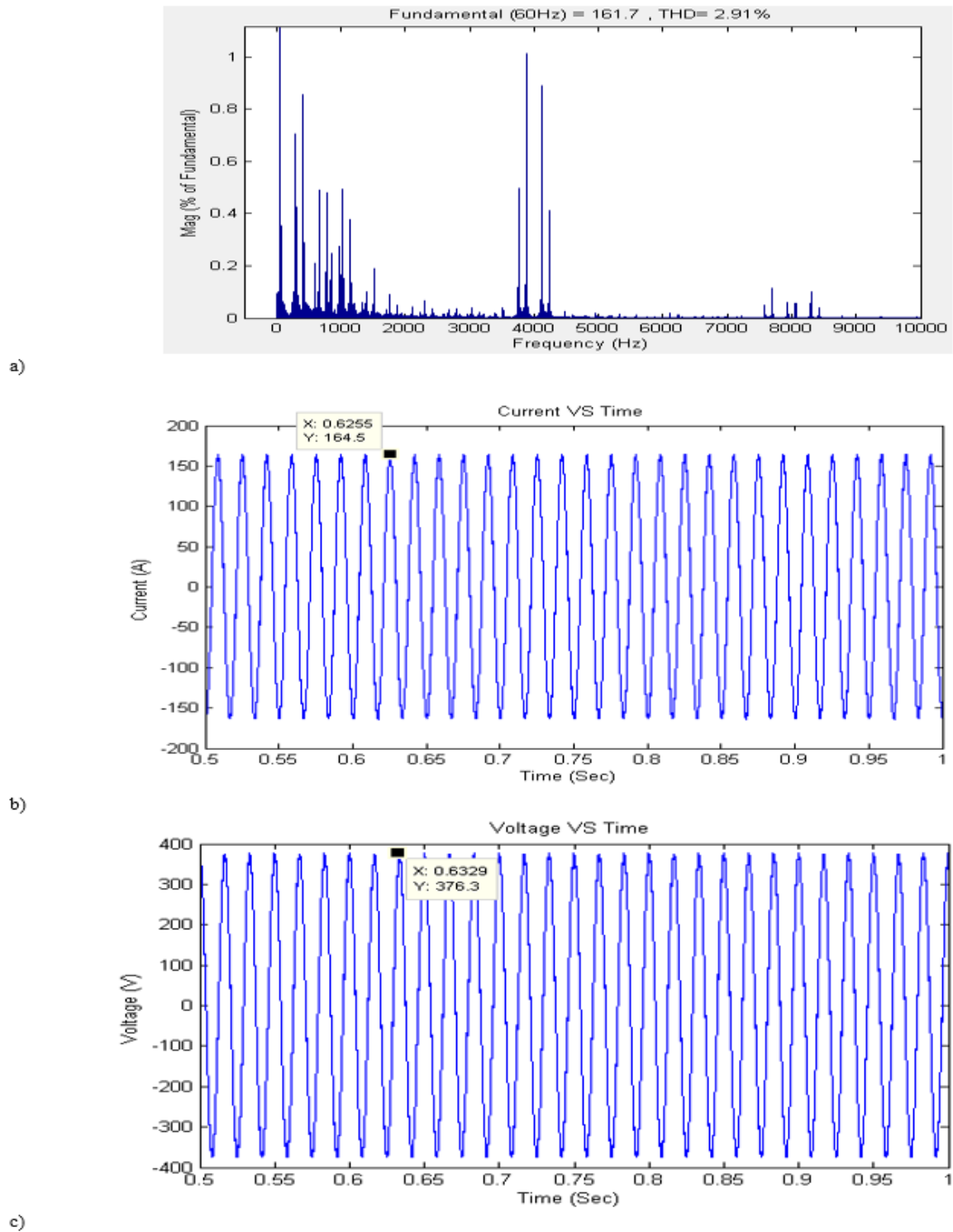
Fig. 4.5: Simulations results for closed current and voltage loops control: a) FFT for current waveform, b) current waveform, and c) voltage waveform.

B. Open Loop:

The open loop is a well-known control technique that uses only references values to actuate an output. There is no automatic feedback to adjust the process, so the operator must make manual adjustments, as shown in Fig. 4.6.
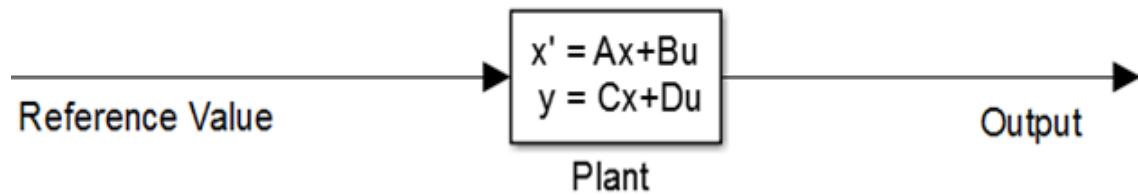
Fig. 4.6: Open control loop.

The response of this open loop control depends mainly on the plant, as shown in Fig. 4.6. When the open loop reached the steady state, the peak of the output current is aproximately 157.A, and the peak of the output voltage is 330 V, with the percentage of total harmonic distortion at approximately 1.90%, as shown in Fig. 4.7. Due to the fact that there is no PI controller in open loops, the adjustments of the process must be made manually.
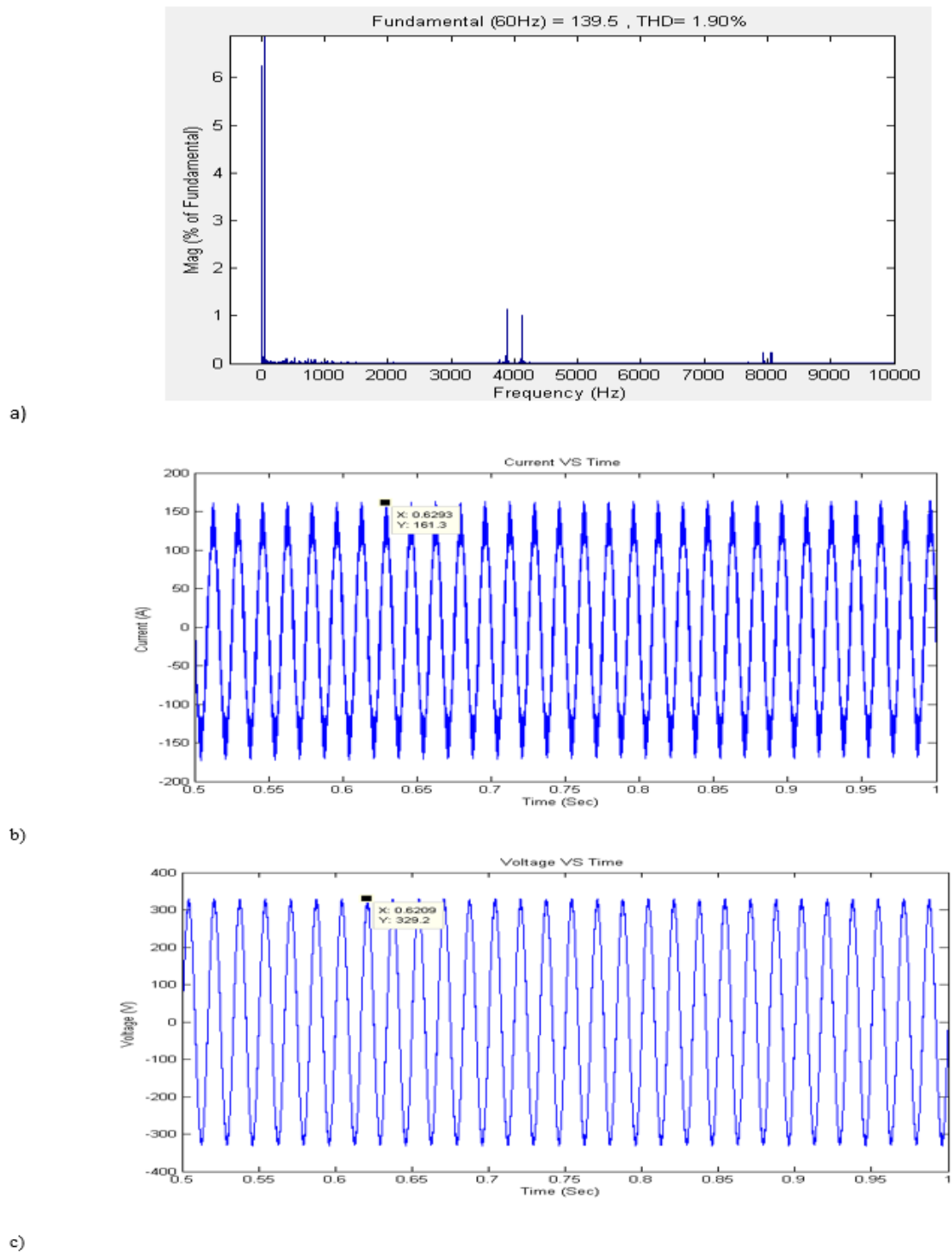
Fig. 4.7: Simulations results for open loop voltage control: a) FFT for the current waveform, b) current waveform, and c) voltage waveform.

Table 4.2 summarizes the simulation results of the first control. It is observed that voltage and current closed loop yield a better performance to use to regulate the converter in microgrid applications since this method has better peak values of the output voltages and currents with middle percentage of the THD.

Loop	Time (sec)	TDH	Current (A)	Voltage (V)	Fig
closed voltage loop	0.62	3.61%	163.7 A	376.3 V	4.4
closed outer voltage loop and inner current loop	0.62	2.91%	164.5 A	376.3 V	4.5
open loop	0.62	2.04%	161.3 A	330 V	4.7

Table 4.2: Summation results.

The main features of this system:

    a.   All available power from renewable energy is transferred to the grid through the power converter.

    b.   The consumed power is decided by the loads, thus, eventually the mismatch between generated and consumed can cause instability to the system.

    c.   PI controllers are used to control the voltage's and the current's loops.

4.1.3 CONTROL ANLYSIS: AVERAGE MODEL FOR THE MICROGRID

An analysis of the power conversion from a DC power source to an AC microgrid is very significant when designing and operating AC microgrids. The power converter is connected to an LCL-filter to reduce the current harmonic as a result of the switching action. Because of this, the power converter has an effect on the power quality of a microgrid.

The design and implementation of this filter are based on two steps: 1) building

the controller, and 2) deriving the transfer functions by using the states space technique,

as shown in Fig. 4.8.
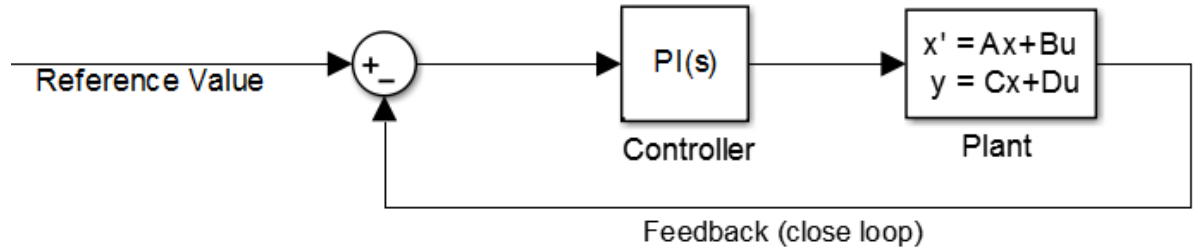
Fig. 4.8: Control of average model for a microgrid.

A. Mathematical Model:

A simplified mathematical model of a filter with a load is shown in Fig. 4.9.

Given the active and reactive power, load resistance and inductor can be calculate as

follows:

$$R_{load} = \frac{3*\left(\frac{V_{nom}}{\sqrt{3}}\right)^2}{P_{load}} \qquad (4.1)$$

$$X_L = \frac{3*\left(\frac{V_{nom}}{\sqrt{3}}\right)^2}{Q_{load}} \qquad (4.2)$$

$$L_c = \frac{X_L}{2\pi*60} \qquad (4.3)$$

Where:

$P_{load} = 100\ KW$ is the load active power at nominal operating condition.

$Q_{load} = 10\ VAR$ is the load reactive power at nominal operating condition.

$V_{norm} = 480\ V$ is the nominal line voltage.

$R_{conv} = 100\ m\Omega$ is the inductor resistance and it is the equivalent resistance.

The circuit of Fig. 4.9 can be simplified as follows:

Neglecting the voltage drop of the capacitor current i_{cf} across the inductance L_f. The

capacitor of the load C and the filter capacitor C_f can be lumped together in one

capacitor C_{eq}. This simplification results in a reduced number of states per phase, from

five states to three per phase.

In order to acquire a mathematical model that can represent the converter

behavior, at the first stage there is a need to introduce the parameters of the filter as

follows:

Parameters	Actual Values	p.u. Values
C_{eq}	100µ F	0.022j
L_{eq}	400 µ H	0.09
R_{eq}	100 $m\Omega$	0.06

Table 4.3: Parameters of simplification circuit in Fig. 4.9.

a)

b)

c)
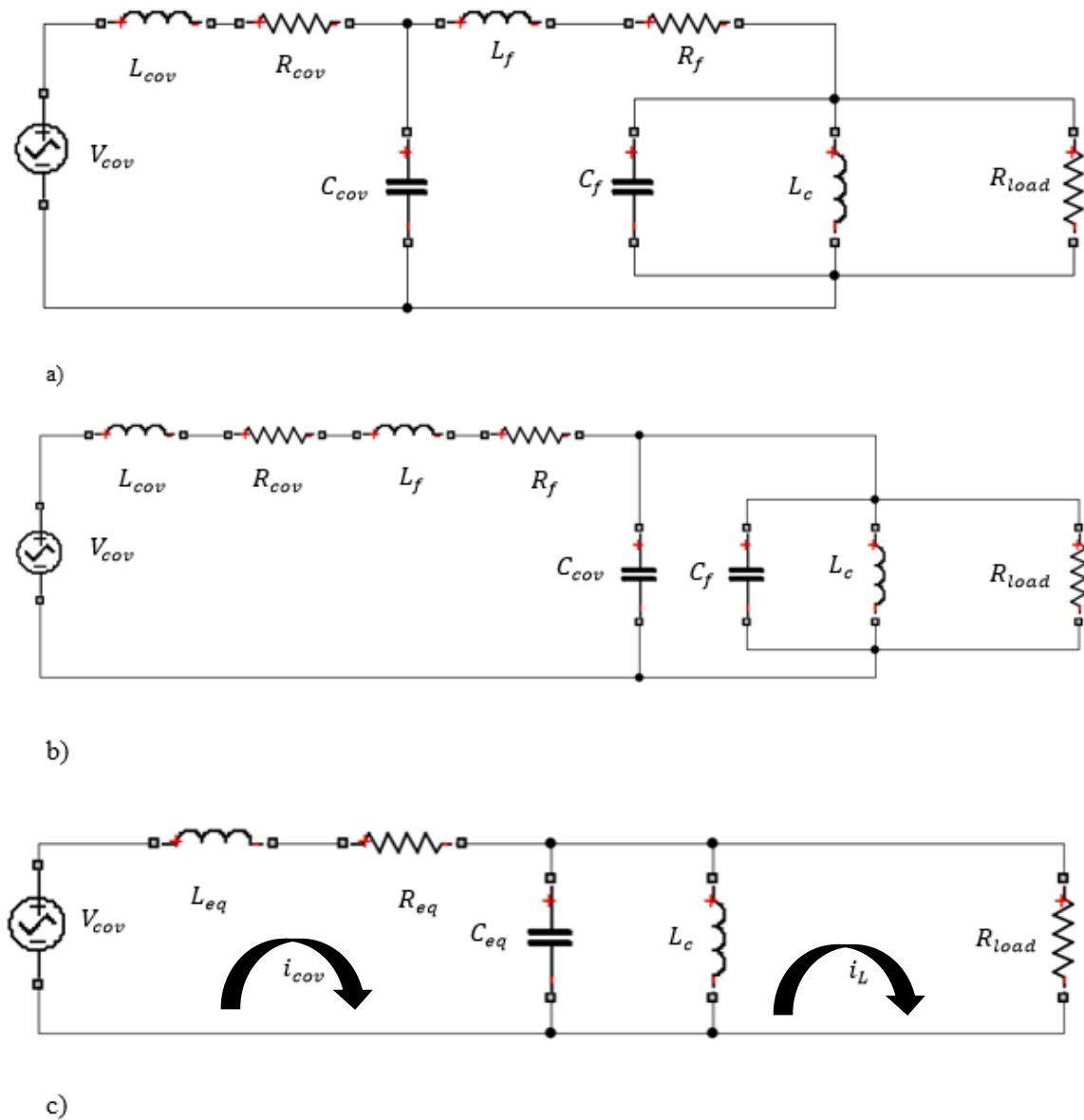
Fig. 4.9: Simplification steps for microgrid filter with a load.

The transfer functions are obtained from the LCL-filter and the load by deriving

the state space model of the system in the form of $[\dot{x} = Ax + Bu]$. The performance of

the developed converter will be compared with that of an LCL-filter and the load-based

DG1 in terms of voltage regulation, control robustness, efficiency, and harmonics [17].

Refer to APPENDIX C for details about the model derivation.

$$
\frac{d}{dt}
\begin{bmatrix}
i_{cova} \\
i_{covb} \\
i_{covc} \\
v_{ca} \\
v_{cb} \\
v_{cc} \\
i_{La} \\
i_{Lb} \\
i_{Lc}
\end{bmatrix}
=
\begin{bmatrix}
\frac{-R_{conv}}{L_{cov}} & 0 & 0 & \frac{-1}{L_{cov}} & 0 & 0 & 0 & 0 & 0 \\
0 & \frac{-R_{conv}}{L_{cov}} & 0 & 0 & \frac{-1}{L_{cov}} & 0 & 0 & 0 & 0 \\
0 & 0 & \frac{-R_{conv}}{L_{cov}} & 0 & 0 & \frac{-1}{L_{cov}} & 0 & 0 & 0 \\
\frac{I}{C} & 0 & 0 & \frac{-1}{C*R_{load}} & 0 & 0 & \frac{-1}{C} & 0 & 0 \\
0 & \frac{I}{C} & 0 & 0 & \frac{-1}{C*R_{load}} & 0 & 0 & \frac{-1}{C} & 0 \\
0 & 0 & \frac{I}{C} & 0 & 0 & \frac{-1}{C*R_{load}} & 0 & 0 & \frac{-1}{C} \\
0 & 0 & 0 & \frac{1}{L_C} & 0 & 0 & 0 & 0 & 0 \\
0 & 0 & 0 & 0 & \frac{1}{L_C} & 0 & 0 & 0 & 0 \\
0 & 0 & 0 & 0 & 0 & \frac{1}{L_C} & 0 & 0 & 0
\end{bmatrix}
$$

$$
\begin{bmatrix}
i_{cova} \\
i_{covb} \\
i_{covc} \\
v_{ca} \\
v_{cb} \\
v_{cc} \\
iL_a \\
iL_b \\
iL_c
\end{bmatrix}
+
\begin{bmatrix}
\frac{1}{L_{cov}} & 0 & 0 & 0 & 0 & 0 & 0 & 0 & 0 \\
0 & \frac{1}{L_{cov}} & 0 & 0 & 0 & 0 & 0 & 0 & 0 \\
0 & 0 & \frac{1}{L_{cov}} & 0 & 0 & 0 & 0 & 0 & 0 \\
0 & 0 & 0 & 0 & 0 & 0 & 0 & 0 & 0 \\
0 & 0 & 0 & 0 & 0 & 0 & 0 & 0 & 0 \\
0 & 0 & 0 & 0 & 0 & 0 & 0 & 0 & 0 \\
0 & 0 & 0 & 0 & 0 & 0 & 0 & 0 & 0 \\
0 & 0 & 0 & 0 & 0 & 0 & 0 & 0 & 0 \\
0 & 0 & 0 & 0 & 0 & 0 & 0 & 0 & 0
\end{bmatrix}
\begin{bmatrix}
v_{cova} \\
v_{covb} \\
v_{covc} \\
0 \\
0 \\
0 \\
0 \\
0 \\
0
\end{bmatrix}
\qquad (4.4)
$$

The operating point of a dynamic system depends on the states of this system at a specific time. The states of this system are the converter current i_{cov}, the current i_L in the inductor L_c and the voltage in the capacitor v_c. Equation 4.4 represents the state space model of the system as $\dot{x} = Ax + Bu$. The stability of the system, the characteristic equations, the pole-zero maps, bode plot, and transfer functions are obtained from

equation 4.4. Therefore, the frequency response and the pole-zero position of the LCL-filter integrated to the load, the Bode diagram, and pole-zero are shown in Fig. 4.10 and Fig. 4.11 respectively.
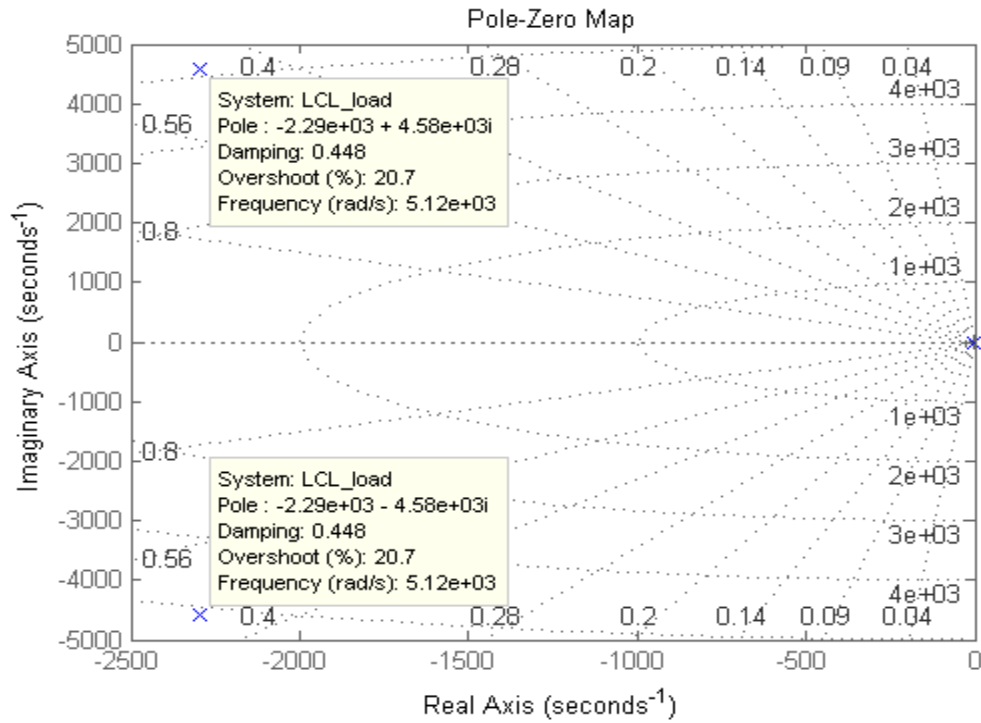
Fig. 4.10: Pole-Zero Maps for LCL-filter and load with damping resistor.
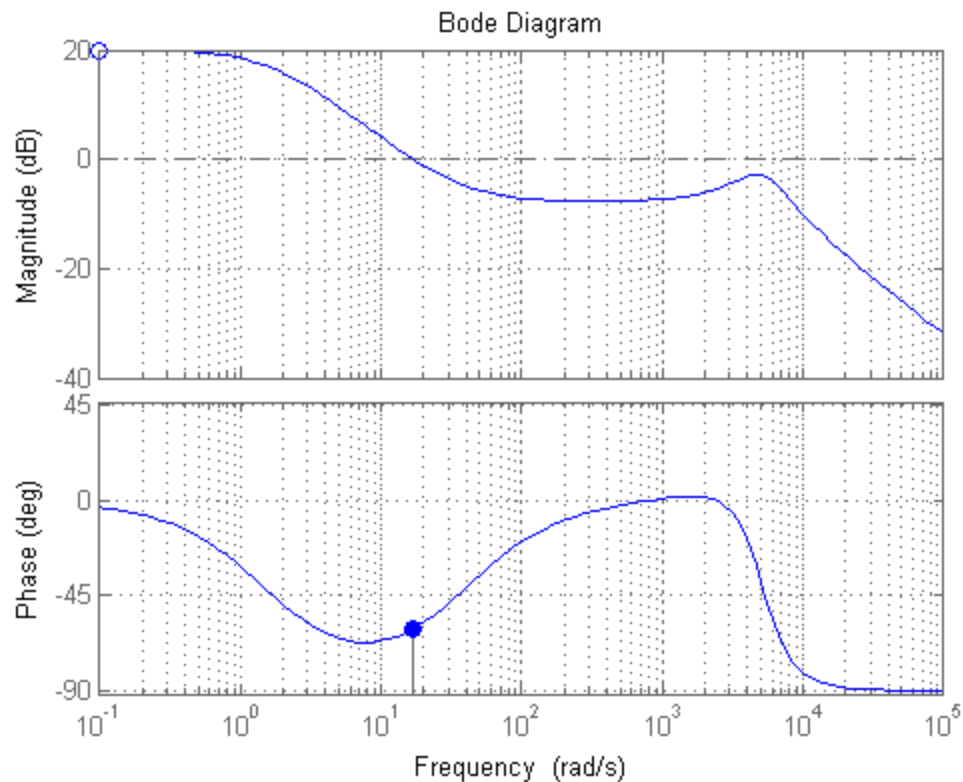
Fig. 4.11: Bode Plot for LCL-filter and the load with damping resistor.

B. Controller Design:

The control strategy for the voltage and current control loops are shown in Fig. 4.12. v_d and v_q are the measured voltages of the d-axis and the q-axis. On the other hand, i_d and i_q are the measured currents of the d-axis and the q-axis, respectively. The voltage control loop, as shown in Fig. 4.11, is mainly responsible for controlling the output voltage. The difference between the desired reference voltage and the actual measured voltage is processed through a PI controller. The output of this PI controller presents a reference current signal that is forwarded to the current control loop. The phase angular used for the d-q transformation is derived by the integration of the angular frequency ω which is the required normal frequency. The voltage and current controller

are both implemented by *PI*. The outer voltage control loop is used to achieve voltage

tracking. [24].
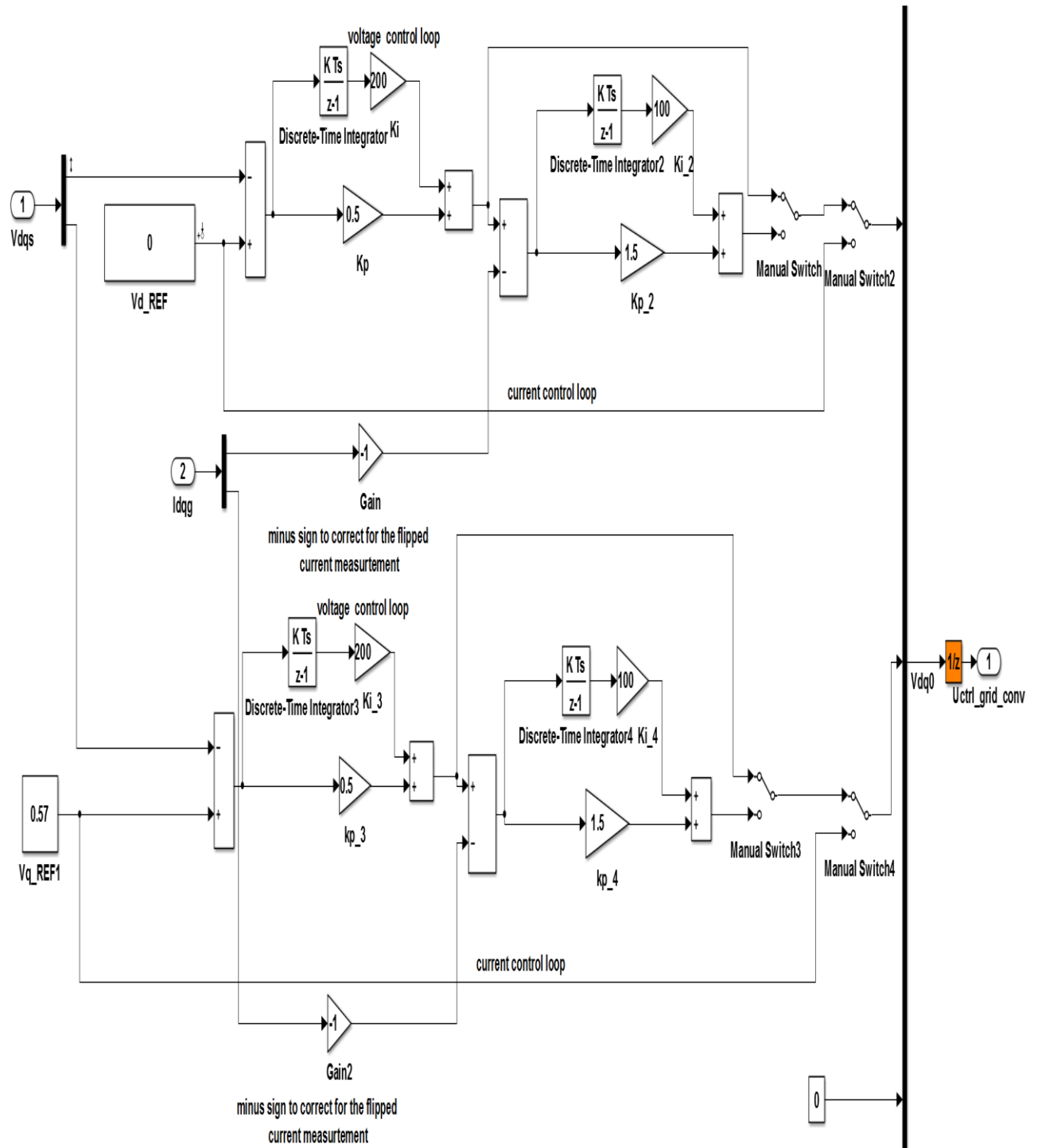
Fig. 4.12: Simulink model for system controller.

4.2 SMALL SIGNALS ANALYSIS:

This control system is designed in the discrete time-domain, as shown in Fig. 4.13. The proposed controller is tested through proper simulations in order to test the stability of this microgrid. A stand-alone mode with the proposed controller was simulated using the control and system parameters shown in Table 4.1. In addition, this grid-side controller, shown in Fig. 4.12, has three different selections to make the control, as shown in Fig. 4.13. These selections are voltage control loop, outer voltage control loop and inner current control loop, and open loop.
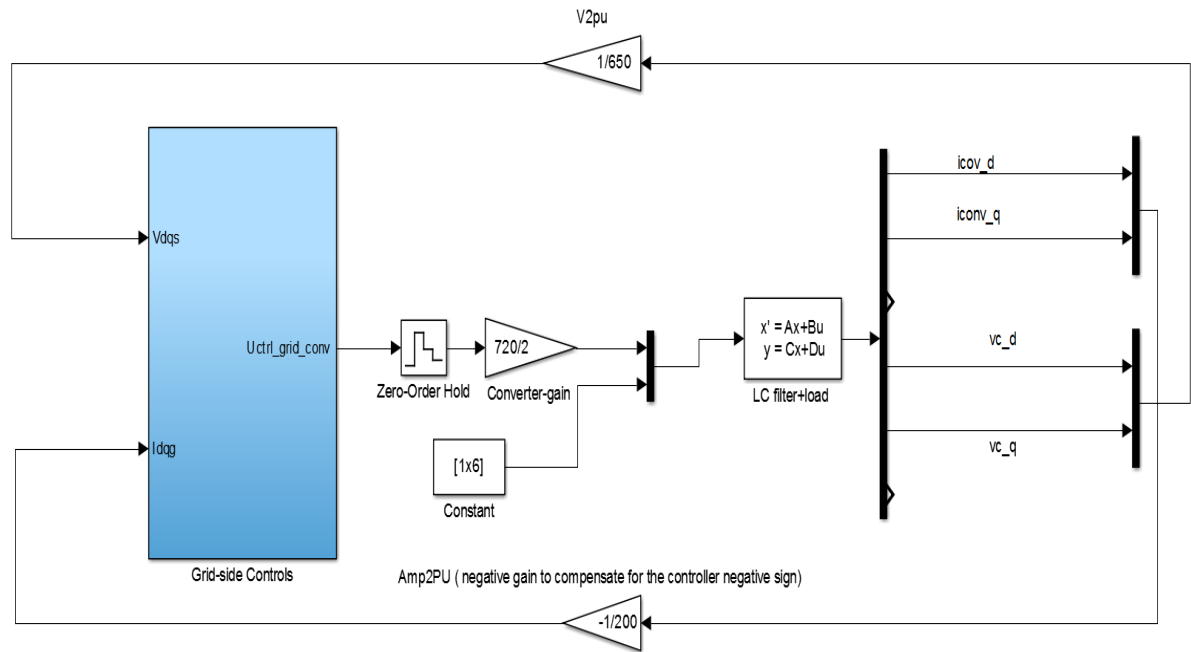
Fig. 4.13: Small signals diagram.

1. Voltage Control Loop:

This loop control is shown in Fig 4.14. The voltage control loop is mainly responsible for controlling the output voltage. The difference between the desired

reference voltage and the actual measured voltage is processed through a PI controller. The output of this PI controller presents a reference voltage signal.
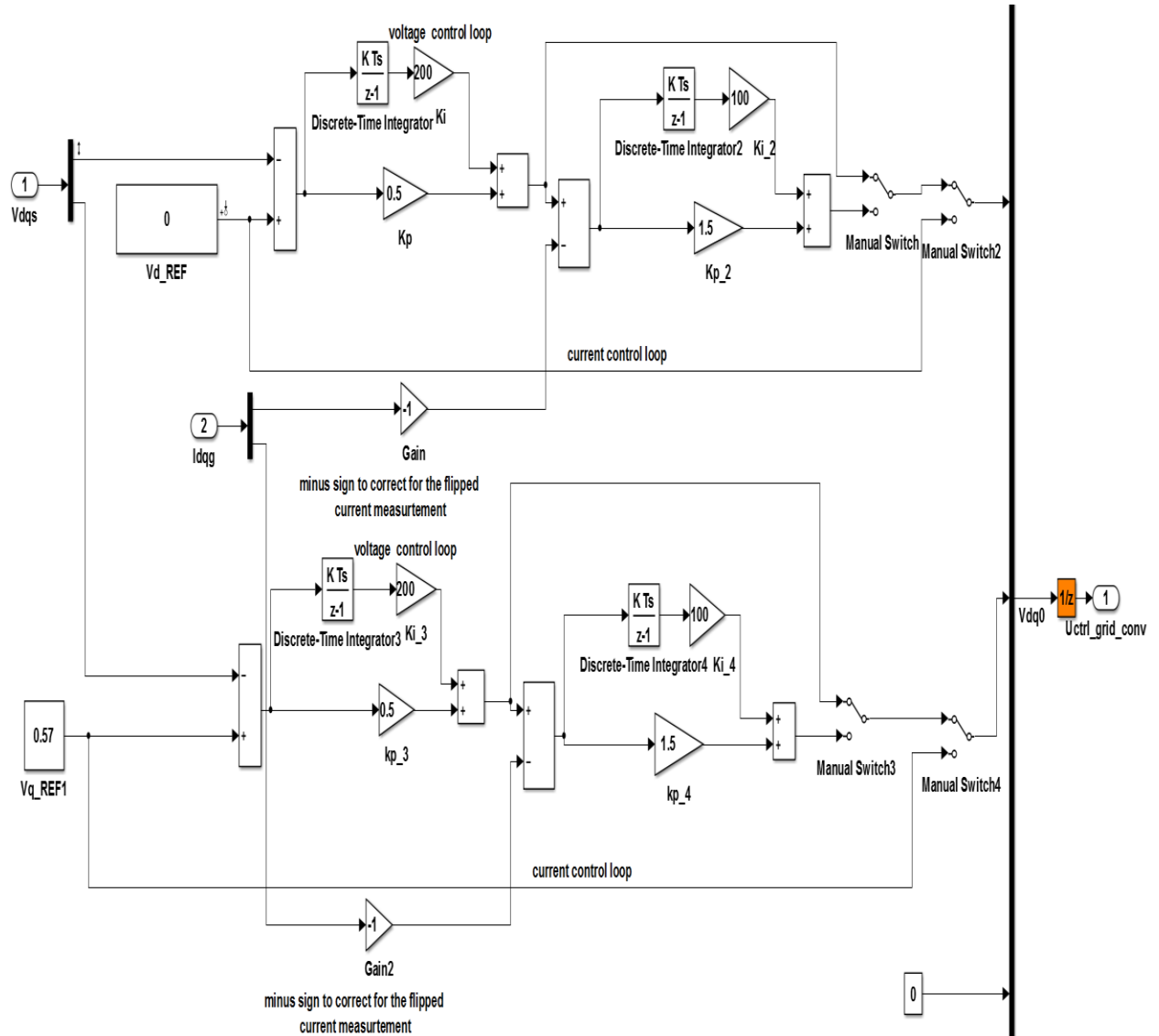
Fig. 4.14: Voltage control loop.

The step response of the model is shown in Fig. 4.15. Note that the system reaches the steady state at 0.07 sec. without overshoot. From Fig. 4.16, the voltage control loop technique provides a gain margin equal to 14.5 dB and phase margin equal

to 103 degrees. In addition, Fig. 4.17 shows the pole-zero map of the voltage control

loop. This Figure shows the location in the complex plane of the poles and zeros of the

system.
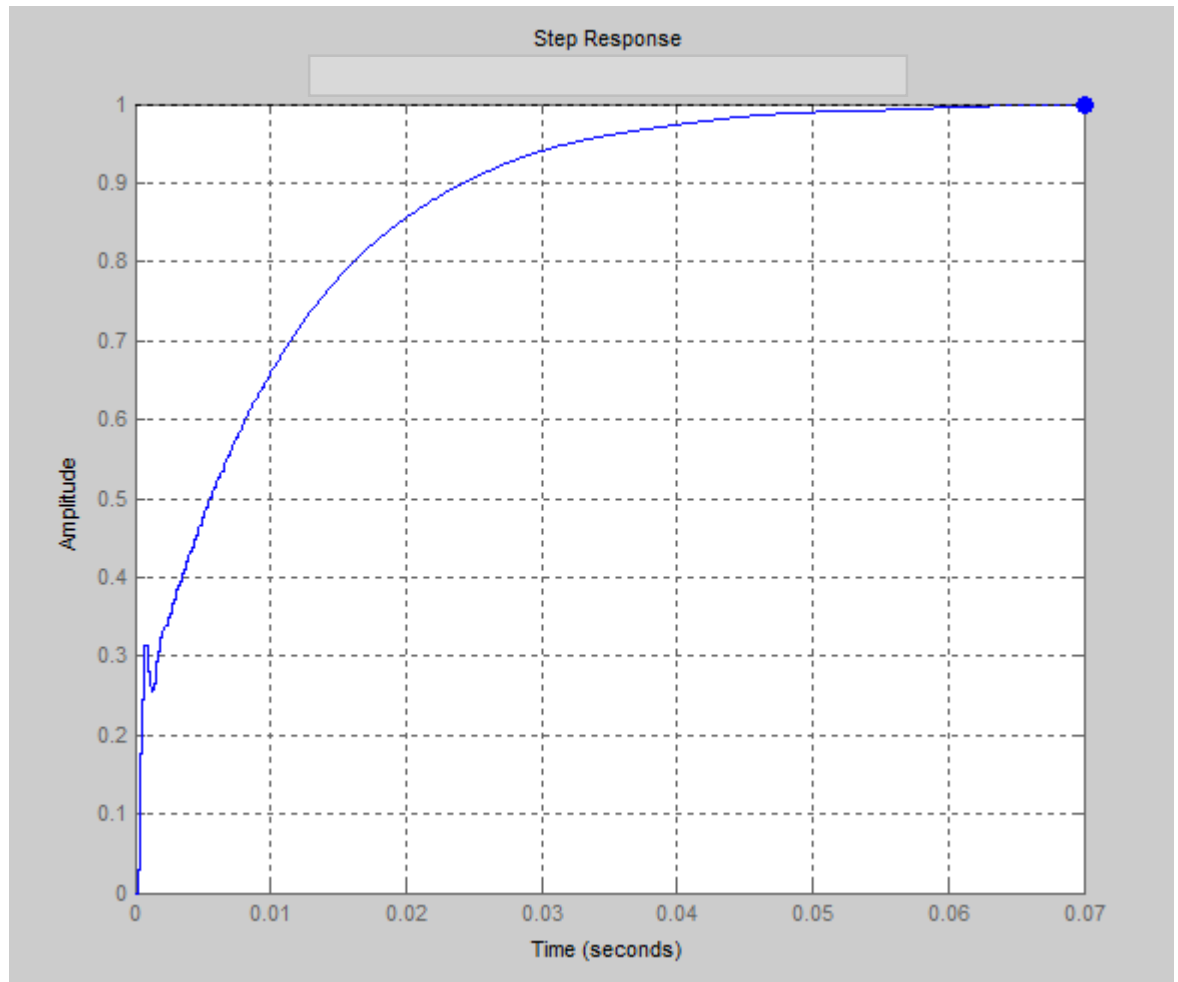
Fig. 4.15: Step response of voltage loop control.
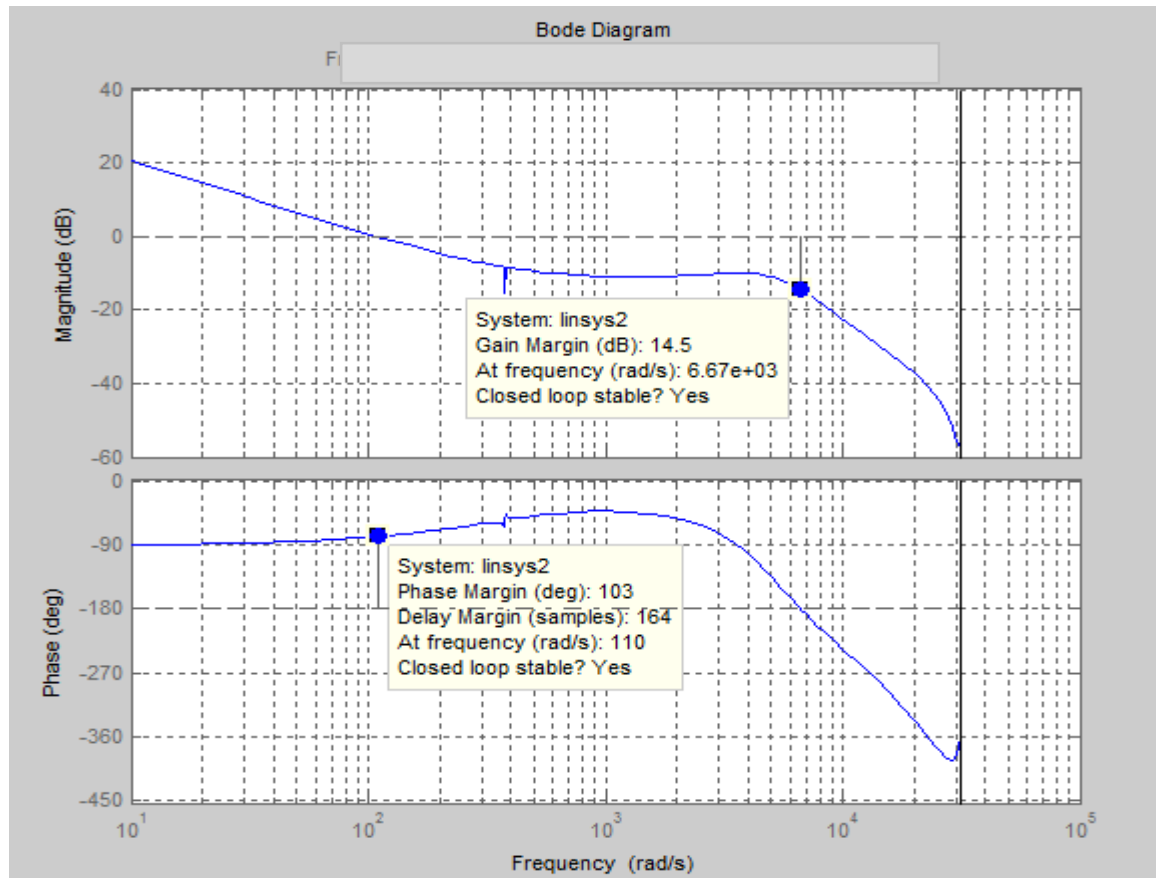
Fig. 4.16: Open loop bode plot for voltage loop control Bode plot of.
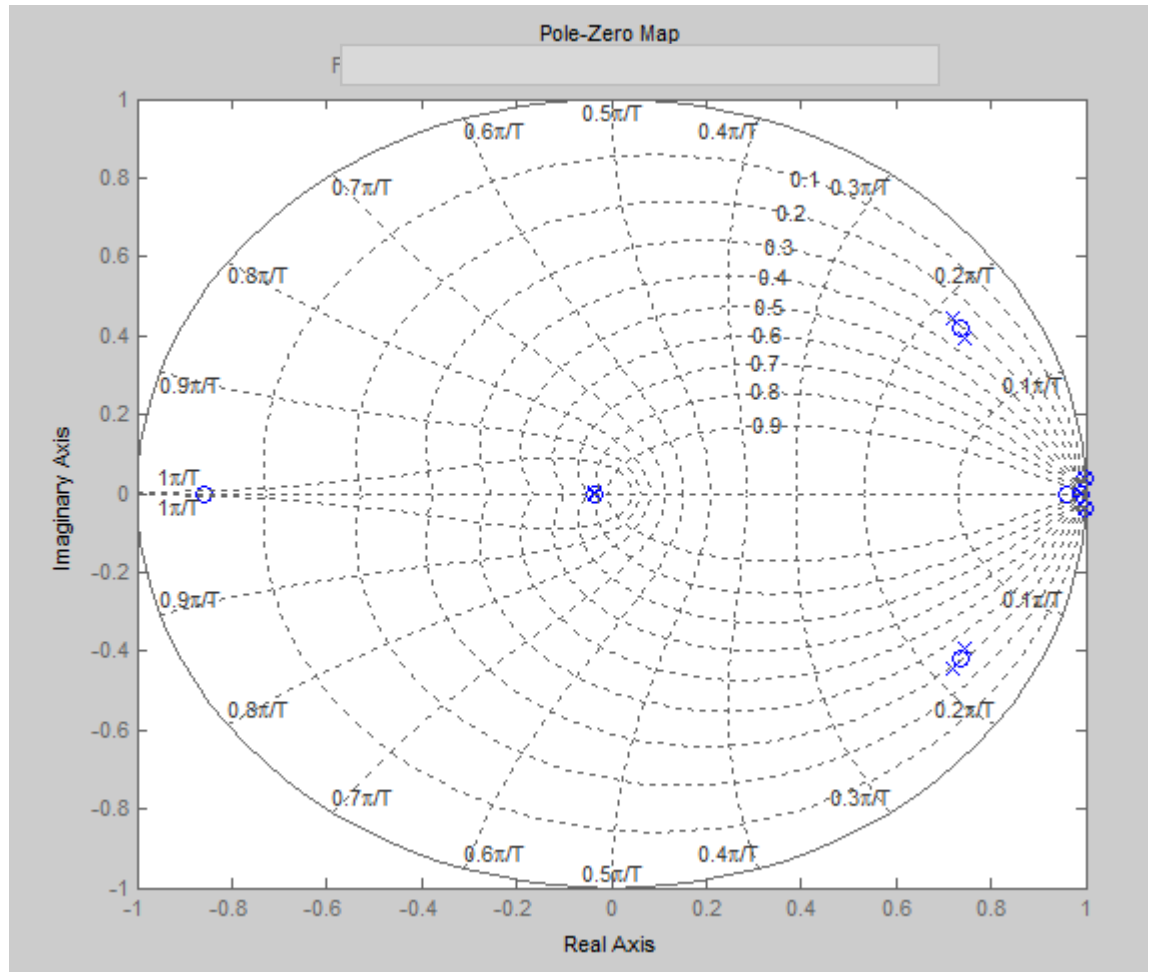
Fig. 4.17: Pole-Zero Map of the system.

2.   Cascade Control :

The structure of the cascade control system is shown in Fig. 4.18. In this case, two loops are used to implement the controller. The voltage loop is mainly responsible for controlling the output voltage. The difference between the desired reference voltage and the actual measured voltage is processed through a PI controller. The output of this PI controller presents a reference current signal that is forwarded to the current control loop. The voltage and current controller are both implemented using a PI regulator.
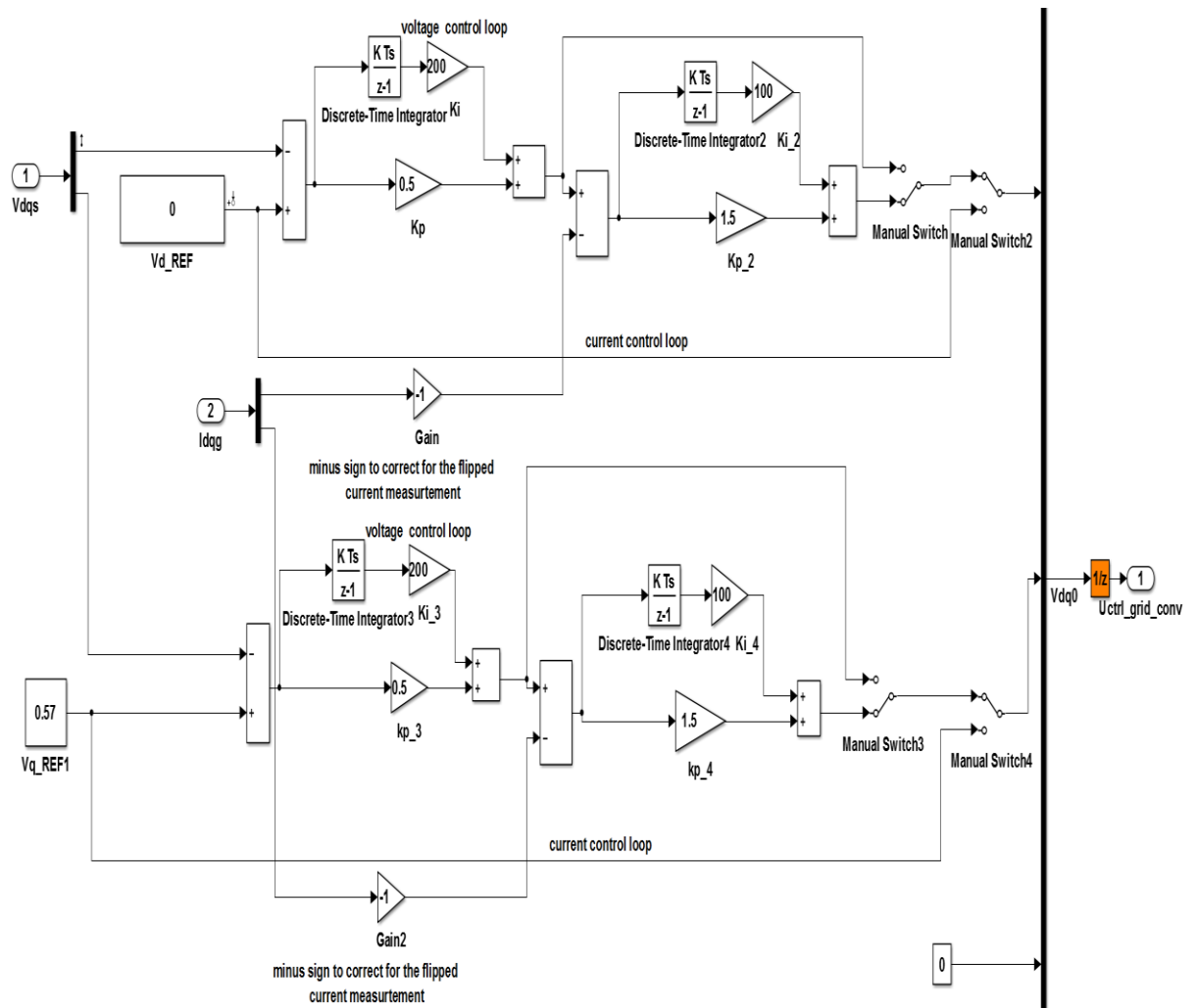
Fig. 4.18: Voltage control loop and inner current control loop.

Fig. 4.19 demonstrates the step response of the model that reaches the steady state at 0.14 sec. with a percentage overshoot of approximately 5.75%. It should be noted from Fig. 4.20 that the voltage control loop technique provides a gain margin equal to 6.85 dB and phase margin equal to 84.8 degrees. In addition, the pole and zero map of the system is shown in Fig. 4.21.
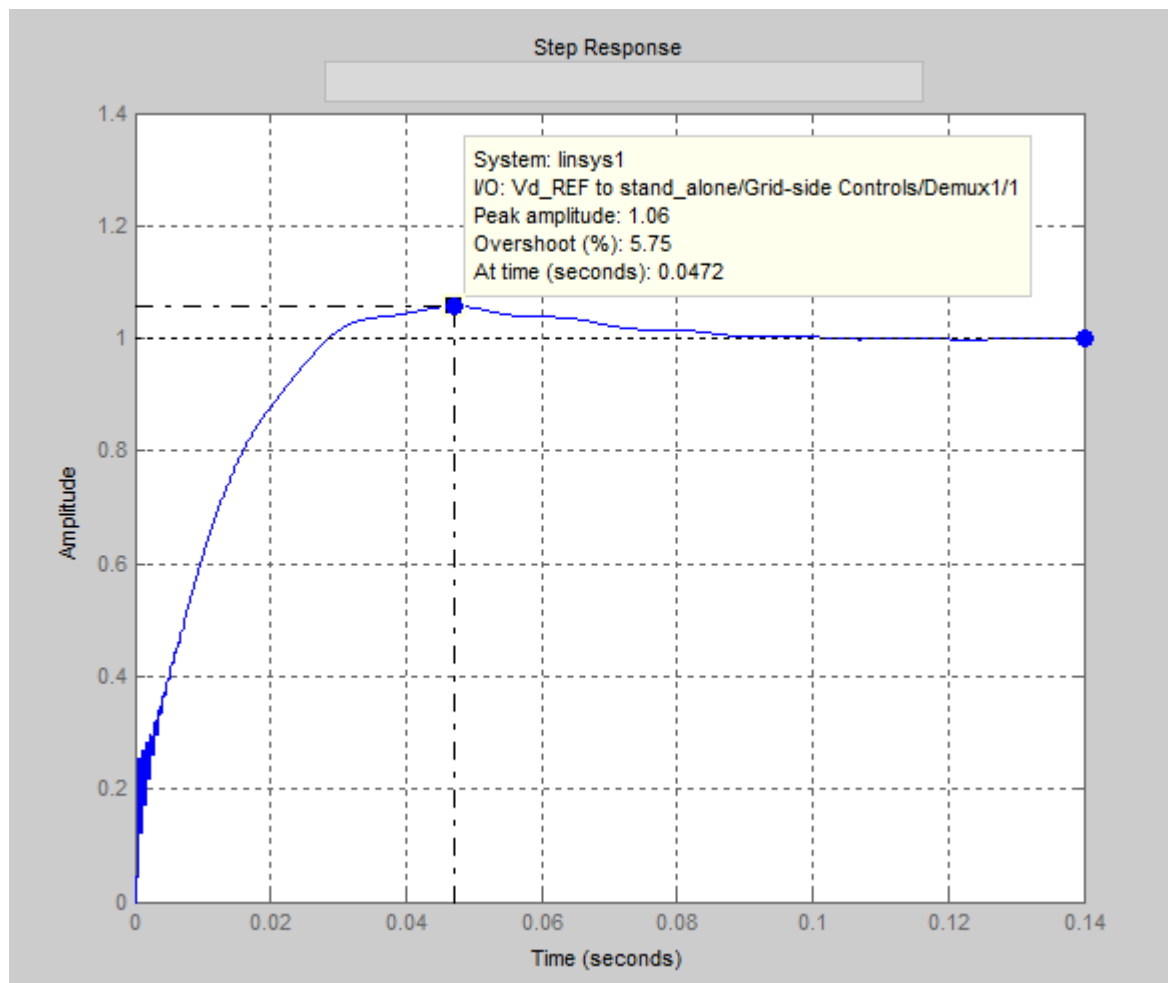
Fig. 4.19: System step response using a cascade control.
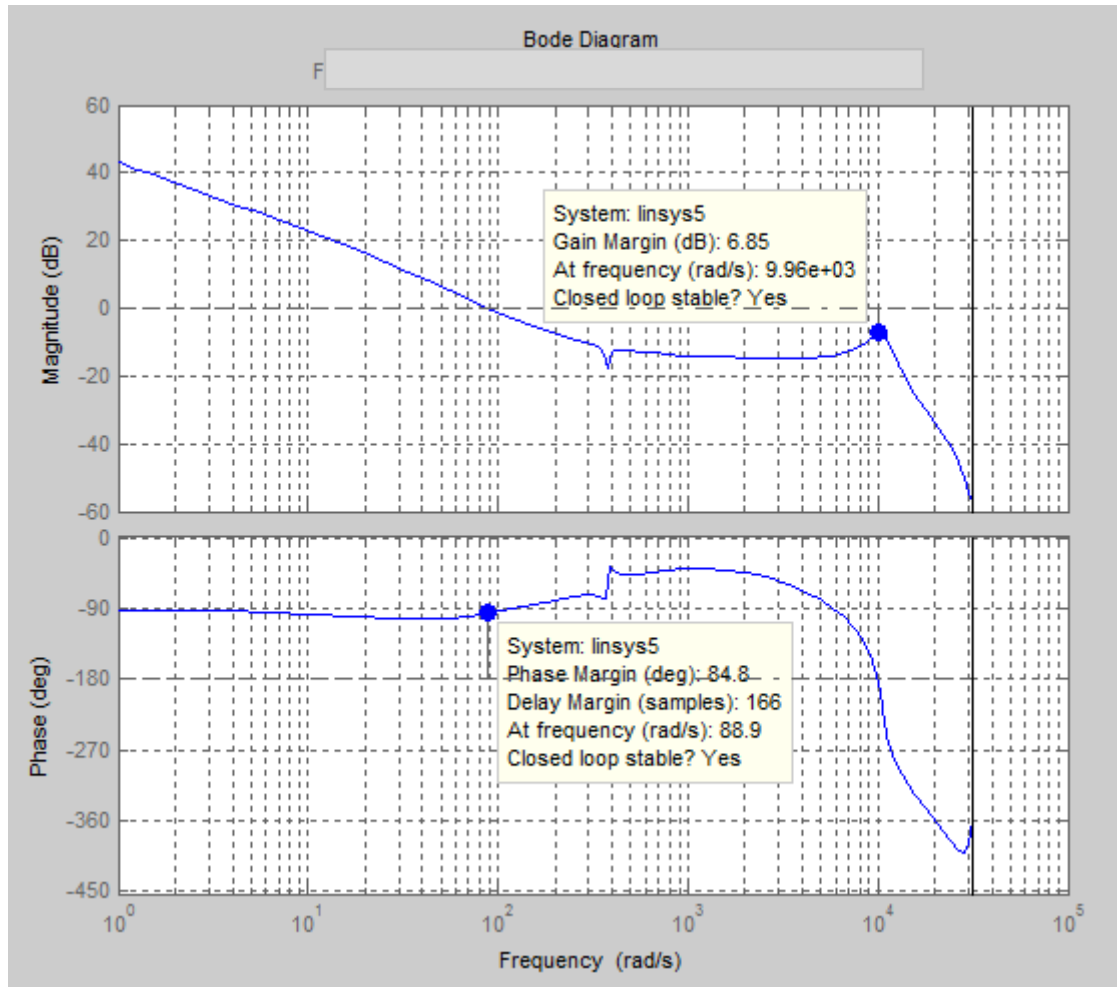
Fig. 4.20: Open loop bode plot for cascade control system.
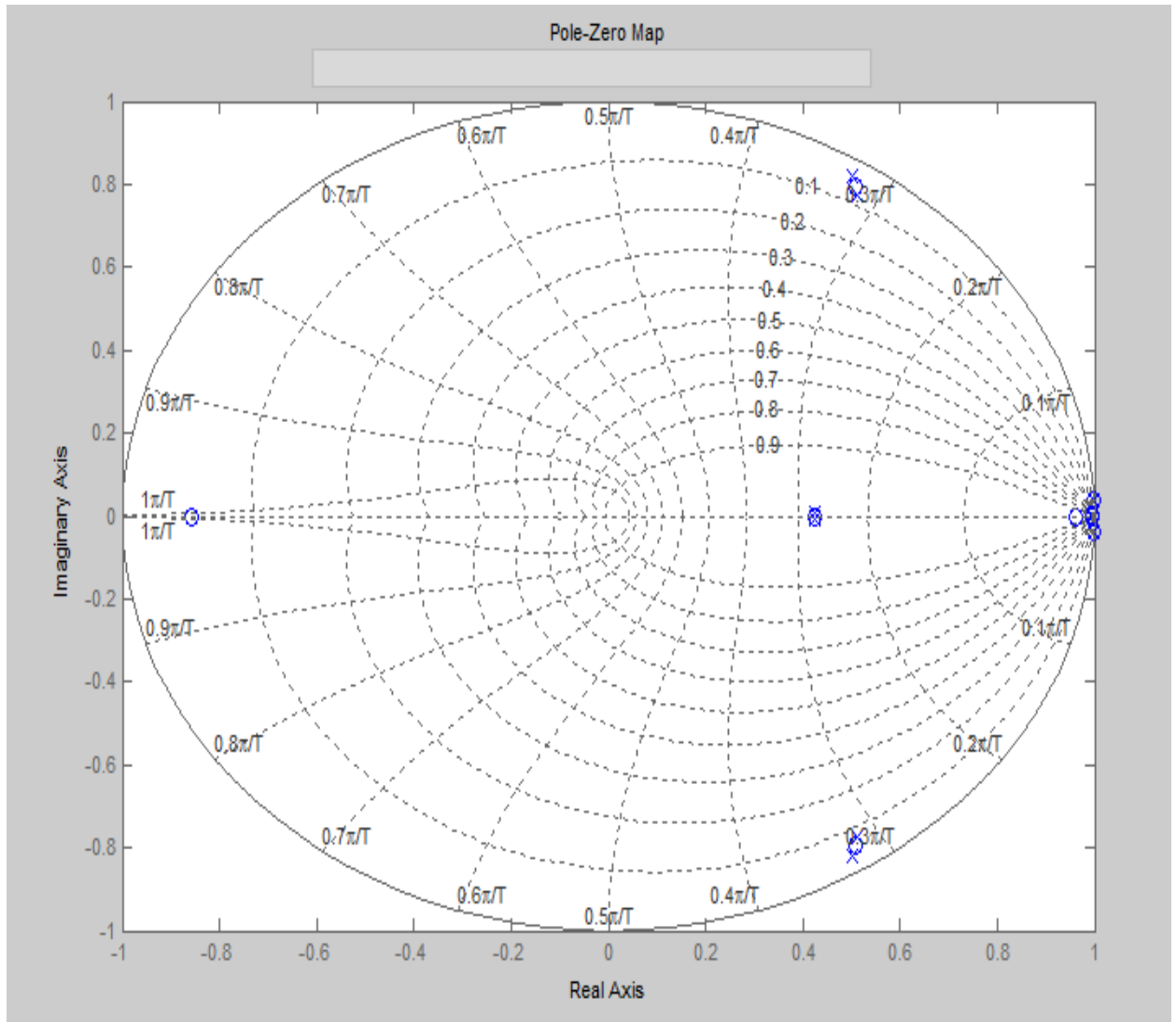
Fig. 4.21: Pole-Zero Map of the cascade control system.

3. Open Loop Control:

It can be noted from Fig. 4.22 that the open loop control is a forward path. It has

the reference values of the voltages V_{dq}. It does not have a PI controller. Hence, the

reference has to be adjusted manually.
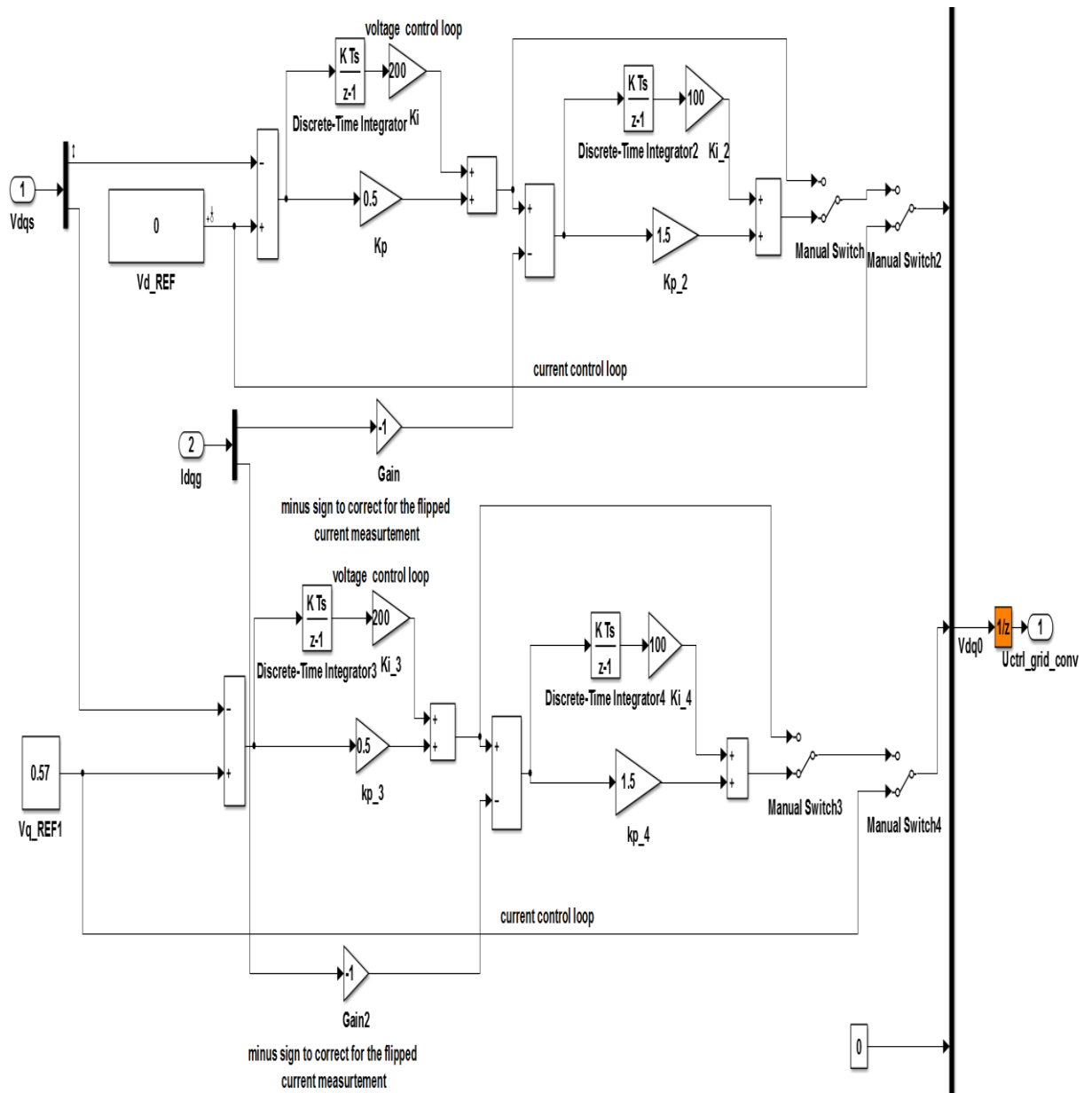
Fig. 4.22: Open loop control.

The step response of the system is shown in Fig. 4.23. It can be noted that the system reached steady state at 0.0025 sec. with a percentage overshoot of approximately 19.75%. The system has a gain margin equal to 8.7 dB, as shown in Fig. 2.24. The pole-zero map of the voltage control loop is shown in Fig. 4.25.
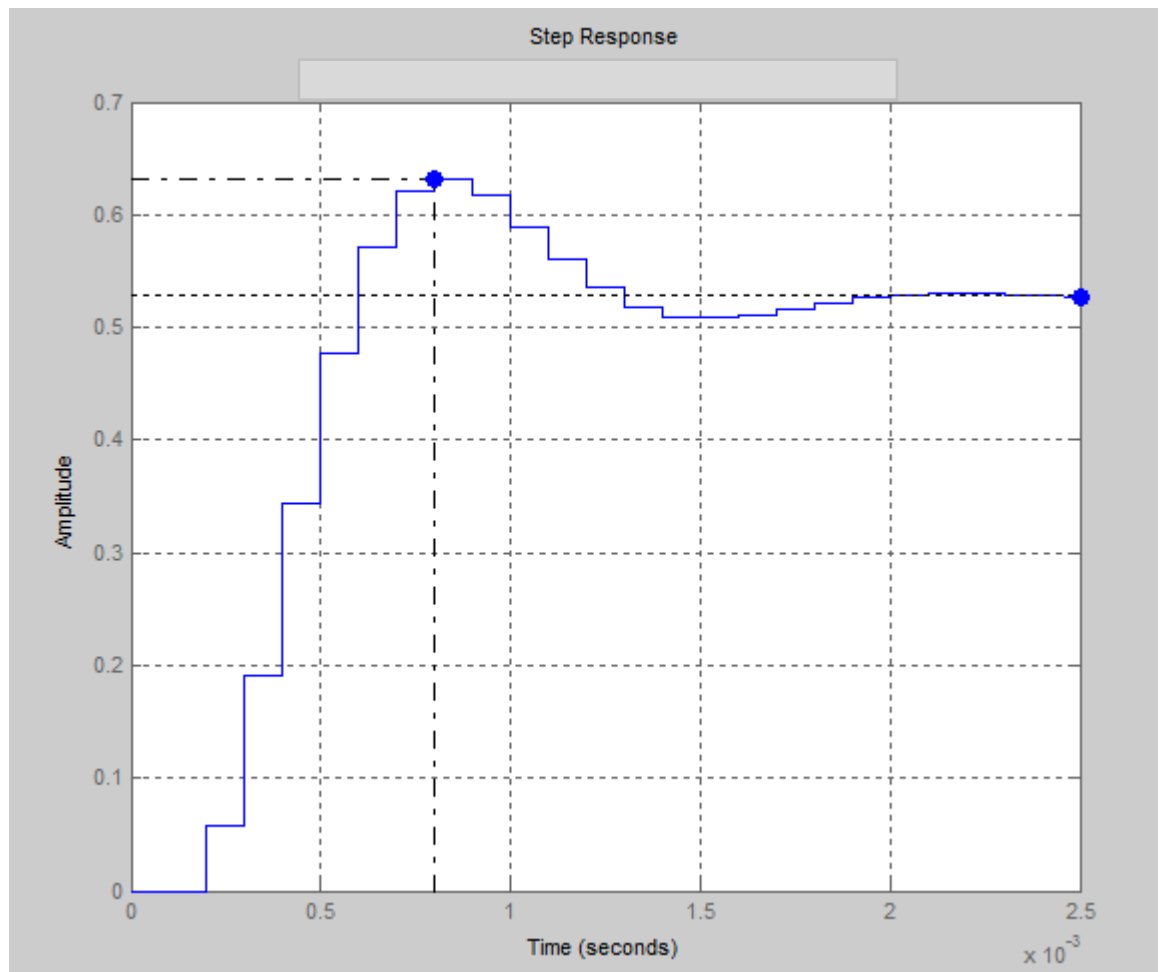
Fig. 4.23: Transient response of the open loop control.
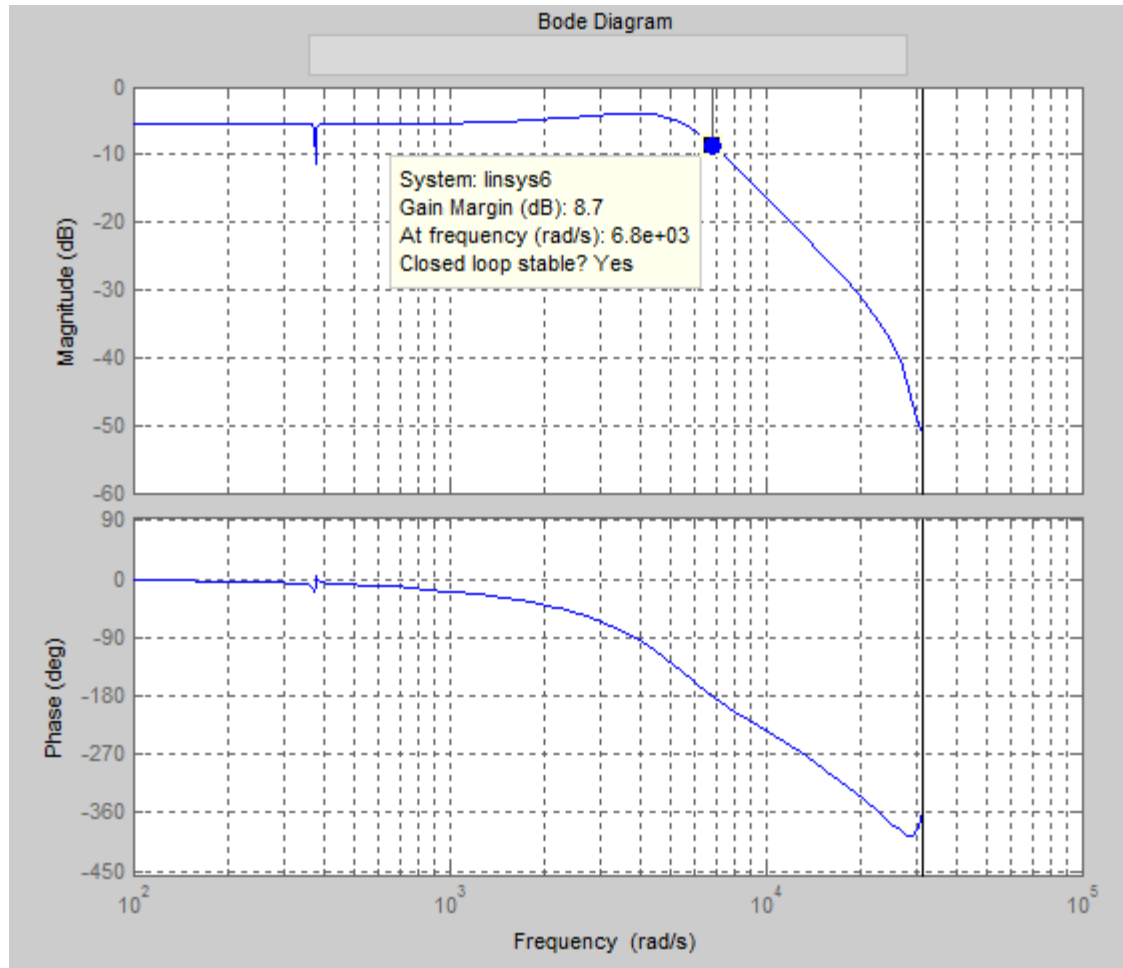
Fig. 4.24: open loop bode plot for the open loop control system
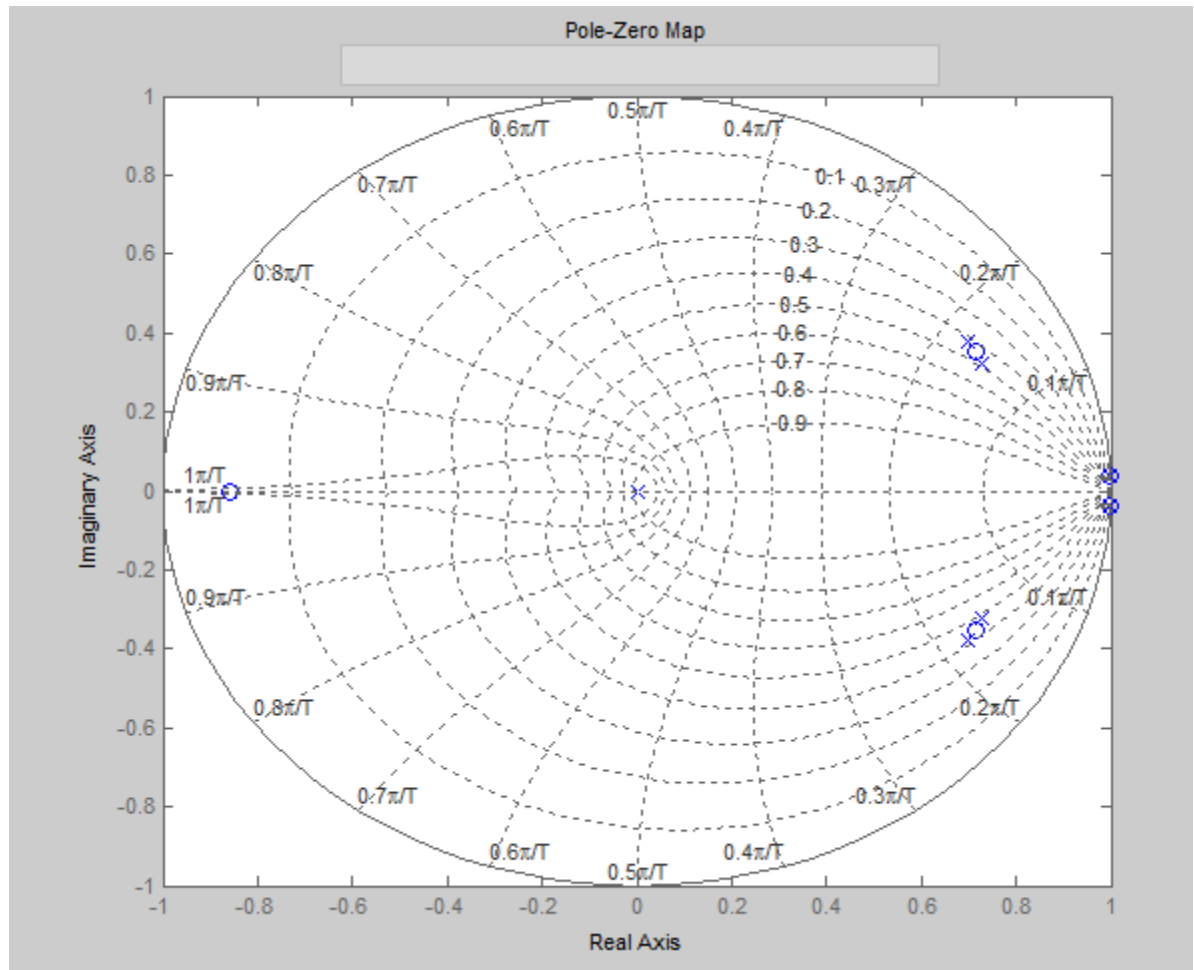
Fig. 4.25: Pole-Zero Map of open loop control.

The results shown in Fig. 4.15 to Fig. 4.25 demonstrate the system response to evaluate the dynamic of this microgrid and the performance of the entire system. In spite of the fact that the complexity of the closed loop system is higher than the open loop system, closed loop yields better results as shown in Table 4.4. The disadvantage of cascade loop is that it has overshoot around 5.75 % and slower response than close loop. On the other hand, cascade loop may provide better distribution rejection which is not studied in this analysis.

Loop	At Steady State	Overshoot %	Gain Margin (dB)	Phase Margin (degree)
closed voltage loop	0.07	0	14.5	103
closed outer voltage loop and inner current loop	0.14	5.75	6.85	84.8
open loop	0.0025	19.5	8.7	-

Table 4.4: Simulation results of signals analysis.

4.3 SUMMARY:

The control structures of an AC microgrid in stand-alone mode were investigated in this chapter by showing the simulations results. In addition, the filter of this type of grid was discussed in this chapter, as well as the reason for the simplification of the LCLfilter with the load. Finally, the microgrid performance was tested by using the simulation results of small signals analysis.

CHAPTER 5: MICROGRID SYSTEM IN STAND-ALONE APPLICATION WITH SHARING SOURCE

5.0   INTRODUCTION:

A large number of low voltage microgrids connected to the grid through the distribution and transportation systems is the future of the power supply system. In this situation, a new scenario is using small energy sources to create new supply systems, which is the microgrid. The use of this technique of power supply sources is not only to ensure the quality of the power supply but also to ensure more efficient use of the renewable energy resources [25].

In this chapter, power quality and power reliability are investigated. Their effects on a microgrid system are shown and discussed. In general, power quality events do not lead to electrical loss. Poor power quality can damage the power in the end-use processes, affecting equipment performance and durability [26]. Distributed energy sources have the potential to increase system reliability and power quality because of the regionalization of supply. The development in reliability levels can be obtained from DG.

The amalgamation of renewable energy sources into the power system arrange for unique challenges to the designers of the electrical system. The central generation is required to provide the base power supply, along with backup power, when the sun is not shining or the wind is not blowing because of the intermittent nature of the sources.

A microgrid with source sharing offers three major advantages over a microgrid without source sharing, as follows:

A. Supplies more utilities.

B. Provides better quality of power delivered to the requirements of the end
users.

C. Creates a more promising environment for energy efficiency and small-scale renewable generation investments.

D. Borrows or buys power from other users.

Therefore, a microgrid with source sharing is preferable. The majority of recent research illustrates the technical difficulty of efficient control of a microgrid with multiple sources sharing as a complete system. It is important to introduce approaches for the design of the control algorithms of a microgrid, as shown in Fig. 5.1. Functionally, a microgrid must operate within three control hierarchical levels:
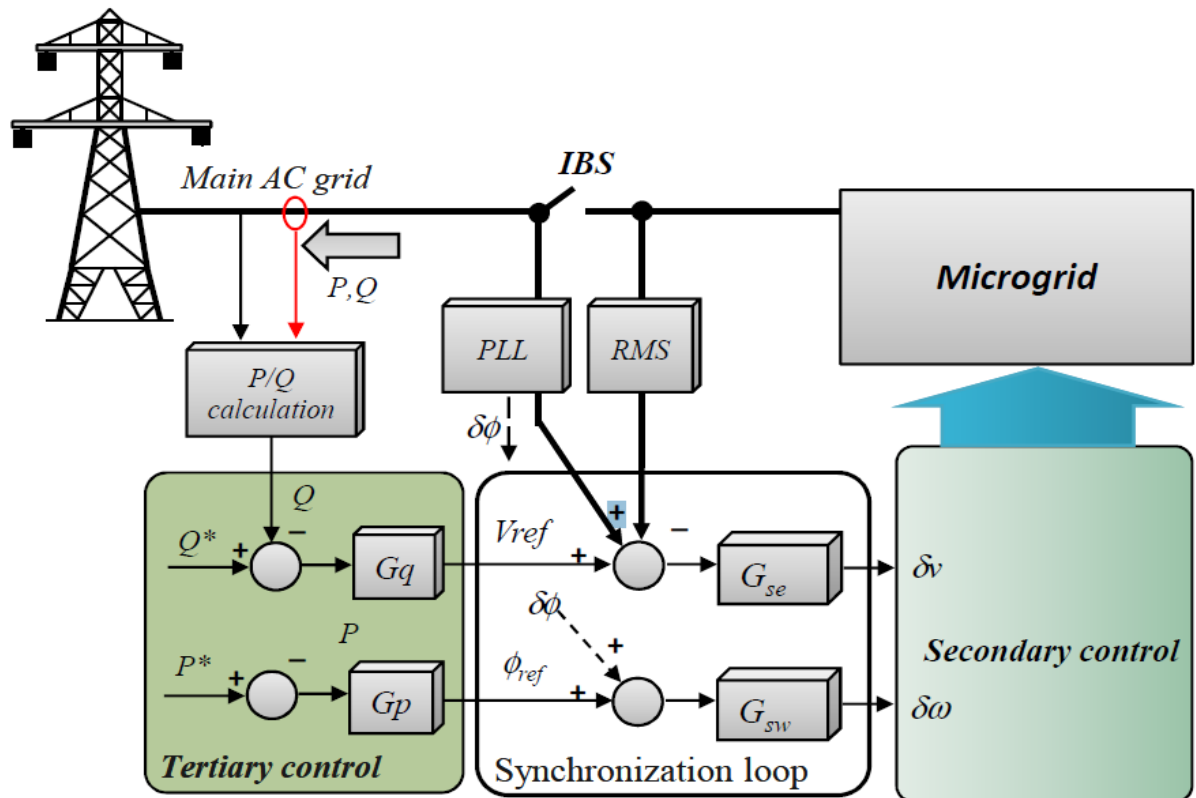
Fig. 5.1: Primary and secondary control of a microgrid with source sharing [2].

- **Primary Control: P/Q Droop Control:**

Droop control is a control strategy for distributed systems and is used in islanded microgrids. This control strategy is based on active and reactive power, which uses locally measured feedback to achieve load current sharing [24].

- **Secondary Control: Frequency-Voltage Restoration and Synchronization:**

This type of control has a supervisor system send signals using low-bandwidth communication to restore the microgrid voltage to nominal values. The power distribution over the control is based on the relationship between frequency and power, and it is implemented as a droop scheme. Similarly, frequency and voltage restoration to their nominal values have to be adjusted when a load change is realized. For some parallel sources, this displacement could not be produced equally because of the measured errors. Furthermore, if the power sources are connected in islanded mode through the main grid at different times, the load behavior could not be completely ensured since all of the initial conditions from the DGs are different [2].

- **Tertiary Control: P/Q Import and Export:**

This control is the adjustment of the references of the power converters and the generators to link them to the microgrid to achieve the maximum power point tracking. Consequently, the energy flow can be optimized. The set points of the microgrid inverters can be adjusted to control the power flow in global (the Microgrid imports/exports energy) or local terms (hierarchy of spending energy). Each controller must respond autonomously to the system changes without requiring load data, the *IBS,* or other

sources, as shown in Fig. 5.1. Therefore, the controller uses a power and voltage

feedback control based on the real-time measured values of P, Q, frequency, and AC

voltage to generate the desired voltage amplitude and phase angle by means of the droop

control [2].

The scope of this chapter focuses on primary control, which is the droop control

method. This system is shown in Fig. 5.2. Also, a review of droop control and power

flow are presented. Finally, model and design LCL-filter with a load are provided with

simulation results.
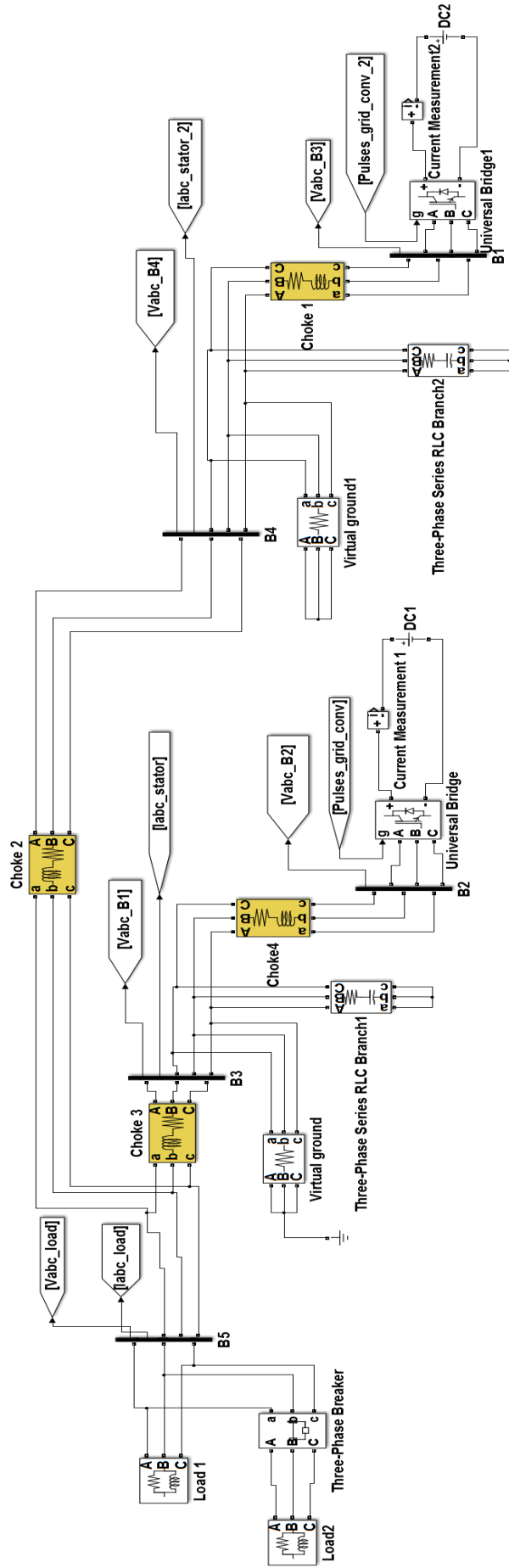
Fig. 5.2: Scheme of a microgrid sharing loads and sources.

5.1   DROOP CONTROL METHOD:

The control strategy for three-phase parallel DGs inverters is shown in Fig. 5.2. This method is introduced with the proposed inductance since it is more robust, and also deals with coupling the frequency and the amplitude related to active and reactive power.

A stability study is provided for designing the droop coefficients and the inductance. This section is divided into four parts:

1. The concept of control theory is presented for connecting the AC power units in parallel.

2. An inductor is implemented in a power sharing loop to accomplish precise load current sharing.

3. States space model is used to analyze the stability of the system.

4. Simulations are conducted to verify the efficiency of this control approach.

First, Droop Control Method:

The two DC sources are converted into AC sources and connected with a common AC bus, as shown in Fig. 5.2. The equivalent circuit of the Fig. 5.2 is shown in Fig. 5.3,

where:

$V = V \angle 0$ is the voltage of the common AC bus.

$E = E \angle \emptyset$ is the output voltage of the inverter.

$\emptyset$ is the phase angle between the inverter and the common AC bus.

$\overline{Z}$ is the transmission line impedance.

θ is the phase angle of the transmission line impedance.
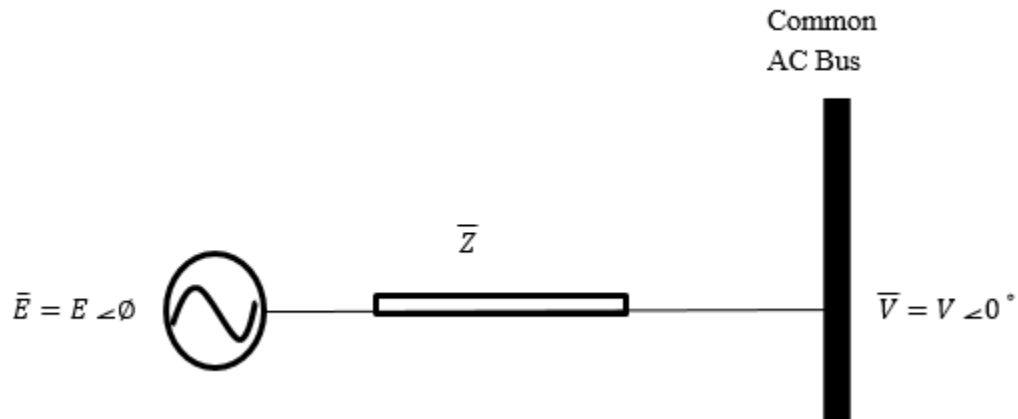
Fig. 5.3: Equivalent circuit of parallel AC source.

As seen from Fig. 5.2, the apparent power can be expressed as follows [22]:

$$S = P + jQ = V I^*$$

$$= V \left(\frac{E_{\angle\emptyset} - V_{\angle 0}}{\overline{Z}}\right)^*$$

$$= V \left(\frac{E*e^{j\emptyset} - V}{\overline{Z}}\right)^*$$

$$= V \left(\frac{E(cos\emptyset + jsin\emptyset) - V}{Ze^{j\emptyset}}\right)$$

$$= V \left(\frac{E(cos\emptyset + jsin\emptyset) - V}{Z}\right) * (cos\theta + jsin\theta)$$

$$S = V \left(\frac{(Ecos\emptyset - V)cos\theta + EVsin\emptyset sin\theta)}{Z}\right) + jV \left(\frac{(Ecos\emptyset - V)sin\theta - EVsin\emptyset cos\theta}{Z}\right) \qquad (5.1)$$

From 5.1:

$$P = V \left(\frac{(Ecos\emptyset - V)cos\theta + EVsin\emptyset sin\theta)}{Z}\right)$$

$$Q = V \left(\frac{(Ecos\emptyset - V)sin\theta - EVsin\emptyset cos\theta}{Z}\right)$$

$$P = V \left(\frac{E - V}{Z}\right) cos\theta + \left(\frac{EV.\emptyset}{Z}\right) sin\theta$$

$$Q = V\left(\frac{E-V}{Z}\right)\sin\theta - \left(\frac{EV.\emptyset}{Z}\right)\cos\theta$$

Then,

$$P = V\left(\frac{E-V}{Z}\right)\cos\theta \left(\frac{EV.\emptyset}{Z}\right)\sin\theta$$

$$Q = V\left(\frac{E-V}{Z}\right)\sin\theta - \left(\frac{EV.\emptyset}{Z}\right)\cos\theta \tag{5.2}$$

From (5.2) when $\emptyset$ is too small, we can make these assumptions:

$$\sin\emptyset = \emptyset \ and \ \cos\emptyset = 1$$

$$V(E - V) = Z\ (P\cos\theta + Q\sin\theta) \tag{5.3}$$

$$EV.\emptyset = Z\ (P\sin\theta - Q\cos\theta) \tag{5.4}$$

Power angle is provided the active power *(P-ω)* while output voltage is provided the reactive

Power *(Q-E)*

Then this relation can be expressed as follow:

$$\omega = \omega^* - mP \ \& \ E = E^* - nQ \tag{5.5}$$

From Fig. 5.4, calculating the slopes:

$$\frac{\omega - \omega^*}{P - P^*} = m \tag{5.6}$$

$$\omega = \omega^* - m(P - P^*)$$

Likewise:

$$\frac{E - E^*}{Q - Q^*} = n \tag{5.7}$$

$$E = E^* - n(Q - Q^*)$$

Where ω and E^* are the frequency and the amplitude of the output voltage. m and n

coefficients define the corresponding slopes. P^* and Q^* are the active and reactive power

references.
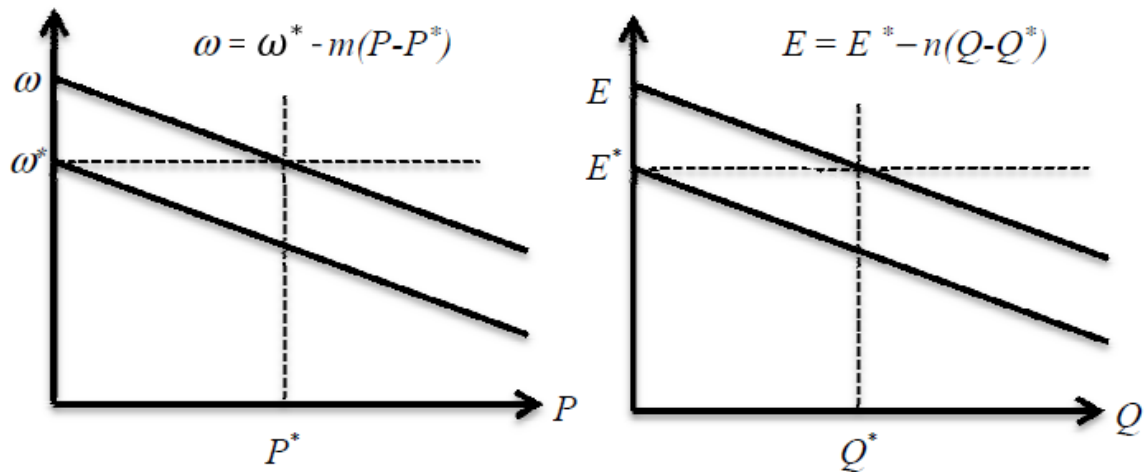
Fig. 5.4: The droop control method.

Second , Power Sharing Loop:

By using the instantaneous power theory, active power p and reactive power q can

be written as:

$$p = v_d \, i_{od} + uv_q i_{oq} \tag{5.8}$$

$$q = v_q \, i_{od} - v_d i_{oq} \tag{5.9}$$

Where, uv_d , v_q , i_{od} and i_{oq}, are the three-phase output voltages and the load currents

obtained from the Park transformation, respectively.

The active and reactive power of the fundamental components are obtained by a

low-pass filter to allow for a necessary time-scale separation between the power sharing

loop and the voltage control loop [28], as follows:

$$P_{filter} = \frac{w_c}{s+w_c} \, p \tag{5.10}$$

$$Q_{filter} = \frac{w_c}{s+w_c} q \tag{5.11}$$

Where w_C is the cutoff frequency.

P and Q are the active and reactive power respectively of the fundamental components.

p and q are the instantaneous active and reactive power.

The voltage reference of the inverter in the *d-q* synchronous rotating frame is represented as

$$[V_{dref} \ V_{qref}]^T = [V_{drf} \ 0 \ ]^T \tag{5.12}$$

Where V_{ref} is the reference of the output voltage amplitude obtained from the park transformation. Therefore, the $P - \omega$ and $Q - E$ method under *d-q* frame is written by:

$$\omega = \omega^* - mP$$

$$V_{dref} = V_{ref} - nQ$$

$$V_{qref} = 0 \tag{5.13}$$

Third, Power Flow Analysis of Islanding Mode:

A mathematical model is given in this sub-section. General transmission line impedance is considered in this derivation. A small signal analysis is completed to analyze the stability of the system, as shown in Fig. 5.3:

$$I^* = \frac{\bar{E}-\bar{V}}{JX} = \frac{E_d+JE_q-V_d-JV_q}{JX}$$

$$I_d + JI_q = \frac{(E_d-V_d)+J(E_q-V_q)}{JX}$$

$$I_d + JI_q = \frac{-J(E_d-V_d)}{X} + \frac{J(E_q-V_q)}{X}$$

$$I_d = \frac{E_q-V_q}{X} \ , I_q = \frac{E_d-V_d}{X} \ , P = V_d(\frac{E_q-V_q}{X}) - V_q(\frac{E_d-V_d}{X})$$

$$I_d + JI_q = \frac{\bar{E} - \bar{V}}{\bar{Z}}$$

$$= \frac{(e_d - je_q) - V}{\bar{Z}}$$

$$= \frac{(e_d - je_q) - V}{Z}(cos\theta + Jsin\theta)$$

$$= \frac{(e_d - V) + je_q}{Z}(cos\theta + Jsin\theta)$$

$$i_{od} = \frac{1}{Z}(e_d - V)cos\theta + e_q sin\theta)$$

$$i_{oq} = \frac{-1}{Z}(e_d - V)sin\theta - e_q cos\theta) \tag{5.15}$$

Now, by linearizing the (5.15) for i_{od} and i_{oq} :

$$\Delta i_{od} = \frac{1}{Z}(\Delta e_d)cos\theta + \Delta e_q sin\theta)$$

$$\Delta i_{oq} = \frac{-1}{Z}(\Delta e_d)sin\theta - \Delta e_q cos\theta) \tag{5.16}$$

$$P + jQ = V(i_{od} + ji_{oq})^* = Vi_{od} - jVi_{oq} \tag{5.17}$$

Now linearize (5.17) gives:

$$\Delta p = V \Delta i_{od} = \frac{1}{Z}(V.\Delta e_d)cos\theta + V.\Delta e_q sin\theta)$$

$$\Delta q = -V \Delta i_{oq} = \frac{1}{Z}(V.\Delta e_d)sin\theta + V.\Delta e_q cos\theta) \tag{5.18}$$

Assuming that the output voltage achieves zero error tracking, thus $e_d = V_{dref}$ and

$e_q = V_{qref}$.

By linearizing (5.5), the dynamic of the proposed control strategy can be written as:

$$\Delta \omega = -\frac{w_c}{s + w_c} m \Delta p$$

$$\Delta e_d = -n\frac{w_c}{s + w_c} \Delta q \tag{5.19}$$

Since $\Delta \omega = \Delta \emptyset$, substituting (5.18) into (5.19) yields:

$$\Delta \ddot{\emptyset} + \omega_c . \Delta \dot{\emptyset} = -m. \omega_c \Delta p$$

$$\Delta \dot{e}_d + \omega_c \cdot \Delta e_d = -n \cdot \omega_c \Delta q$$

$$\Delta \dot{e}_q + \omega_c \cdot \Delta e_q \qquad (5.20)$$

Where, $\emptyset = \tan^{-1} \frac{e_q}{e_d}$ \qquad (5.21)

By linearizing $\emptyset$ yields:

$$\Delta \emptyset = -e_q \Delta \frac{e_d}{e_d^2 + e_q^2} + e_d \Delta \frac{e_q}{e_d^2 + e_q^2} \qquad (5.22)$$

Solve 5.22 for Δe_q :

$$\Delta e_q = \frac{e_d^2 + e_q^2}{e_d} + \Delta \emptyset \frac{e_q}{e_d} \Delta e_d \qquad (5.23)$$

Based on (5.16), (5.18), (5.20), and (5.23) and assume that $= \frac{\pi}{2}$, the state space equation

for the system is written as:

$$\begin{bmatrix} \Delta \dot{\emptyset} \\ \Delta \ddot{\emptyset} \\ \Delta \dot{e}_d \end{bmatrix} = \begin{bmatrix} 0 & 1 & 0 \\ \frac{-mVw_c}{z} & w_c & \frac{-mVe_qW_C}{Ze_d} \\ 0 & 0 & \frac{-w_c - nVw_c}{z} \end{bmatrix} \begin{bmatrix} \Delta \emptyset \\ \Delta \dot{\emptyset} \\ \Delta e_d \end{bmatrix} \qquad (5.24)$$

Forth, Simulations are conducted to Verify the Efficiency of This Control

Approach:

Equation (5.24) expresses the state space model of the system $\dot{x} = Ax$. To

investigate the stability of the system, the characteristic equation $/ sI - A /=0$ displays the

system root and poles location. Further increasing or decreasing the droop control

coefficients with the impedance L values causes the system to be over damped, and

change the pole and zero locations, which results in instability.

$V_{(L-L)}$	480 V
e_d	360 V
e_q	83.1384 V
L	400 $\mu\,H$
m	5 m
n	0.4 m
f	60 Hz
w_c	2πf

Table 5.1: Simulation parameters.

When the coefficients n = 0.0004, m = 0.005, and L = 400 $\mu\,H$, the overshoot of

the pole is 68%, and the damping ratio is 0.11, as shown in Fig. 5.5. On the other hand,

when the value of L is increased to 400 $m\,H$, the overshoot became zero and the damping

ratio is one, as shown in Fig. 5.6. Hence, L should be designed to satisfy the desired

damping performance in order to ensure the stability and share the load current among

the units. Finally, when coefficients values changed to be n = 30, m = 40 and L = 400 μ,

the overshoot of the pole is 99.6%, and the damping ratio is 0.00132, as shown in Fig.

5.7, which may cause instability to the system. Therefore, the droop control coefficients

must be considered in the design according to the desired power flow.
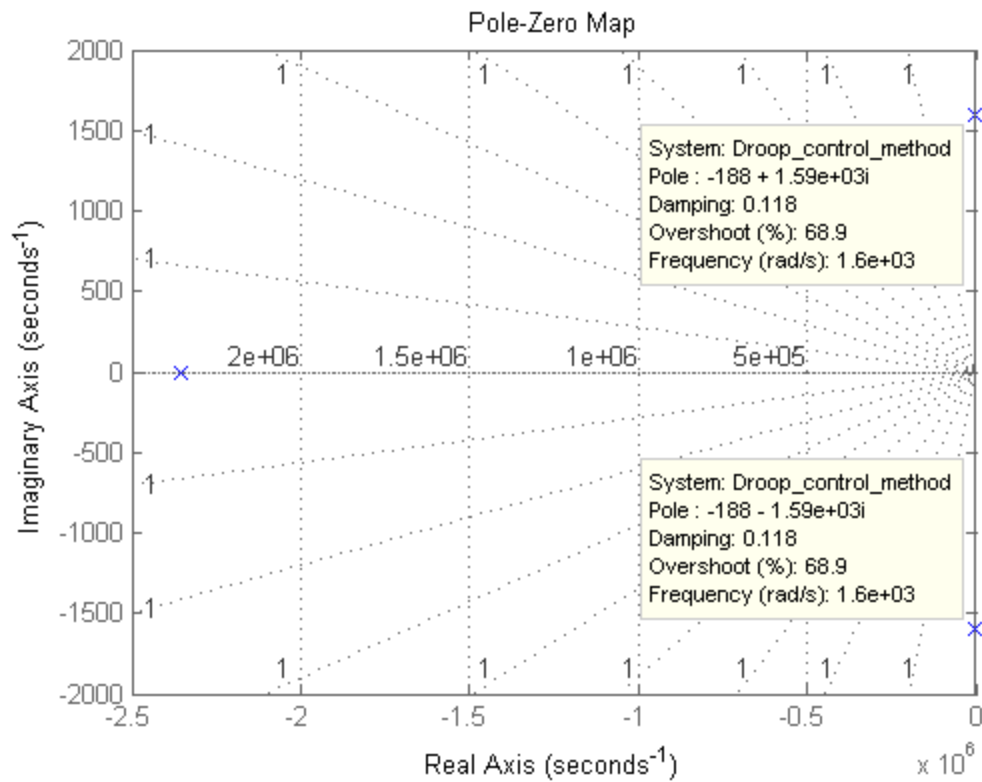
Fig. 5.5: Pole-Zero Maps when L= 400μ , m = 0.005 and n =0.0004
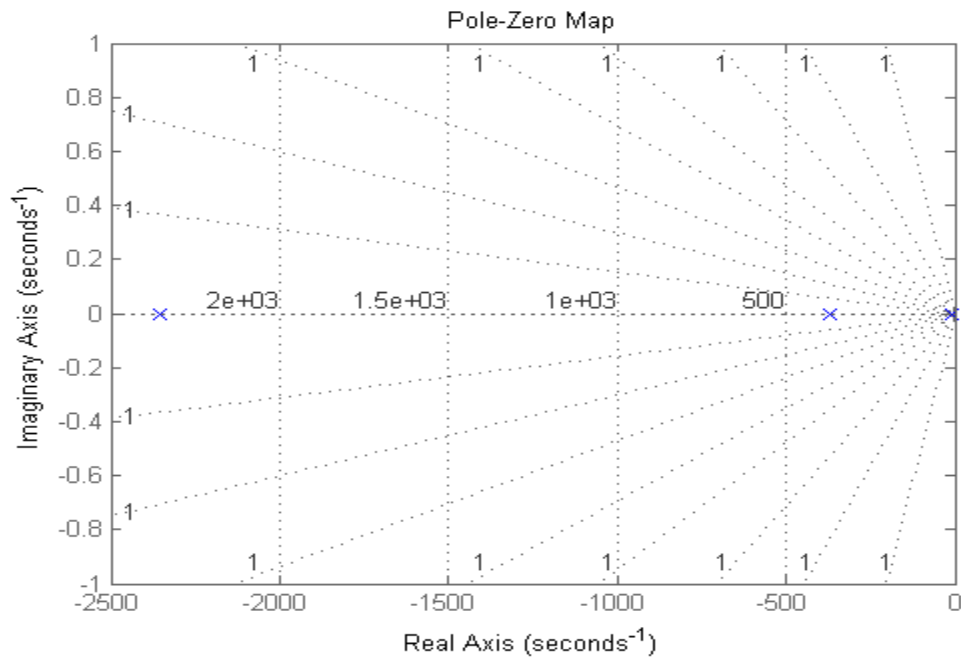
Fig. 5.6: Pole-Zero Map when L= 400 *m* , m = 0.005 and n =0.0004
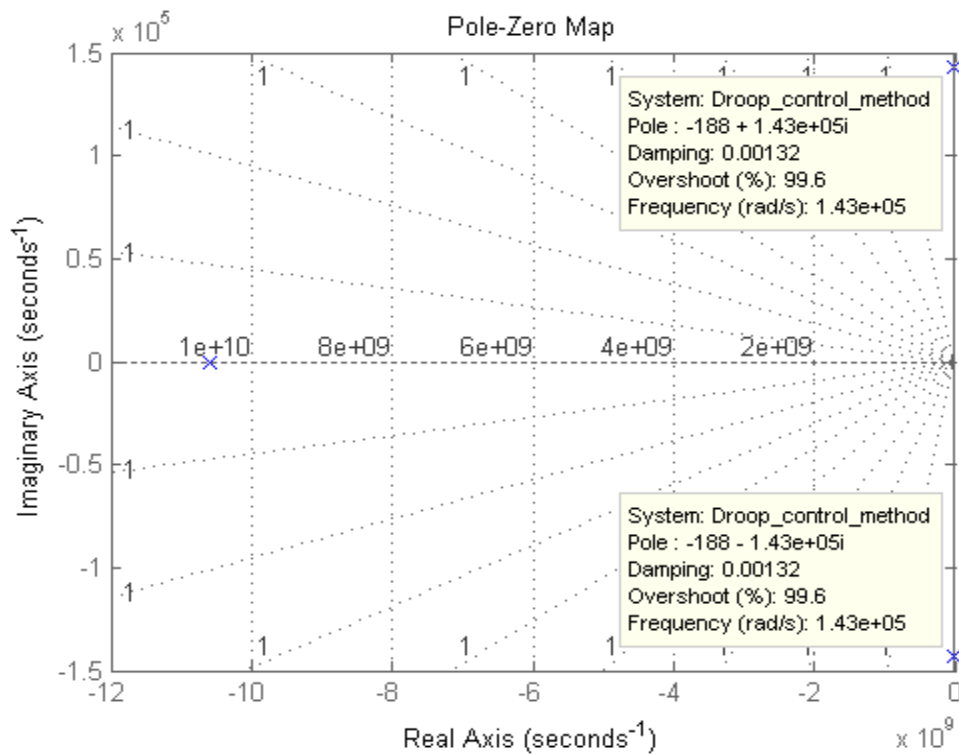
Fig. 5.7: Pole-Zero Map when L= 400µ , m = 40 and n =30

The simulation results of the two paralleled converters are shown in Fig. 5.2. The

output waveform of the currents and voltages are stable for both power converters. From

Fig. 5.8a and Fig. 5.9a, the peak current is 271 A at 0.61 sec. In addition, from Fig. 5.8b

and Fig. 5.9b, the peak voltage is 392 V at 0.62 sec. These results show that by using the

droop control method, the system illustrates the stability with reasonable values of the

coefficients n and m. The most important parameter to be considered is the inductance

since it has major effect in the droop control method as the aforementioned concerns in

this chapter.

In order to identify the importance of   DCM , . Fig 5.10a and Fig 5.11a are

shown the currents for DG1 and DG2 without using DCM. In , additions , Fig 5.10b and

Fig 5.11b are shown the voltages for DG1 and DG2 without using DCM . These figures show the highly distorted currents waveform and voltage waveform when DCM is not used.
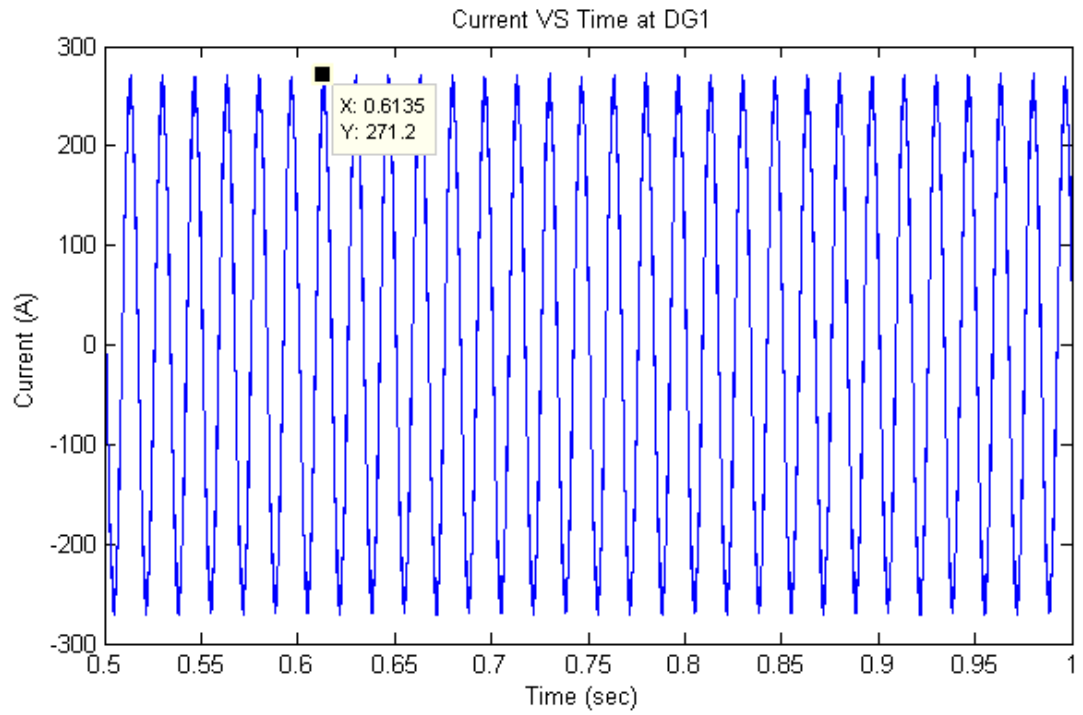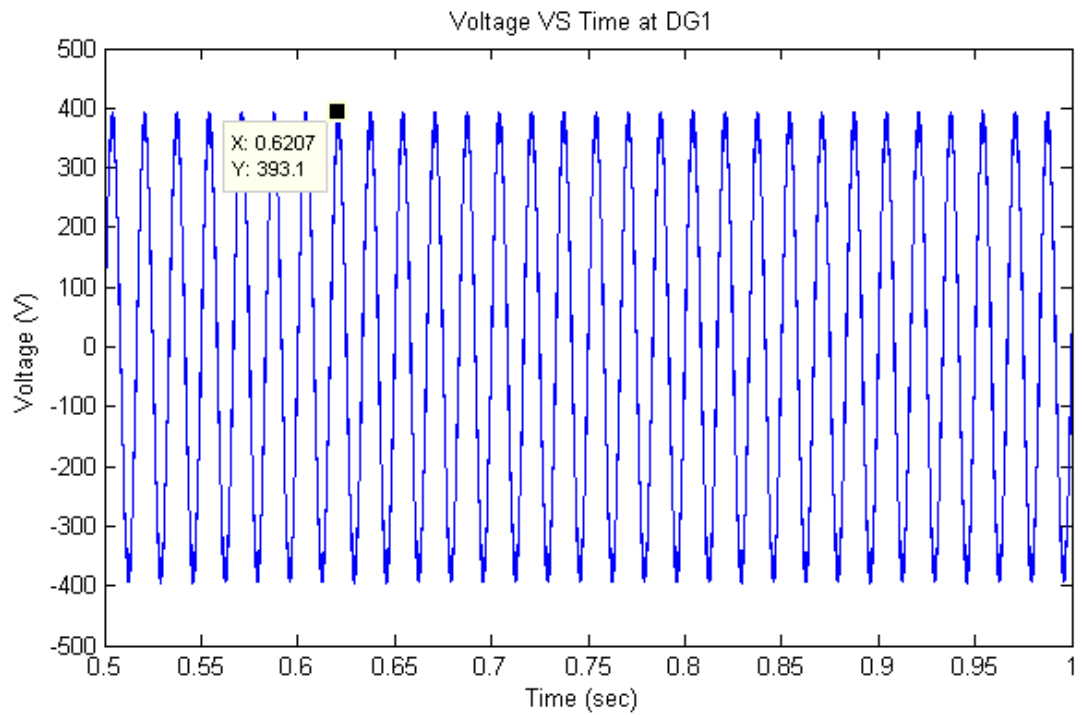
Fig. 5.8: a) current and b) voltage at DG1.
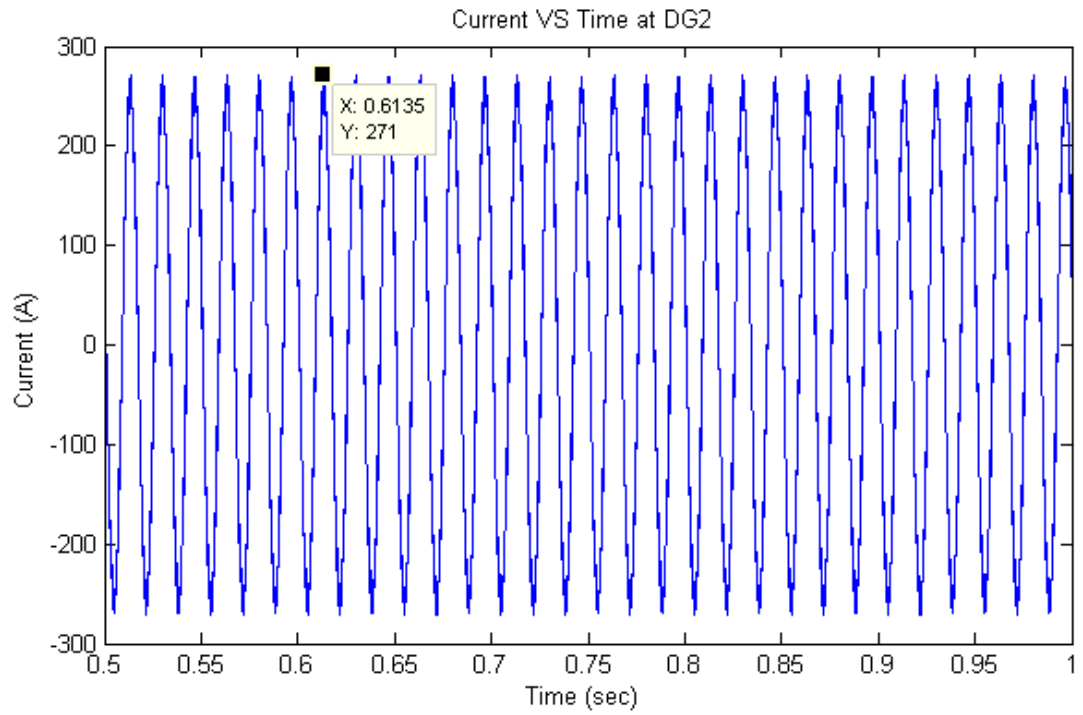
a)
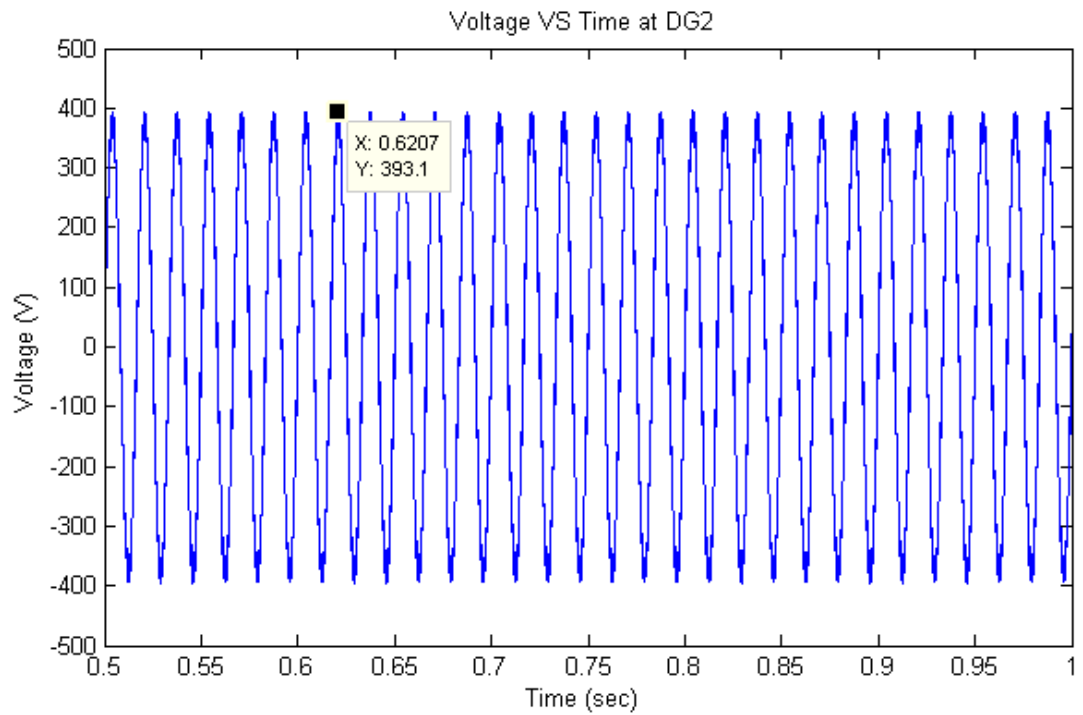
b)

Fig. 5.9: a) current and b) voltage at DG2.
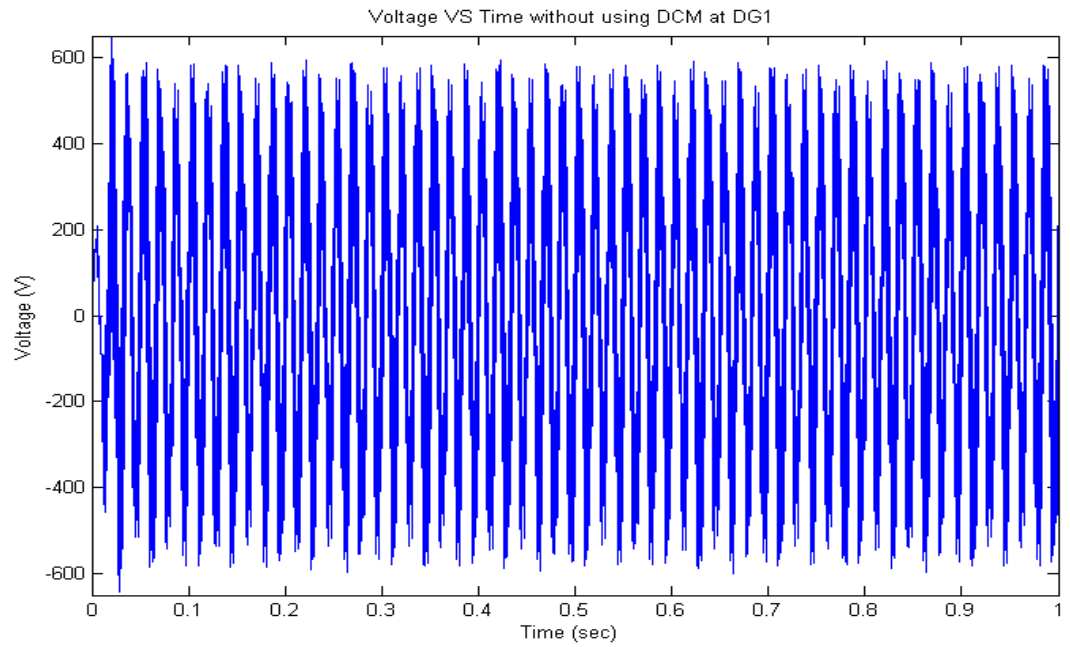
a)
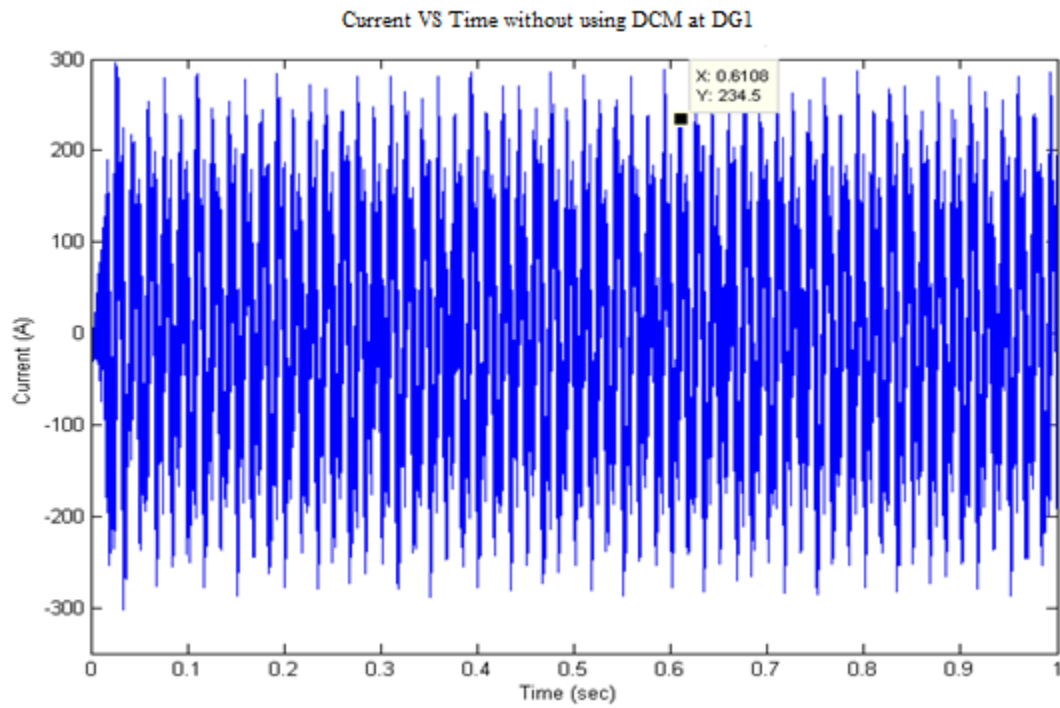
b)

Fig. 5.10: a) current and b) voltage without using DCM at DG1.
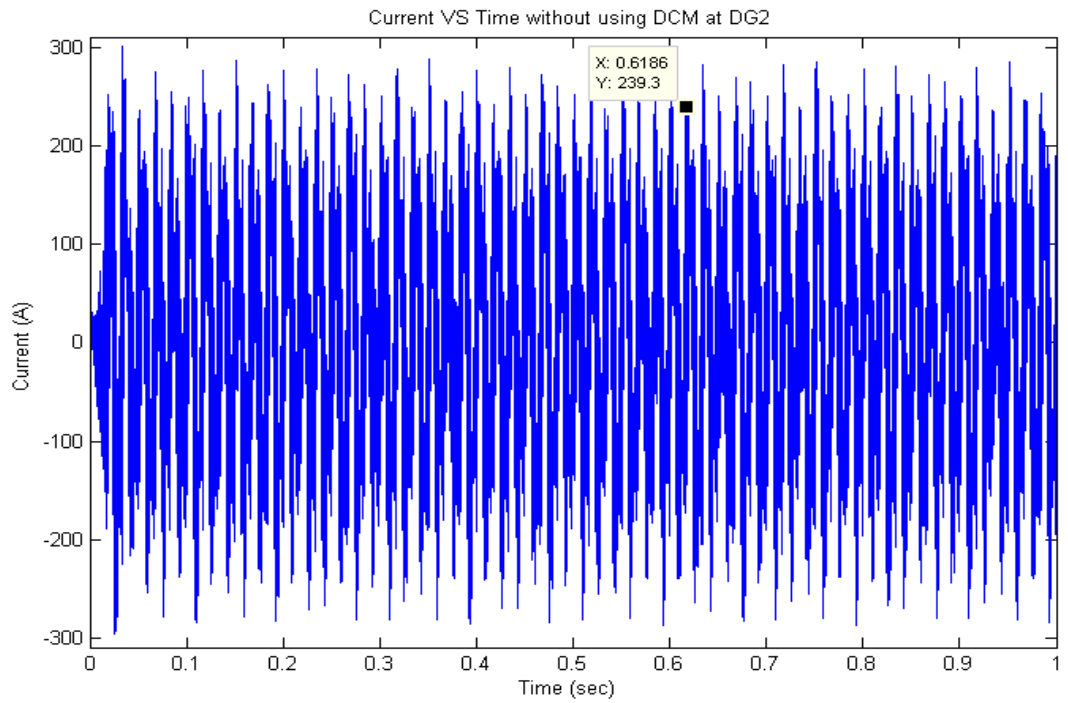
a)
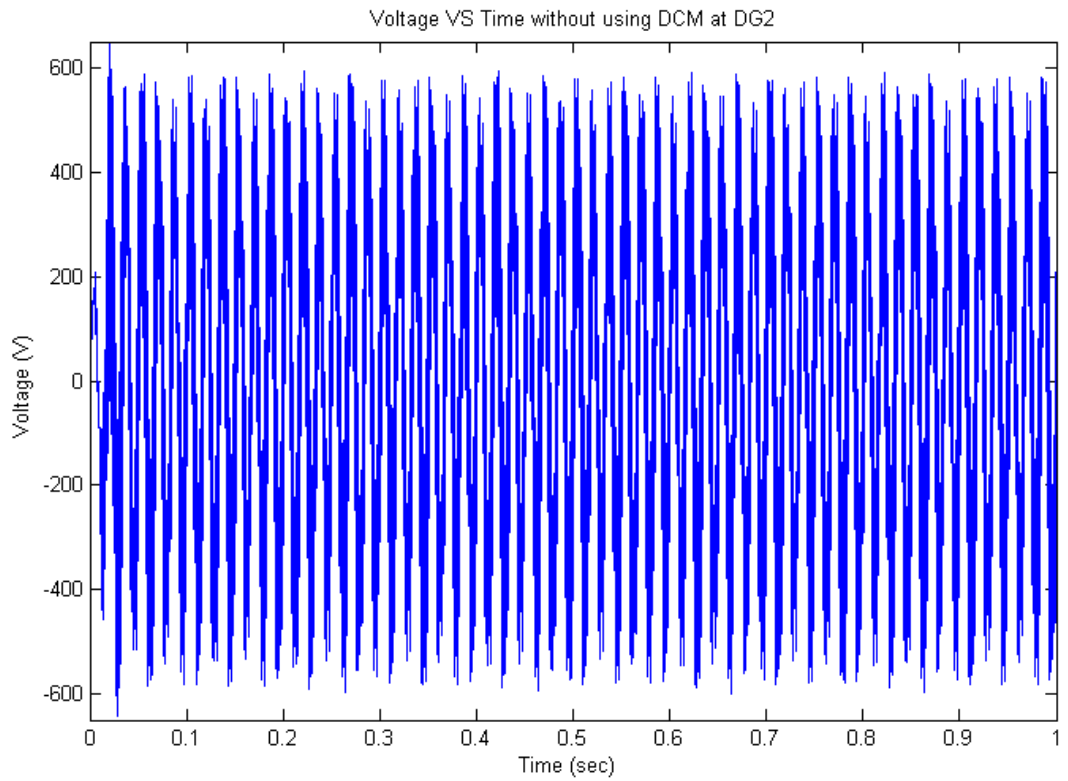
b)

Fig. 5.11: a) current and b) voltage without using DCM at DG2.

5.2   SUMMARY:

The method of sharing the output current among paralleled inverters suitable for DG systems was introduced in this chapter. An inductor implementation in the synchronous d-q frame was discussed. In this microgrid, the output current is perfectly shared among the inverters. Finally, a model and design LCL-filter was provided with simulation results.

CHAPTER 6: CONCLUSION AND FUTURE WORK

6.0. CONCLUSION:

The main contributions of the this thesis is to provide analysis of power converter control techniques in an AC smart grid for microgrid applications. Power converters have an outstanding potential in smart grid and microgrid applications that require flexible and fast power control, as well as rigid voltage regulation at the point of common coupling. Power converters are required to properly operate under several modes of operation such as grid-tie and microgrid modes of operations.

In Chapter 2, the control system was designed to enable proper load sharing between several units. Several control techniques have been proposed in the literature to address most of the control requirements of the power converters under different operating modes. These control techniques are divided into three types:

1.   Voltage Oriented Control (VOC).

2.   Direct Power Control (DPC).

3.   Virtual Direct Torque Control (VDTC).

Also, details of the VOC were introduced and compared to the DPC and VDTC.

In Chapters 3 and 4, a detailed investigation of power converter control techniques in grid-tie and AC smart grid and microgrid applications were introduced. This analysis was based on detailed nonlinear time domain simulation, as well as average and small signal models for system stability assessment and performance evaluation. The filter of smart grid and microgrid was investigated by using detailed time domain simulations and the state space technique to model the control system.

Furthermore, the stability of the converter control system, including the outer, inner, open, and closed loop was discussed in Chapters 3 and 4.

In addition, the controllers and the impact of the different objectives for active and reactive power control were investigated in Chapter 3. This control was based on the transformation from *abc* frame of reference to *dq* frame of reference. The current controller is the inner control loop, which corrects the error between the reference, and the measured currents values for this two axis. The references are provided by the voltage controller.

The comprehensive study presented here combines an analysis of the power converters' control and power flow in stand-alone mode, using the droop control method.

6.1. FUTURE WORK:

A. Hierarchical Control of AC Microgrids:

Although, the control technology of power converters in AC smart grid and microgrid applications was developed several decades ago, more intelligent control approaches need to be developed. For example, multiple power-generation systems based on different technologies and power ratings are interconnected in a microgrid. Therefore, it is required to implement a hierarchical control structure to reduce the operation cost, while making best use of efficiency, reliability, and controllability. The main issues to be considered when determining the optimum operation point of a microgrid are power ratings, distribution of loads and generation systems, electrical market prices, generation costs, and energy availability from primary sources [28]–[29]. Consequently, the

hierarchical control of microgrids can be systematized into three main layers. They are primary, secondary, and tertiary control, as presented in Fig. 6.2. Some extra ancillary services, the majority of them implemented locally in the generation units, are shown in Fig. 6.1.

The primary control is devoted to control local variables, such as frequency and voltage as explained in Chapter 5. In this thesis the local controllers were not dealing with implementing virtual impedance in designing the droop control techniques. However, the method of using virtual inductance is considered for future work since it is more robust and also deals with the coupling of the frequency and the amplitude related to active and reactive power.

The virtual impedance control is a line current feed-forward. It is added to the DG voltage reference..

In fact, when the output impedance is resistive, the $P - \omega$ and $Q - E$ droop control is not effective. A virtual inductor is proposed to improve the output impedance features [12]. Therefore, the output impedance is designed for the inverters to accomplish precise load current sharing and an elimination of the harmonic voltage distortion. For three-phase inverters transformed in the synchronous reference frame, the voltage and current vectors are shown in Fig. 6.1. The voltage drop across the inductor leads the current by 90° and it is written by:

$$V_{dLg} + jV_{qLg} = j\omega \, L_g\left(i_{od} + Ji_{oq}\right) = -\omega L_g i_{oq} + Jwi_{od}$$

Then:

$$V_{dLg} = -\omega L_g \, i_{oq}$$

$$V_{qLg} = -\omega L_g \, i_{od} \qquad\qquad\qquad (6.1)$$
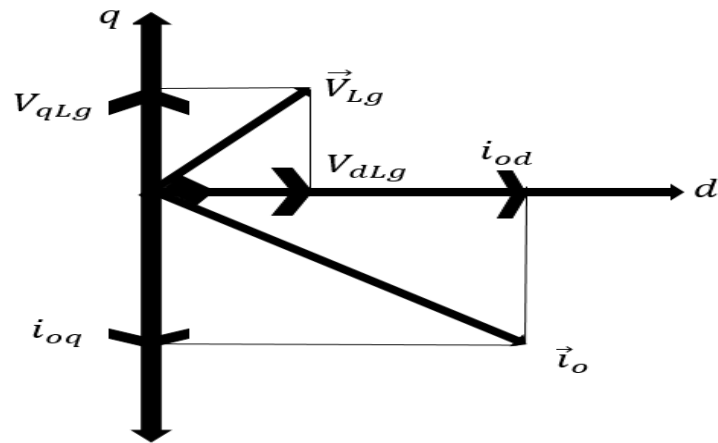
Fig. 6.1: Phase diagram d-q frame.

The secondary control acts as an automatic generation controller since it restores the steady-state errors in the microgrid voltage and frequency to their nominal values. Moreover, the secondary control is in charge of controlling the voltage profile in the AC buses to keep it within its operational limits at any point of the microgrid [3].

The tertiary control level is in charge of optimizing the microgrid operation and setting its interaction with the distribution network by regulating the active and reactive power references for all DGs unit [3]. This control is usually based on financial criteria since it considers the relationship between the energy supply balance and demand with the marginal generation cost of all DG units. The approximation in the short-term load changes the generation forecast and energy storage capability, along with the specific demands set by the Transmission System Operators (TSO) and the prize signals provided by the electrical market [29]. Furthermore, the tertiary control level is in charge of restoring the secondary control reserve, managing eventual congestions, and providing

support to the secondary control if needed [3]. In this thesis, the investigation details were given for primary control only. However, it is planned for future work to investigate in-depth the secondary and tertiary control, as well.
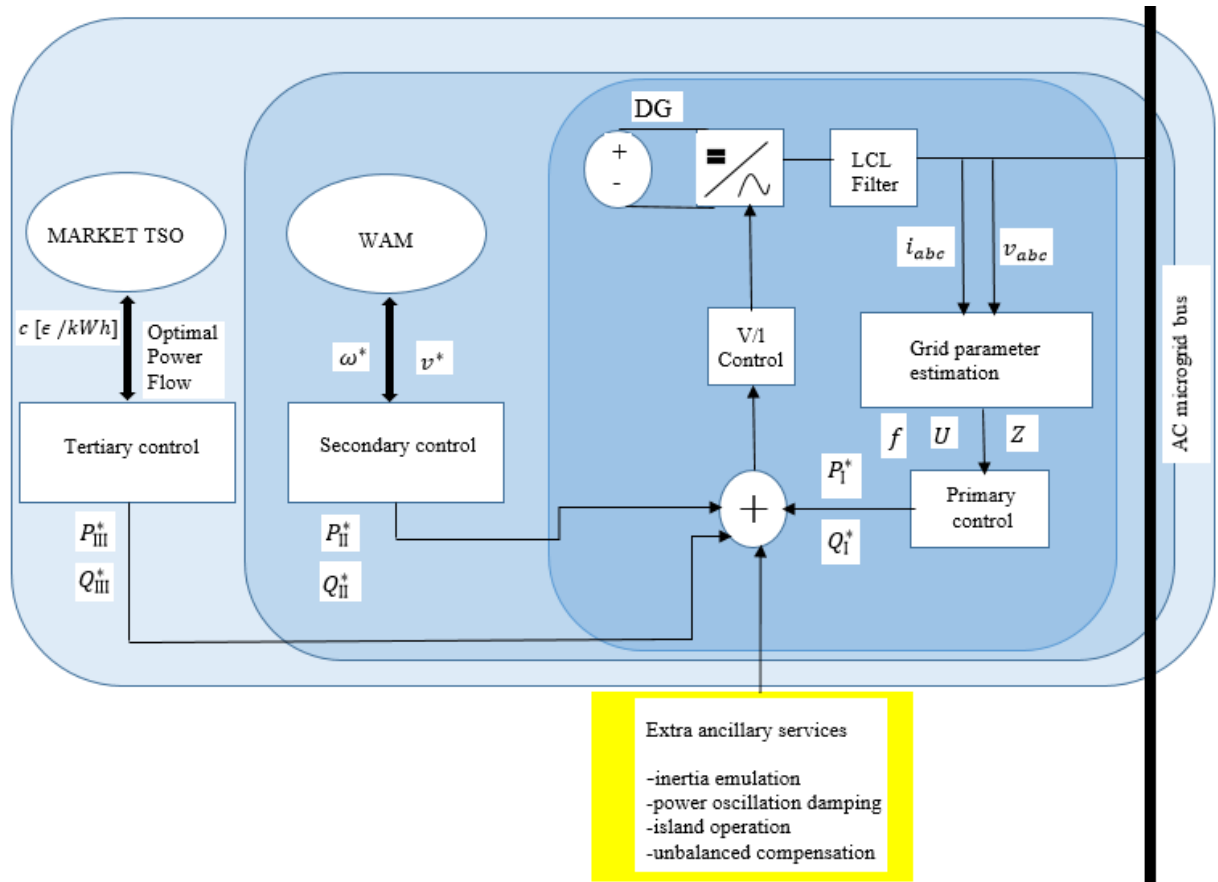
Fig. 6.2: Block diagram of primary, secondary, and tertiary microgrid control.

B. DC Microgrid:

A majority of research focuses on AC smart grid and microgrid while DC smart grid and microgrid have not been considered recently. Although a majority of our buildings have devices that internally operate on a DC power source, we still plug these

devices into a typical AC power source outlet, and then convert AC to DC to operate the devices. This process of conversion wastes energy because it is not 100 % efficient.

These days, many newly constructed buildings are deploying renewable energy sources, such as solar, which generate DC power. Since these buildings have a large number of DC-powered devices, the need for a DC microgrid is increasing in order to eliminate the conversion waste and maximize the use of DC power generated by renewables. Therefore, investigation and development of the DC microgrid is considered for future future work.

BIBLIOGRAPHY

[1] Keyhani, A. (2011). *Design of Smart Power Grid Renewable Energy Systems.* Hoboken: John Wiley & Sons, Inc.

[2] V´asquez, Q. J. (2009, June 10). *Decentralized Control Techniques Applied to Electric Power Distributed Generation in Microgrids*. Barcelona, Spain.

[3] Rocabert, Joan, Alvaro Luna, Frede Blaabjerg, and Pedro Rodriguez. (2012, November 11). *Control of Power Converters in AC Microgrids.* pp. 4734-4749. IEEE TRANSACTIONS ON POWER ELECTRONICS, VOL. 27, NO. 11. Retrieved from IEEE: ieee.org.

[4] Tedorescu, R., M. Liserre, and P. Rodriguez. (2011). *Grid Converters for Photovoltaic and Wind Power Systems.* West Sussex: John Wiley & Sons, Ltd.

[5] Larminie, James (1 May 2003). *Fuel Cell Systems Explained, Second Edition*. SAE International. ISBN 0-7680-1259-7.

[6] Mohan, M. (2006). *First Course on Power System.* Minneapolis: MNPERE.

[7] Ringwald, A. (2009, July 13). *Theenergy Collective.* Retrieved from http://theenergycollective.com/watthead/28514/smart-microgrids-discussing-efficient-energy-management-solutions-valence-energy.

[8] Sanjuan, S. L. (2010). *Voltage Oriented Control of Three-Phase.* Göteborg, Sweden. 10- Masters G., "Renewable and Efficient Electric Power Systems", John Wiley & Sons Inc., 2004. Dr. Dan M. Ionel, Renewable Energy Module, Spring 2012, Part 5.

[9] M. Liserre, A. Dell'Aquila, and F. Blaabjerg. "Genetic Algorithm-Based Design of the Active Damping for an LCL-Filter Three-Phase Active Rectifier" Power Electronics, *IEEE Transactions on power electronics,* Volume 19, No 1, Jan. 2004: 76-86.

[10] M. Liserre, A. Dell'Aquila, and F. Blaabjerg. *"Design and Control of an LCL-filter based Three-phase Active Rectifier",* Industry Applications Conference, 2002. 37th IAS Annual Meeting Volume 2, 13-18 Oct. 2002: 1181-88.

[11] RADUCU, G. A. (2008). *Control of Grid Side Inverter in a B2B Configuration for WT Applications.* Aalborg, Denmark

[13] Lindgren, M. (1998). *Modeling and Control of Voltage Source Converters Connected to the Grid.* Goteborg, Sweden.

[14] Teodorescu, R. and F. Blaabjerg. *"Flexible control of small wind turbines with grid failure detection operating in stand-alone and grid-connected mode" IEEE Transactions on power electronics,* Volume 19, No. 5, Sept. 2004: 1323-1332.

[15] Svensson, Jan. (1998). *Grid-Connected Voltage Source Control Principle and Wind Energy Applications.* Goteborg, Sweden.

[16] Ahmed Mohamed, Arash Nejadpak, and Osama Mohammed. (2012). *LCL-Filter-Based Bi-Directional Converter for Connectivity of Microgrids Involving Sustainable Energy Sources.* Retrieved from IEEE: http://ieeexplore.ieee.org/xpls/abs_all.jsp?arnumber=6336334&tag=1

[17] Hammerstrom, J. "AC Versus DC Distribution Systems --- Did We Get It Right?," IEEE Power Engineering Society General Meeting, 2007: 1-5.

[18] Nilsson and A. Sannino. "Efficiency Analysis of Low- and Medium-Voltage DC Distribution Systems," IEEE PES General Meeting, 2004.

[19] Salomonsson and A. Sannino, "Low-Voltage DC Distribution System for Commercial Power Systems With Sensitive Electronic Loads," IEEE Trans. on Power Delivery, Vol. 22, No. 3, July 2007: 1620-27.

[20] Engelen, K., E. L. Shun, P. Vermeyen, L. Pardon, R. D'hulst, J. Driesen, and R. Belmans, "The Feasibilty of Small-Scale Residential DC Distribution"

[21] Hirofumi Akagi, Edson Hirokazu Watanabe, Mauricio Aredes. (n.d.). *Instantaneous Power Theory and Applications to Power Conditioning.* Wiley-IEEE Press; 1 edition (March 9, 2007).

[22] Zhiqiang Guo, Deshang Sha, and Xiaozhong Liao. (2013, May 3). *Wireless Paralleled Control Strategy of Three-phase Inverter Modules for Islanding Distributed Generation Systems.* Retrieved from Journal of Power Electronics: http://dx.doi.org/10.6113/JPE.2013.13.3.479.

[23] Vandenbergh, M., A. Engler, R. Geipel, M. Landau, and P. Strauss. *Microgrid management with a high share of renewable energy sources.* In *21st International Conference on European Photovoltaic Solar Energy*, 2006.

[24] Bollman, A. (2009). *Microgrid, an Experimental Study of Frequncy Droop Control in a Low - Inertia.* Urbana, Illinois, USA.

[25] Jiangbiao He, Sizov Y. Gennadi, Peng Zhang, and Nabeel Demerdash, "A Review of Mitigation Methods for Overvoltage in Long-Cable-Fed PWM AC Drives," IEEE EnergyConversion Congress and Exposition (ECCE), Phoenix, 2011: 2160-66.

[26] Jinwei He, Yun Wei Li, Josep M. Guerrero, Frede Blaabjerg, and Juan C. Vasquez. (2013). *Microgrid Reactive and Harmonic Power Sharing Using.* Retrieved from IEEE.

[27] F. Z. Peng, Y. W. Li, and L. M. Tolbert. "Control and Protection of Power Electronics Interfaced Distributed Generation Systems in a Customer-driven Microgrid," in *Proc. IEEE   Power Energy Soc. General Meet.*, 2009: 1–8.

[28] S. Chowdhury, S. P. Chowdhury, and P. Crossley. *Microgrids and Active Distribution Networks. vol. 1.* London, U.K.: Inst. Eng. Technol., 2009.

[29] K. De Brabandere, K.Vanthournout, J. Driesen, G. Deconinck, and R. Belmans. "Control of Microgrids," in *Proc. IEEE Power Eng. Soc. General Meet.*, 2007: 1–7.

Appendix A

Equivalent two-phase system, $\alpha\beta$-transformation (Park):

A three-phase system can be designated with only two components d and q (real and imaginary respectively). In addition, we call a space vector the coordinate system rotating with the frequency ω

$$v_{dq} = v_d + jv_q \tag{A.1}$$

$$T = \begin{bmatrix} v_d \\ v_q \\ v_0 \end{bmatrix} = K \begin{bmatrix} \sin(\omega t) & \sin(\omega t - \frac{2\pi}{3}) & \sin\left(\omega t + \frac{2\pi}{3}\right) \\ \cos(\omega t) & \cos(\omega t - \frac{2\pi}{3}) & \cos(\omega t + \frac{2\pi}{3}) \\ \frac{1}{3} & \frac{1}{3} & \frac{1}{3} \end{bmatrix} \begin{bmatrix} v_a \\ v_b \\ v_c \end{bmatrix} \tag{A.2}$$

Where K is a scaling constant. The transformation from ABC-to-dq (Park transformation) is dependent on the scaling constant K[8]:

Amplitude invariant	$K = 1$
RMS-value invariant	$K = 1/\sqrt{2}$
Power invariant	$K = \dfrac{2}{3}$

Table A1: K values.

Appendix B

Design Considerations for LCL-Filter:
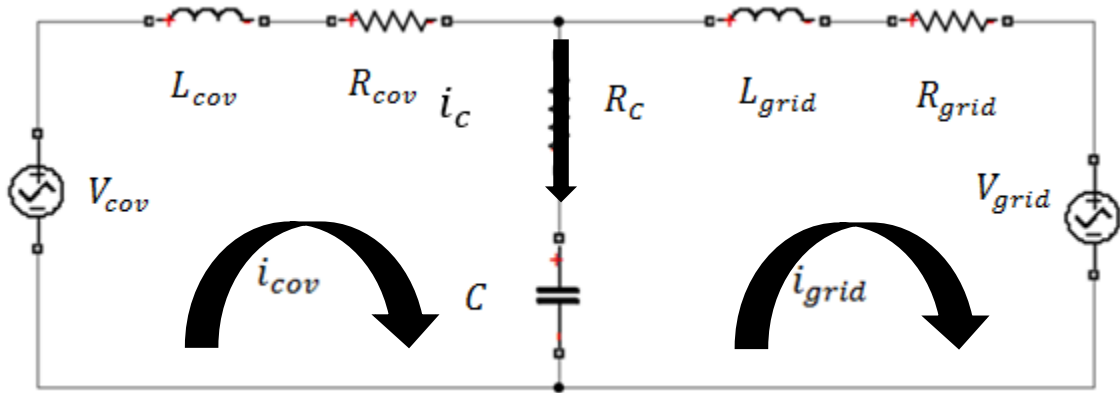
Fig B.1: LCL filter

V_{cov} is the input of the converter side .

V_{grid} is the input of the grid side.

i_{cov} is the converter side current

i_{grid} is the grid side current.

v_c is the capacitor voltage.

Where V_{cov} and V_{grid} are the inputs of the three-phase system a,b,c while i_{cov} , i_{grid} and

v_c are the three states of the three-phase system a,b,c as shown in Fig. B.1.

- Writing the equations for phase (a):

$$V_{cov} - R_{cov}\, i_{cov} - L_{cov}\frac{di_{cov}}{dt} - R_c i_c - V_c = 0$$

$$\frac{i_{cov}}{dt} = \frac{1}{L_{cov}}\,[\ V_{cov} - R_{cov}\, i_{cov} - R_c i_c - V_c \qquad\qquad\qquad \text{(B.1)}$$

$$V_c - R_{grid}\, i_{grid} - L_{grid}\frac{di_{grid}}{dt} + R_c i_c - V_{grid} = 0$$

$$\frac{i_{grid}}{dt} = \frac{1}{L_{grid}} \left[V_c - R_{grid}\, i_{grid} + R_c i_c - V_{grid} \right] \tag{B.2}$$

$$\dot{v}_c = \frac{1}{c} \left[i_{cov} - i_{grid} \right] \tag{B.3}$$

- Writing the equations for phase (b):

$$V_{cov} - R_{cov}\, i_{cov} - L_{cov}\frac{di_{cov}}{dt} - R_c i_c - V_c = 0$$

$$\frac{di_{cov}}{dt} = \frac{1}{L_{cov}} \left[V_{cov} - R_{cov}\, i_{cov} - R_c i_c - V_c \right] \tag{B.4}$$

$$V_c - R_{grid}\, i_{grid} - L_{grid}\frac{di_{grid}}{dt} + R_c i_c - V_{grid} = 0$$

$$\frac{di_{grid}}{dt} = \frac{1}{L_{grid}} \left[V_c - R_{grid}\, i_{grid} + R_c i_c - V_{grid} \right] \tag{B.5}$$

$$\dot{v}_c = \frac{1}{c} \left[i_{cov} - i_{grid} \right] \tag{B.6}$$

- Writing the equations for phase (c):

$$V_{cov} - R_{cov}\, i_{cov} - L_{cov}\frac{di_{cov}}{dt} - R_c i_c - V_c = 0$$

$$\frac{di_{cov}}{dt} = \frac{1}{L_{cov}} \left[V_{cov} - R_{cov}\, i_{cov} - R_c i_c - V_c \right] \tag{B.7}$$

$$V_c - R_{grid}\, i_{grid} - L_{grid}\frac{di_{grid}}{dt} + R_c i_c - V_{grid} = 0$$

$$\frac{di_{grid}}{dt} = \frac{1}{L_{grid}} \left[V_c - R_{grid}\, i_{grid} + R_c i_c - V_{grid} \right] \tag{B.8}$$

$$\dot{v}_c = \frac{1}{c} \left[i_{cov} - i_{grid} \right] \tag{B.9}$$

- From questions (B.1) to (B.9), the steady space model $(\dot{x} = Ax + Bu)$ can be arranged in three phases (a, b, c) as follows:

$$
\frac{d}{dt}\begin{bmatrix} i_{cova} \\ i_{covb} \\ i_{covc} \\ i_{grida} \\ i_{gridb} \\ i_{gridc} \\ v_{ca} \\ v_{cb} \\ v_{cc} \end{bmatrix} =
\begin{bmatrix}
\frac{-R_{cov}-R_c}{L_{cov}} & 0 & 0 & \frac{R_c}{L_{cov}} & 0 & 0 & \frac{-1}{L_{cov}} & 0 & 0 \\
0 & \frac{-R_{cov}-R_c}{L_{cov}} & 0 & 0 & \frac{R_c}{L_{cov}} & 0 & 0 & \frac{-1}{L_{cov}} & 0 \\
0 & 0 & \frac{-R_{cov}-R_c}{L_{cov}} & 0 & 0 & \frac{R_c}{L_{cov}} & 0 & 0 & \frac{-1}{L_{cov}} \\
\frac{R_c}{L_{grid}} & 0 & 0 & \frac{-R_c-R_{grid}}{L_{grid}} & 0 & 0 & \frac{1}{L_{grid}} & 0 & 0 \\
0 & \frac{R_c}{L_{grid}} & 0 & 0 & \frac{-R_c-R_{grid}}{L_{grid}} & 0 & 0 & \frac{1}{L_{grid}} & 0 \\
0 & 0 & \frac{R_c}{L_{grid}} & 0 & 0 & \frac{-R_c-R_{grid}}{L_{grid}} & 0 & 0 & \frac{1}{L_{grid}} \\
\frac{1}{C} & 0 & 0 & \frac{-1}{C} & 0 & 0 & 0 & 0 & 0 \\
0 & \frac{1}{C} & 0 & 0 & \frac{-1}{C} & 0 & 0 & 0 & 0 \\
0 & 0 & \frac{1}{C} & 0 & 0 & \frac{-1}{C} & 0 & 0 & 0
\end{bmatrix}
$$

$$
\begin{bmatrix} i_{cova} \\ i_{covb} \\ i_{covc} \\ i_{grida} \\ i_{gridb} \\ i_{gridc} \\ v_{ca} \\ v_{cb} \\ v_{cc} \end{bmatrix} +
\begin{bmatrix}
\frac{1}{L_{cov}} & 0 & 0 & 0 & 0 & 0 & 0 & 0 & 0 \\
0 & \frac{1}{L_{cov}} & 0 & 0 & 0 & 0 & 0 & 0 & 0 \\
0 & 0 & \frac{1}{L_{cov}} & 0 & 0 & 0 & 0 & 0 & 0 \\
0 & 0 & 0 & \frac{-1}{L_{grid}} & 0 & 0 & 0 & 0 & 0 \\
0 & 0 & 0 & 0 & \frac{-1}{L_{grid}} & 0 & 0 & 0 & 0 \\
0 & 0 & 0 & 0 & 0 & \frac{-1}{L_{grid}} & 0 & 0 & 0 \\
0 & 0 & 0 & 0 & 0 & 0 & 0 & 0 & 0 \\
0 & 0 & 0 & 0 & 0 & 0 & 0 & 0 & 0 \\
0 & 0 & 0 & 0 & 0 & 0 & 0 & 0 & 0
\end{bmatrix}
\qquad \text{(B.10)}
$$

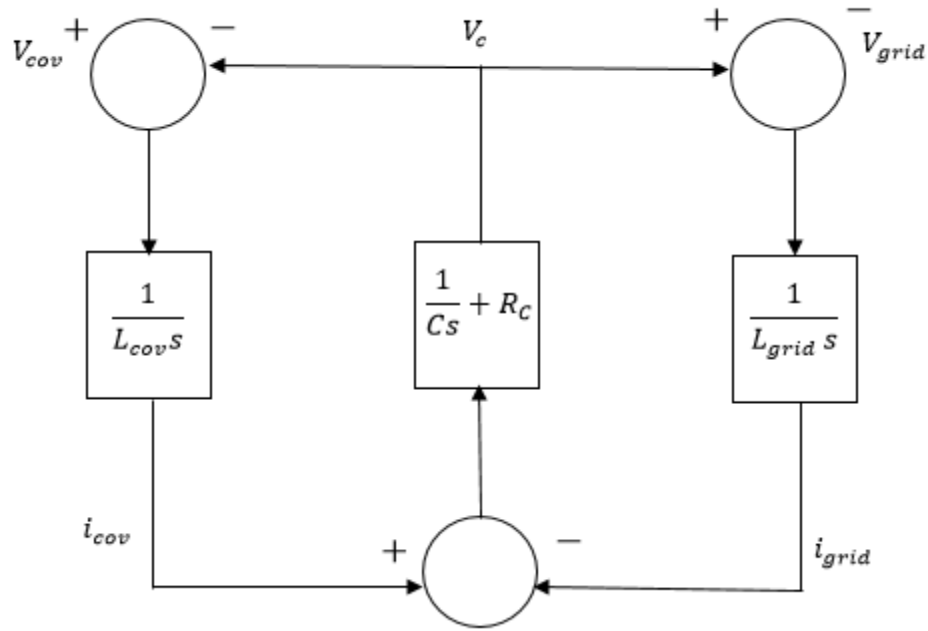- Driving the transfer function of this system as follows:

Fig. B.2: Single phase LCL model in s-plane.

Determines the transfer function of the LCL model by using Fig. B.2.

$$v_{cov} = z_{11}i_{cov} + z_{12}i_{grid} \qquad \text{(B.11)}$$

$$v_{grid} = z_{21}i_{cov} + z_{22}i_{grid} \qquad \text{(B.12)}$$

$$z_{11}i_{cov} = v_{cov} - z_{12}i_{grid}$$

$$i_{cov} = \frac{[v_{cov} - z_{12}i_{grid}]}{z_{11}}$$

$$\frac{i_{cov}}{v_{cov}} = \frac{\left[\frac{v_{cov} - z_{12}i_{grid}}{z_{11}}\right]}{v_{cov}} \qquad \text{(B.13)}$$

$$z_{11} = L_{cov}s + \frac{1}{Cs} + R_C \qquad \text{(B.14)}$$

$$z_{12} = -[\frac{1}{Cs} + R_C] \qquad \text{(B.15)}$$

$$z_{21} = -[\frac{1}{Cs} + R_C] \tag{B.16}$$

$$z_{22} = -[L_{grid} \, s + \frac{1}{Cs} + R_C] \tag{B.17}$$

$$H(s) = \frac{I(s)_{cov}}{v(s)_{cov}} = \frac{L_{grid} \, C \, s^2 + R_C \, C \, s + 1}{L_{cov} \, L_{grid} \, s^3 + R_C \, C \, (L_{cov} \, L_{grid})s^2 + (L_{cov} \, L_{grid})s} \tag{B.18}$$

- The transformation from *abc* frame of reference to *dqo* frame of reference as follows:

$$\dot{x}_{abc} = Ax_{abc} + Bu \tag{B.19}$$

$$x_{abc} = Tx_{dq} \tag{B.20}$$

$$\dot{x}_{abc} = \dot{T}x_{dq} + T\dot{x}_{dq} \tag{B.21}$$

$$\dot{T}x_{dq} + T\dot{x}_{dq} = ATx_{dq} + TBu_{dq} \tag{B.22}$$

$$T\dot{x}_{dq} = ATx_{dq} - \dot{T}x_{dq} + BTx_{dq} \tag{B.23}$$

$$\dot{x}_{dq} = (TA^{-1}T)x_{dq} - (T^{-1}\dot{T})x_{dq} + (T^{-1}B\,T)x_{dq} \tag{B.24}$$

Where T is given in Appendix A.

Appendix C

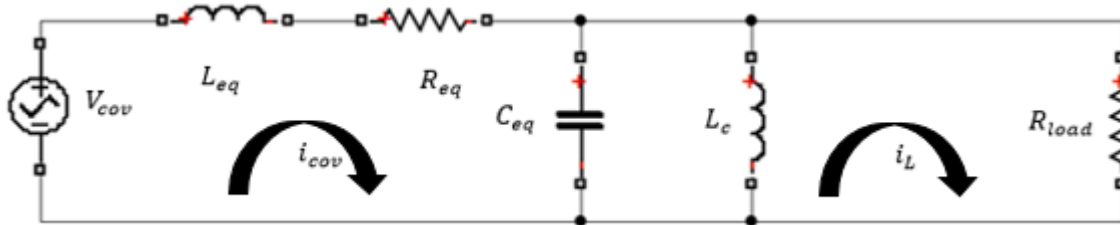## Design Considerations for LCL-Filter With a Load:

Fig. C1: LCL-filter with a load.

V_{cov} is the input of the converter side.

i_{cov} is the converter side current.

v_c is the capacitor voltage.

L_{eq} is the equivalent inductor of the convert side.

R_{eq} is the equivalent resistorof the convert side.

Where V_{cov} is the inputs of the three-phase system a,b,c, while i_{cov} , i_{Lc} and v_c are the

three states of the three-phase system a,b,c as shown in Fig. C.1.

- Writing the equations for phase (a):

$$V_{cov} - R_{eq}\, i_{cov} - L_{eq} \frac{di_{cov}}{dt} - V_c = 0$$

$$\frac{di_{cov}}{dt} = \frac{1}{L_{eq}} [\ V_{cov} - R_{eq}\, i_{cov} - V_c\ ] \qquad\qquad (C.1)$$

$$i_{cov} - i_L - \frac{V_c}{R_{load}} - \frac{\dot{v}_c}{c}$$

$$\dot{v}_c = \frac{1}{c} [\ i_{cov} - i_L - \frac{V_c}{R_{load}}\ ] \qquad\qquad (C.2)$$

$$\frac{di_L}{dt} i_L = V_c$$

$$\frac{di_L}{dt} = \frac{V_c}{i_L} \tag{C.3}$$

- Writing the equations for phase (b):

$$V_{cov} - R_{eq} i_{cov} - L_{eq} \frac{di_{cov}}{dt} - V_c = 0$$

$$\frac{di_{cov}}{dt} = \frac{1}{L_{eq}} [\, V_{cov} - R_{eq} i_{cov} - V_c \,] \tag{C.4}$$

$$i_{cov} - i_L - \frac{V_c}{R_{load}} - \frac{\dot{v}_c}{c}$$

$$\dot{v}_c = \frac{1}{c} [\, i_{cov} - i_L - \frac{V_c}{R_{load}} \,] \tag{C.5}$$

$$\frac{di_L}{dt} i_L = V_c$$

$$\frac{di_L}{dt} = \frac{V_c}{i_L} \tag{C.6}$$

- Writing the equations for phase (C):

$$V_{cov} - R_{eq} i_{cov} - L_{eq} \frac{di_{cov}}{dt} - V_c = 0$$

$$\frac{di_{cov}}{dt} = \frac{1}{L_{eq}} [\, V_{cov} - R_{eq} i_{cov} - V_c \,] \tag{C.7}$$

$$i_{cov} - i_L - \frac{V_c}{R_{load}} - \frac{\dot{v}_c}{c}$$

$$\dot{v}_c = \frac{1}{c} [\, i_{cov} - i_L - \frac{V_c}{R_{load}} \,] \tag{C.8}$$

$$\frac{di_L}{dt} i_L = V_c$$

$$\frac{di_L}{dt} = \frac{V_c}{i_L} \tag{C.9}$$

- From questions (C.1) to (C.9) , the steady space model $(\dot{x} = Ax + Bu)$ can be arranged in three phases (a, b, c) as follows:

$$\frac{d}{dt}\begin{bmatrix} i_{cova} \\ i_{covb} \\ i_{covc} \\ v_{ca} \\ v_{cb} \\ v_{cc} \\ i_{La} \\ i_{Lb} \\ i_{Lc} \end{bmatrix} = \begin{bmatrix} \frac{-R_{conv}}{L_{cov}} & 0 & 0 & \frac{-1}{L_{cov}} & 0 & 0 & 0 & 0 & 0 \\ 0 & \frac{-R_{conv}}{L_{cov}} & 0 & 0 & \frac{-1}{L_{cov}} & 0 & 0 & 0 & 0 \\ 0 & 0 & \frac{-R_{conv}}{L_{cov}} & 0 & 0 & \frac{-1}{L_{cov}} & 0 & 0 & 0 \\ \frac{I}{C} & 0 & 0 & \frac{-1}{c*R_{load}} & 0 & 0 & \frac{-1}{c} & 0 & 0 \\ 0 & \frac{I}{C} & 0 & 0 & \frac{-1}{c*R_{load}} & 0 & 0 & \frac{-1}{c} & 0 \\ 0 & 0 & \frac{I}{C} & 0 & 0 & \frac{-1}{c*R_{load}} & 0 & 0 & \frac{-1}{c} \\ 0 & 0 & 0 & \frac{1}{L_C} & 0 & 0 & 0 & 0 & 0 \\ 0 & 0 & 0 & 0 & \frac{1}{L_C} & 0 & 0 & 0 & 0 \\ 0 & 0 & 0 & 0 & 0 & \frac{1}{L_C} & 0 & 0 & 0 \end{bmatrix}$$

$$\begin{bmatrix} i_{cova} \\ i_{covb} \\ i_{covc} \\ v_{ca} \\ v_{cb} \\ v_{cc} \\ iL_a \\ iL_b \\ iL_c \end{bmatrix} + \begin{bmatrix} \frac{1}{L_{cov}} & 0 & 0 & 0 & 0 & 0 & 0 & 0 & 0 \\ 0 & \frac{1}{L_{cov}} & 0 & 0 & 0 & 0 & 0 & 0 & 0 \\ 0 & 0 & \frac{1}{L_{cov}} & 0 & 0 & 0 & 0 & 0 & 0 \\ 0 & 0 & 0 & 0 & 0 & 0 & 0 & 0 & 0 \\ 0 & 0 & 0 & 0 & 0 & 0 & 0 & 0 & 0 \\ 0 & 0 & 0 & 0 & 0 & 0 & 0 & 0 & 0 \\ 0 & 0 & 0 & 0 & 0 & 0 & 0 & 0 & 0 \\ 0 & 0 & 0 & 0 & 0 & 0 & 0 & 0 & 0 \\ 0 & 0 & 0 & 0 & 0 & 0 & 0 & 0 & 0 \end{bmatrix} \begin{bmatrix} v_{cova} \\ v_{covb} \\ v_{covc} \\ 0 \\ 0 \\ 0 \\ 0 \\ 0 \\ 0 \end{bmatrix} \quad (C.10)$$

- The transformation from *abc* frame of reference to *dqo* frame of reference as it is explained in appendix A.